#### **INFORMATION TO USERS**

This manuscript has been reproduced from the microfilm master. UMI films the text directly from the original or copy submitted. Thus, some thesis and dissertation copies are in typewriter face, while others may be from any type of computer printer.

The quality of this reproduction is dependent upon the quality of the copy submitted. Broken or indistinct print, colored or poor quality illustrations and photographs, print bleedthrough, substandard margins, and improper alignment can adversely affect reproduction.

In the unlikely event that the author did not send UMI a complete manuscript and there are missing pages, these will be noted. Also, if unauthorized copyright material had to be removed, a note will indicate the deletion.

Oversize materials (e.g., maps, drawings, charts) are reproduced by sectioning the original, beginning at the upper left-hand corner and continuing from left to right in equal sections with small overlaps.

Photographs included in the original manuscript have been reproduced xerographically in this copy. Higher quality 6" x 9" black and white photographic prints are available for any photographs or illustrations appearing in this copy for an additional charge. Contact UMI directly to order.

Bell & Howell Information and Learning 300 North Zeeb Road, Ann Arbor, MI 48106-1346 USA 800-521-0600



·		

#### **NOTE TO USERS**

This reproduction is the best copy available.

**UMI** 

# Advances in On-line Ultrasonic Monitoring of Injection Molding Process



#### Szu-sheng Wen

Department of Electrical Engineering
McGill University
Montréal, Québec, Canada
July 1998

A thesis submitted to the Faculty of Graduate Studies and Research in partial fulfillment of the requirements of the degree of M. Eng.

© Szu-sheng Wen 1998



National Library of Canada

Acquisitions and Bibliographic Services

395 Wellington Street Ottawa ON K1A 0N4 Canada Bibliothèque nationale du Canada

Acquisitions et services bibliographiques

395, rue Wellington Ottawa ON K1A 0N4 Canada

Your file Votre reference

Our file Notre référence

The author has granted a non-exclusive licence allowing the National Library of Canada to reproduce, loan, distribute or sell copies of this thesis in microform, paper or electronic formats.

The author retains ownership of the copyright in this thesis. Neither the thesis nor substantial extracts from it may be printed or otherwise reproduced without the author's permission.

L'auteur a accordé une licence non exclusive permettant à la Bibliothèque nationale du Canada de reproduire, prêter, distribuer ou vendre des copies de cette thèse sous la forme de microfiche/film, de reproduction sur papier ou sur format électronique.

L'auteur conserve la propriété du droit d'auteur qui protège cette thèse. Ni la thèse ni des extraits substantiels de celle-ci ne doivent être imprimés ou autrement reproduits sans son autorisation.

0-612-55124-5



#### **Abstract**

On-line ultrasonic monitoring of conventional and gas-assisted injection molding processes, and temperature measurement using ultrasound, are carried out. A technique utilizing reflection coefficients obtained by a pulse/echo technique is established to monitor the local polymer melt arrival, end of filling, pressure overshoot, solidification, part detachment, plunger retraction, and part ejection in conventional injection molding. The same technique is applied to monitor additional process parameters such as the local gas arrival, start and end of gas injection, gas penetration, and gas blow-through in gas-assisted injection molding. During solidification monitoring of a high-density polyethylene part, the solidification front is observed. Also the thickness of solidified layers is determined, and its application in obtaining temperature within the molded part is demonstrated. An approach to determine the local flow front speed of the molten polymer is also proposed.

A high-performance buffer rod is fabricated and calibrated as a new type of ultrasonic temperature probe to measure temperature during the extrusion process. The temperature obtained using the ultrasonic technique is comparable with calibrated conventional thermocouples. Comparison between ultrasonic sensors and conventional pressure and temperature probes is also discussed in this study.

#### Résumé

Des mesures utilisant des techniques ultrasonores en ligne ont été pour les procédés de moulage par injection conventionnel et assisté par gaz. Une technique utilisant le coefficient de réflexion obtenu par la méthode pulse/echo a été implantée pour le suivi en ligne de certains paramètres pendent le moulage. Ces paramètres sont: le front d'écoulement du polymère liquide, la fin du remplissage, les variations de pression, la solidification, le décollement des parois, le retrait de la vis et l'éjection de la pièce. La même technique est utilisée pendent le moulage assisté par gaz pour obtenir, en plus des informations cités précédemment, certains paramètres additionnels: l'arrivée du gaz, le début et la fin de l'injection des gaz, la pénétration des gaz et le "blow-through" du gaz. De plus, une approche a été développée pour démontrer la relation entre l'épaisseur des couches de solidification et la température interne des polymères pendent le solidification lors de moulage de polyéthylène de haute densité. Une méthode y est aussi proposée pour déterminer la vitesse du front d'écoulement du polymère liquide.

Une ligne à délai ultrasonore de haute performance a été fabriquée et calibrée pour mesurer la température dans le procéde de l'extrusion. Les mesures de température obtenues sont comparables à aux obtenues par des thermocouples traditionnels. La comparaison entre le capteur ultrasonore et les capteurs conventionnel de pression et de température est également discutée dans cette étude.

#### **Acknowledgments**

I would like to thank the Lord for His initiation, provision, and leading in my studies, and my parents, my grandparents, and my brother for their endless care, encouragement, and support throughout my years of study.

I also want to thank my thesis supervisor, Dr. C.-K. Jen for his love and effort in caring and raising up a student, his timely and continual guiding of this project, and instructions about ultrasound, which made the completion of this study possible.

Dr. K.T. Nguyen and Dr. A. Derdouri are also greatly appreciated for their help in my understanding of the injection molding process and its monitoring. I would like to express my gratitude to Dr. T.-F. Chen, and acknowledge his contribution in implementing the real-time Kalman filter to assist the signal processing for temperature measurement. Mr. B. Cao and Mr. H. Hébert are also acknowledged for their implementation of original data acquisition and signal processing programs.

In addition, I would like to thank Mr. Y. Simard for operating injection molding machines, Dr. A. Steele and Mr. D. Gee for their instructions and help in carrying out calibration of temperature sensors, and Mr. A. Bloch for proof-reading this thesis.

Special thanks are given to the Industrial Material Institute, National Research Council (IMI-NRC) where all ultrasonic monitorings were carried out, and the Institute for National Measurement Standards, National Research Council (INMS-NRC) where temperature sensors were calibrated.

Financial support from the Natural Sciences and Engineering Research Council of Canada from an operating and a strategy (STR0192858) grant and Le Fonds pour la Formation de Chercheurs et l'Aide à la Recherche (Fonds FCAR) are gratefully acknowledged.

#### **Dedication**

To My Parents

and Grandparents

#### **Abbreviations and Nomenclature**

ABS acrylonitrile-butadiene-styrene

CAE computer-aided engineering

DCR corrected Dynisco thermocouple reading

DE detachment from external mold

DI detachment from internal mold

DR Dynisco thermocouple reading before correction

EF end of filling

EMCI external mold/cavity interface

EMGI external melt/gas interface

FA flow front arrival

GA gas arrival

GAIM gas-assisted injection molding

HDPE high density polyethylene

IMCI internal mold/cavity interface

IR infrared

L liquid layer
MA melt arrival

PRTD platinum resistance temperature detector

PS polystyrene S solid layer

SG start of gas injection
SLI solid/liquid interface
SNR signal-to-noise ratio
UT ultrasonic transducer

VI virtual instrument

A temperature gradient
B surface temperature

D diameter of UT

distances between end of the ultrasonic probe and the 1st discontinuity and

between discontinuities

FA<sub>c,d,PT</sub> flow front arrival monitored at locations c, d, and by pressure transducer

h<sub>mea,eff</sub> measured and effective wall thickness

h<sub>l.s-ex.s-in</sub> thicknesses of the liquid, external and internal solid layers

 $L_{a,b}$  echoes reflected from the 1<sup>st</sup> and 2<sup>nd</sup> discontinuities

L<sup>1</sup> 1<sup>st</sup> return echo from EMCI

L<sub>2,4,6,2g</sub> 1<sup>st</sup>, 2<sup>nd</sup>, and 3<sup>rd</sup> return echoes from IMCI and 1<sup>st</sup> return echo from EMGI

N near field length

P,P<sub>A,B,h,l</sub> pressure, pressure measured at locations A and B, high and low pressure

T,T<sub>c,measurable</sub> temperature, crystallization, and measurable temperatures

t<sub>A,B,S,R,G</sub> time at location A, B, switch-over, time for mechanical response, gate

freezing

V,V<sub>h,i,avg</sub> ultrasonic wave velocity, high, low, average ultrasonic wave velocity

 $Z_1, Z_2$  acoustic impedance, acoustic impedance in the 1<sup>st</sup> and the 2<sup>nd</sup> media

α 1<sup>st</sup> order thermal response time

 $\Delta\Gamma_{c,d}$  change in reflection coefficient at locations c and d

 $\Delta P$ ,  $P_G$  change in pressure of molded part and gas pressure

 $\Delta \tau$  change in time delay

Γ reflection coefficient

 $\lambda$  wavelength

 $\mu_{x,y}$  means in the x and y direction

Π transmission coefficient

ρ density

σ standard deviation

 $\tau, \tau_{l.s-ex.s-in}$  time delay, travel time in the liquid, external, internal solid layers

 $\tau_{m,g,1,2}$  time delay between L<sub>2</sub> and L<sup>1</sup>, between L<sub>2g</sub> and L<sup>1</sup>, between L<sub>a</sub> and L<sup>1</sup>,

between La and Lb

#### **Table of Contents**

Abstract	i
Résumé	ii
Acknowledgments	iii
Dedication	iv
Abbreviations and Nomenclature	v
Table of Contents	vi
List of Figures	ix
List of Tables	xi
Chapter 1: Introduction	1
1.1 Background	1
1.2 Ultrasound, pulse/echo method, and acquisition system	2
1.3 The injection molding process and its monitoring	6
1.4 Gas-assisted injection molding, its advantages and monitoring	9
1.5 Thesis content	11
1.5.1 Objective	11
1.5.2 Content	11
Chapter 2: Advances in On-line Ultrasonic Monitoring	
of Injection Molding Process	14
2.1 Introduction	14
2.2 Experimental setup	14
2.2.1 Setup and the sample	14
2.2.2 Operating conditions	17
2.3 Cavity pressure	18
2.4 Filling monitoring	20
2.5 Effect of overshoot	25
2.6 Flow front speed monitoring	31
2.7 Solidification monitoring	37

2.8 Detachment monitoring	42
2.9 Summary	47
Chapter 3: On-line Ultrasonic Monitoring of Gas-assisted Injection Moldin	g
and Off-line Measurement for Co-injection Molding	50
3.1 Introduction	50
3.2 Gas-assisted injection molding (GAIM)	51
3.2.1 Experimental setup and the sample	51
3.2.2 Operating conditions of the injection molding machine	52
3.2.3 Cavity pressure	53
3.2.4 Principle of on-line monitoring of GAIM	55
3.2.5 Results	57
3.3 Co-injection molding	64
3.4 Summary	67
Chapter 4: Ultrasonic Temperature Measurement	70
4.1 Introduction	70
4.2 Ultrasonic techniques in temperature measurement	70
4.3 Calibration of ultrasonic probe	76
4.3.1 Setup	77
4.3.2 Steady state calibration	78
4.3.3 Temperature measurement in fluids	80
4.4 Temperature measurement in polymer extrusion	83
4.5 Summary	86
Chapter 5: Conclusions	88
5.1 Thesis summary	88
5.2 Original contributions	94
5.3 Future work	95
Defense	07

#### **List of Figures**

Fig. 1-1: Transmission and reflection of ultrasound at an interface	3
Fig. 1-2: Schematics of acquisition system	4
Fig. 1-3: Serial acquisition VI used to acquire and save ultrasonic signals	5
Fig. 1-4: VI used to determine the amplitude of a chosen ultrasonic echo	5
Fig. 1-5: One cycle of injection molding monitored from cavity	7
Fig. 1-6: One cycle of gas-assisted injection molding	10
Fig. 2-1: Engel 150-ton co-injection molding machine	15
Fig. 2-2: Molded box and its dimensions	16
Fig. 2-3: Top and side views of cross-section	16
Fig. 2-4: Installation of UTs onto the outside surface of external mold	17
Fig. 2-5: Characteristic cavity pressure curve in injection molding	19
Fig. 2-6: Pressure reduction at section 1 due to isolation from pressure source	
as section 2 is solidified	20
Fig. 2-7: Molded boxes from complete and incomplete cavity filling	22
Fig. 2-8: Filling Monitoring for injection molding	23
Fig. 2-9: Monitoring the end of filling (EF) using ultrasonic technique	25
Fig. 2-10: An injection molding run without overshoot	27
Fig. 2-11: An injection molding run with overshoot	28
Fig. 2-12: Tripartite (P-V-T) relationship for HDPE	29
Fig. 2-13: Average ultrasonic wave velocity, pressure, and temperature	
of the molded part	31
Fig. 2-14: Error in flow front speed measurement with two ultrasonic	
transducers (UTs)	32
Fig. 2-15: Flow front speed measurement with one ultrasonic transducer (UT)	33
Fig. 2-16: Far field Gaussian distribution of ultrasonic intensity for circular UT	
and integration (energy transmission) across it	35
Fig. 2-17: Injection phase in injection molding with different plunger speeds	36

Fig. 2-18: On-line monitoring of solidification	38
Fig. 2-19: Solidification fronts and thickness of liquid and solid layers	39
Fig. 2-20: Detachment mechanism	43
Fig. 2-21: On-line monitoring of detachment from internal mold (DI)	
and external mold (DE)	44
Fig. 2-22: Effect on $\Gamma$ due to detachment and plunger retraction	46
Fig. 2-23: Summary of on-line monitoring of injection molding using $\Gamma$ plots	48
Fig. 3-1: Husky injection molding machine and Cinpres 2-cylinder	
gas injection unit	51
Fig. 3-2: Installation of UTs on the external mold wall	52
Fig. 3-3: HDPE sample made by GAIM	53
Fig. 3-4: Gas pressure by discontinuous gas generation unit	55
Fig. 3-5: Typical polymer melt and gas pressure curves in GAIM	55
Fig. 3-6: Principle of ultrasonic on-line monitoring of GAIM	56
Fig. 3-7: Echo (L <sub>2g</sub> ) (indicated by arrows) reflected from external melt/gas	
interface (EMGI)	58
Fig. 3-8: Ultrasonic on-line monitoring of GAIM	59
Fig. 3-9: Diminishing of echo (L <sub>2</sub> ) reflected from internal mold/cavity	
interface (IMCI) and developing of echo (L2g) reflected from	
external melt/gas interface (EMGI)	61
Fig. 3-10: Ultrasonic on-line monitoring of GAIM - A complete part,	
monitored from location "B"	62
Fig. 3-11: Ultrasonic on-line monitoring of GAIM - Gas blow-through case,	
monitored from location "A"	63
Fig. 3-12: Top and bottom views of co-injected plate under study	65
Fig. 3-13: Five co-injected samples (S1~S5) co-injected with different	
amounts of ABS and mixed ABS	65
Fig. 3-14: Sample and ultrasonic transducers (UT) setup in immersion tank	
for interface measurement of co-injected plate	66
Fig. 3-15: Interface echoes (marked by arrows) observed in co-injected	

plates from both top and bottom surfaces	67
Fig. 3-16: Summary of on-line monitoring of GAIM using reflection	
coefficient (Γ) plots	68
Fig. 4-1: Slot ultrasonic probe with two discontinuities inside the die	72
Fig. 4-2: Dimensions of the slot probe and discontinuities "a" and "b"(in mm).	72
Fig. 4-3: Machined ultrasonic probe with Dynisco temperature and	
pressure sensors	73
Fig. 4-4: Step ultrasonic probe with discontinuities "a" and "b"	74
Fig. 4-5: L <sup>1</sup> , L <sub>a</sub> , and L <sub>b</sub> from (a) uncladded and (b) cladded step probe	
using UTs with different central frequencies	75
Fig. 4-6: Frequency spectrum of L <sup>1</sup> with cladded step probe	75
Fig. 4-7: Two conventional temperature sensors used in injection	
molding machines	76
Fig. 4-8: Water and oil bath at INMS-NRC with acquisition system	
used in calibration of temperature probes	78
Fig. 4-9: Setup for calibration of ultrasonic temperature probe	78
Fig. 4-10: Calibration curves for the two conventional temperature sensors	
(Dynisco TPT463E-1M and J-type mold control thermocouple)	79
Fig. 4-11: Calibrated ultrasonic wave velocity inside the slot ultrasonic	
probe versus PRTD temperature readings using ultrasonic	
transducers (UTs) of different central frequencies	80
Fig. 4-12: Response to step temperature change for all temperature sensors	81
Fig. 4-13: Installation of ultrasonic and Dynisco temperature and pressure	
probes in the die of the extruder on a PLACO co-extrusion blow	
molding machine	83
Fig. 4-14: Ultrasonic signals received (a) before and (b) after molten	
polymer arrives at monitoring point using slot ultrasonic probe	84
Fig. 4-15: Temperature readings from slot ultrasonic probe and Dynisco	
TPT463E-1M temperature probe during polymer extrusion process	85

#### List of Tables

Table 2-1: Operating conditions for injection molding	17
Table 2-2: Comparison between ultrasonic and pressure sensors in	
on-line monitoring of injection molding process	49
Table 3-1: Operating conditions for GAIM	52
Table 4-1: Response time for various temperature probes in fluid	
temperature measurement	82
Table 4-2: Comparison between ultrasonic and Dynisco TPT463E-1M	
temperature probes in temperature measurement	87

#### Chapter 1:

#### Introduction

#### 1.1 Background

After mass production techniques such as polymer extrusion and injection molding became prominent since mid-1950s, materials such as glass, metal, and wood have been replaced rapidly by plastics. Due to increasing demands for high quality in products and efficiency in production, material processing underwent a rapid evolution in the past decade [1~5]. Among all processing techniques, injection molding is the most popular and versatile operation, contributing to 32 % by weight of all polymer production [5,6]. It is well known that molding conditions influence significantly the quality of the part such as surface finish, dimensional stability, and mechanical properties of the product [7].

However, injection molding was not understood in the early days due to the complexity of the process [7]. This resulted in the advent of process modeling, analysis, and optimization of parameters. Starting from the 1960s, a great number of investigations have been carried out [8~14]. Mathematical models have been developed to predict material behavior throughout the process, including filling, packing, cooling, shrinkage, and warpage [7,15]. However, simulation software is only useful in the design process if it is accurate [5]. Since computer simulation models often simplify real but complicated situations, verification of the model is crucial [16~20]. In order to identify the sources of inaccuracy and ultimately to improve the model, modeled variables may be measured *in situ* as a verification [5,21,22]. In order to directly measure these process parameters, sensors providing precise measurement are required.

Process control is an important tool to improve production cost and product quality, and reduce material waste [23]. However, since material processes are usually dynamic and difficult to maintain in a steady state, complex control strategies are needed [2~4,24~26]. In order to improve the quality of an injection molded part, process parameters such as temperature (melt and mold), pressure (cavity and hydraulic), and injection speed are monitored and used to control the injection molding process [27]. Consequently, precise feedback of these process parameters to the control system is important to directly supervise the process and indirectly assure consistent quality in the finished product [27]. At present, the lack of proper material processing sensors hampers the advancement of material process control [28]. As a result, demands for the development of cost-effective sensors for on-line measurement are high [2.4,26.29].

#### 1.2 Ultrasound, pulse/echo method, and acquisition system

In order not to perturb process conditions and product qualities in a batch or continuous process, while at the same time performing process control by acquiring desired information fast enough to prevent errors, the ultrasonic sensor is an attractive option due to the ability of ultrasound to interrogate non-invasively, non-destructively, and rapidly the surface and internal regions of objects [30].

When ultrasound propagates in materials, its velocity depends on the material and its temperature and pressure. Therefore, in analogy to electro-magnetic theory, an acoustic impedance (Z) can be defined as the product of the density ( $\rho$ ) and the ultrasonic velocity (V) inside that material. When ultrasound encounters an interface between two different materials, part of the energy will transmit into the other material, and part of the energy will be reflected from the interface. The transmitted portion is referred to as the transmitted wave, and the portion reflected is referred to as the reflected wave. Figure 1-1 shows the incident, transmitted, and reflected waves on both sides of an interface. On oscilloscope screens where the received ultrasonic echo is displayed, the amplitudes of the echoes are observed. As a result, reflection ( $\Gamma$ ) and transmission ( $\Pi$ ) coefficients can

be defined as in Equations 1.1 to represent a measure of amplitude of reflected and transmitted ultrasonic waves on two sides of the interface, respectively.

$$\Gamma = \frac{Z_2 - Z_1}{Z_1 + Z_2}$$

$$\Pi = 2\frac{Z_2}{Z_1 + Z_2} = 1 - \Gamma$$
(1.1)

where  $Z_1$  and  $Z_2$  are acoustic impedances of the 1<sup>st</sup> and the 2<sup>nd</sup> media on two sides of the interface as shown in Figure 1-1, respectively [31]. All the monitoring presented in this paper is done by the pulse/echo technique, in which only one ultrasonic transducer (UT) is utilized both to send and receive ultrasonic waves. As indicated in Figure 1-1, UT not only generates and sends ultrasonic waves into the 1<sup>st</sup> medium, but also receives the reflected wave from the interface.



Fig. 1-1: Transmission and reflection of ultrasound at an interface

Throughout this study, 5 and 10 MHz, longitudinal, 6.35 mm (1/4 inch) diameter, and 20 MHz, longitudinal, 3.18 mm (1/8 inch) diameter UTs made by Panametrics (Waltham, MA) are used to generate and receive ultrasonic waves. The schematic of the acquisition system is shown in Figure 1-2 [32]. The acquisition system includes a Tektronix 7854 oscilloscope, two MP203 pulsers, and MR101 receivers from MetroTek

Inc. with frequency range from 0.5 to 20 MHz. A CompuScope 250 digitizer card from Gage Applied Science Inc. is used to digitize received ultrasonic echoes. The maximum sampling rate is 100 MHz for single channel (one UT) and 50 MHz for dual channels (2 UTs). The digitizer card has 8 MB on-board memory and 8 bits A/D resolution [33]. A Pentium 90 computer is used to run LabView (software from National Instrument). Under the LabView graphical programming environment, VIs (virtual instruments) are created to carry out data acquisition and signal processing. Results presented in this paper are obtained using VIs originating from Cao and Hébert [33] and modified to meet the needs for the study presented in this thesis. Figures 1-3 and 1-4 show the front panels of the acquisition VI, and another signal processing VI that generates the magnitude plot, respectively. The maximum acquisition rate achievable for the overall system is 1000 acquisitions per second [33].

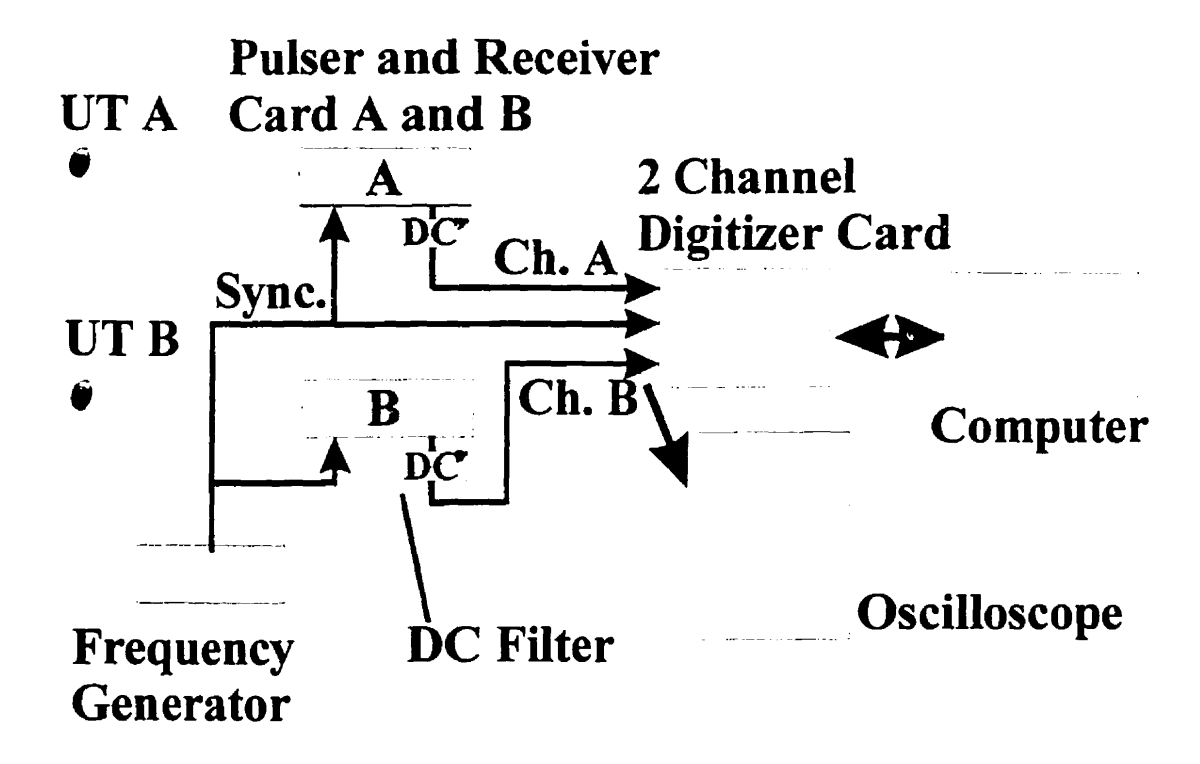


Fig. 1-2: Schematics of acquisition system

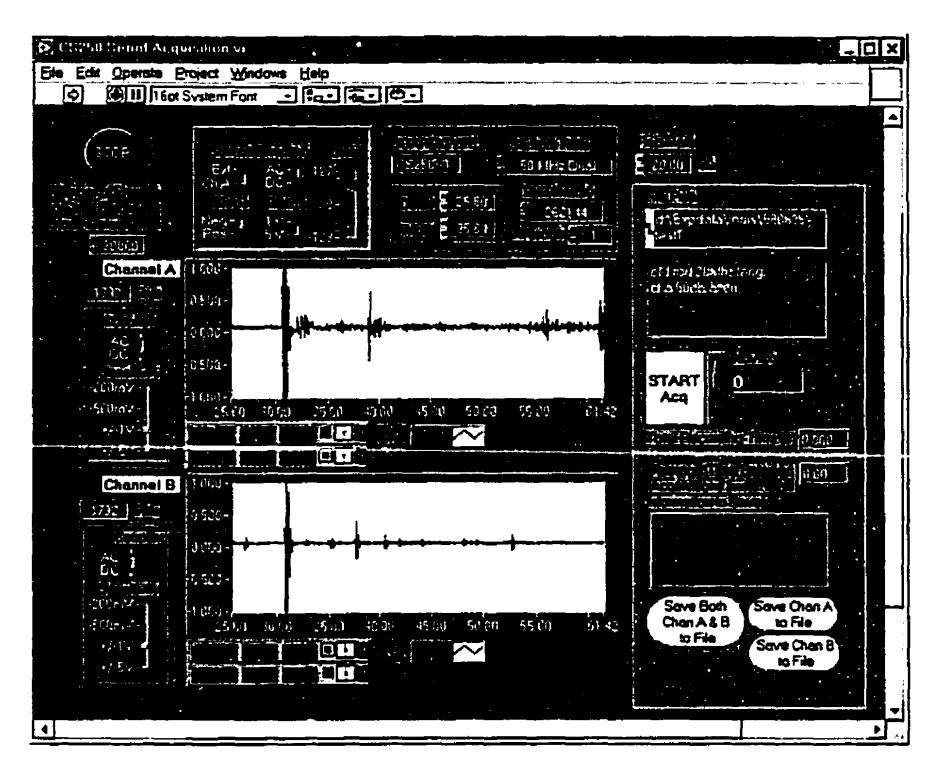


Fig. 1-3: Serial acquisition VI used to acquire and save ultrasonic signals

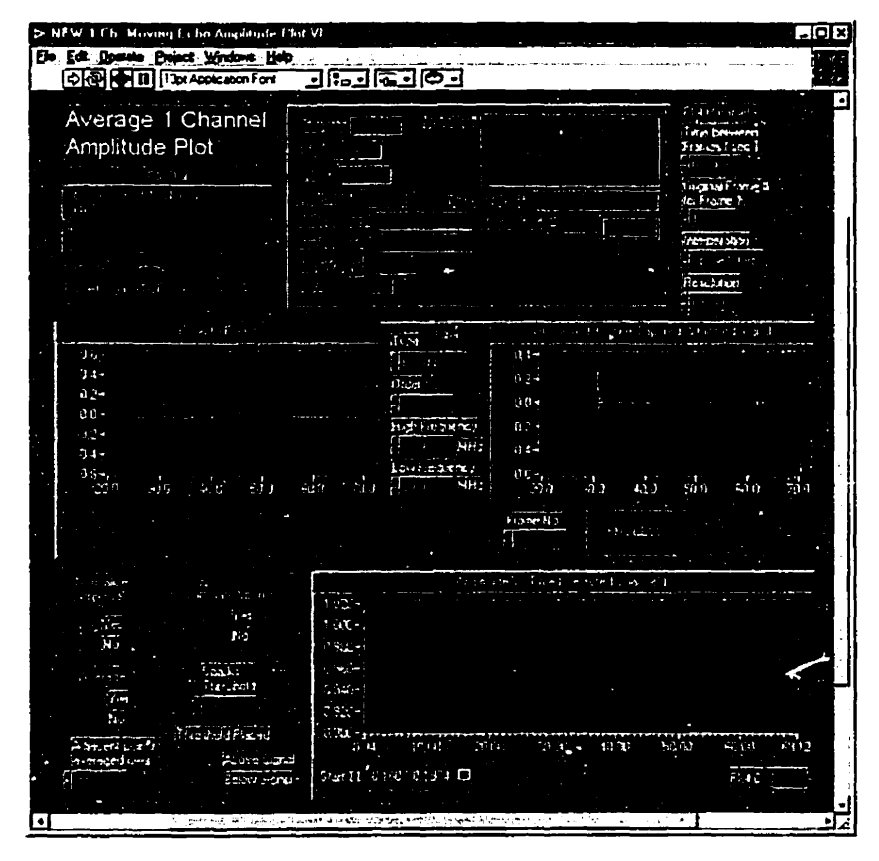


Fig. 1-4: VI used to determine the amplitude of a chosen ultrasonic echo

#### 1.3 The injection molding process and its monitoring

The injection molding process contains four stages: plastication, filling, holding, and cooling. In the plastication stage, plastic pellets are melted in a reciprocating screw extruder. The polymer is mixed and forced toward the nozzle by the rotating screw. As the screw advances at a set time under the action of a hydraulic system, it pushes the polymer into the mold and fills it up during the injection stage. When the cavity is totally filled, the melt will be compressed by the high injection pressure, resulting in a pressure overshoot. In order to avoid pressure overshoot after the cavity is filled, the high injection pressure has to be switched over to a lower holding pressure [5]. The switch-over can be controlled by several techniques, using thresholds set according to time, screw position, cavity pressure, or clamping force [27]. In the holding stage, polymer continues to be forced into the mold by the holding pressure in order to compensate for the volumetric loss as the polymer in the cavity cools and shrinks. After the injection gate freezes, transmission of pressure is blocked and the process enters into the cooling stage, in which the molded part remains inside the cavity until it is solid enough to retain the desired dimensions after ejection [5]. Part ejection completes the injection molding cycle. Since the plastication stage occurs outside the cavity, this stage is not monitored. Figure 1-5 shows one complete cycle of injection molding when monitored from the cavity.

Kamal, et al. have demonstrated barrel temperature measurement by means of thermocouples installed at front and rear zones in the barrel [34] during the plastication stage. Mochuzuki, et al. and others, meanwhile, use ultrasonic techniques to measure the average polymer melt temperature in the barrel and the nozzle [35~37]. Ultrasonic wave velocity can be determined, provided that both temperature and pressure of the material are known [38~41]. By measuring the travel time of ultrasound inside the polymer and the cavity pressure, an average melt temperature inside the barrel and nozzle can be determined.

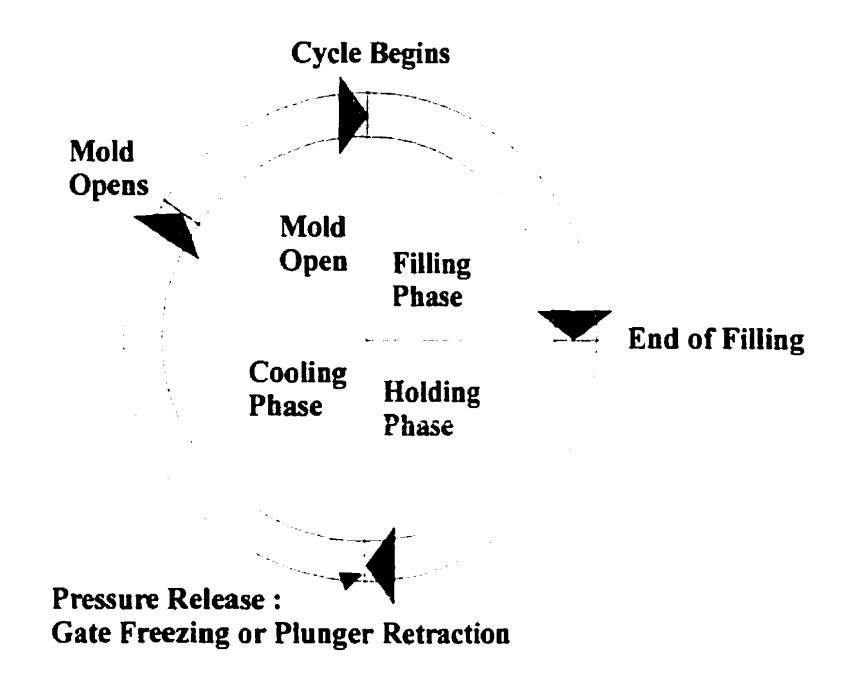


Fig. 1-5: One cycle of injection molding monitored from cavity

In the injection stage, injection speed, melt velocity, melt temperature, hydraulic pressure, *etc.*, are crucial parameters that influence product properties such as crystallinity, viscosity, and surface quality [27]. Injection speed is very easy to measure. Salamon and Donald analyzed flow advancement qualitatively by varying the shot sizes [42]. Pressure sensors not only give acceptable readings for hydraulic and cavity pressures, but also serve to monitor flow advancement quantitatively [13,19]. Cao also demonstrated the capability of ultrasound in on-line monitoring of the flow front advancement [33]. Even though flow front speed was determined, it was only accurate if the flow path was known since the speed was determined by dividing the distance between two sensors by the difference in arrival time.

In the holding stage, switch-over time and cavity pressure have impacts on the completeness of the part, weight, and flash formation. Pressure sensors are used to monitor cavity pressure. Pressure overshoot can also be detected using pressure sensors [27]. Nishiwaki, *et al.* demonstrated the capability of ultrasound in measuring cavity pressure [39]. In their approach, a thin (80µm) metal foil was placed on the surface of

cavity walls. By calibrating the amplitude of the echo reflected from the contacting surface between the thin metal foil and the cavity wall under different pressure, cavity pressure can be measured by ultrasound. In the holding stage, as the polymer cools down it will start to solidify. The solidification will take place first at the contacting surfaces with the mold, since the mold is kept at a lower temperature. With semi-crystalline material such as HDPE, material properties such as density and ultrasonic wave velocity undergo a sharp change at the temperature of crystallization. By identifying such distinct characteristics, Nishiwaki, *et al.* have observed the development of two solid/liquid interfaces inside the polymer, using ultrasonic techniques [43].

Meanwhile, in order to improve cooling (heat removal) and cycle time, cooling line design is very important. To improve the design of cooling lines, mold temperature and its distribution need to be better understood [44]. Furthermore, the cooling efficiency of the molded part and its quality are related to the melt temperature (profile across molded part between cavity walls). By inserting thermocouples into the polymer at different depths, the temperature profile can be measured [45~47]. However, not only is the result hampered by viscous heating effects as the polymer shears against the sensor [36], but the invasive measurement techniques also introduce problems such as heat conduction through thermocouples and melt flow alteration [48]. Le Bot, et al. demonstrated temperature profile measurement using heat flux sensors [49].

Infrared (IR) temperature sensors provide a fast response (10ms) and non-invasive measurement option, and have been used in several studies [50~52]. Not only is the calibration of IR temperature sensors difficult [49], but also error is introduced by detecting additional IR signatures at the metal walls of the equipment [5]. In the optical method of Kalman, et al. and Thomas, fluorescent dyes were doped into the polymer resin and the strong temperature-dependent emission spectrum of the fluorescent dyes was utilized to measure temperature and even temperature profiles in the polymer between cavity walls [5,48]. In addition, Bur, et al. demonstrated the capability of determining mold filling, the start of soli\_ification, crystallinity, part detachment, and

part shrinkage using optical techniques [53,54]. However, the polymer needs to be transparent; thus this approach is not applicable to opaque polymers. Even the mold wall must be modified to accommodate a transparent sapphire window for the transmission of light into the transparent polymer. Moreover, adding fluorescent dyes (foreign material) at even a small concentration into the polymer melt is not considered an attractive solution for industrial applications.

The cooling stage, as generally defined, starts after the injection gate freezes. However, the cooling of the polymer starts once the material enters into the mold cavity. As the part continues to cool down, the part will detach from the mold cavity walls. Nishiwaki, *et al.* have reported that the heat flow from polymer to steel molds underwent a discontinuity when detachment occurred [55]. This means that heat transfer became less efficient after part detachment. This temperature drop is caused by thermal contact resistance [56,57]. Therefore, the time of part detachment, if determined quantitatively, could be used as an improved strategy to reduce energy consumption. Cao utilized ultrasound to monitor the gap development during injection molding [58,59]. However, the time when detachment occurred was not clearly identified. Nishiwaki, *et al.* demonstrated the principle of identifying both detachment from moving (referred to in this thesis as external) and stationary (referred to in this thesis as internal) molds using ultrasonic techniques [43].

### 1.4 Gas-assisted injection molding, its advantages and monitoring

Though injection molding is very popular in the plastic processing industry, several difficulties remain. For example, sink marks will occur when injection molding thick-walled parts. This is because the volume contraction cannot be completely compensated for [6]. As a result, numerous attempts have been made to produce parts which cannot be produced by conventional injection molding. Gas-assisted injection molding (GAIM) is one of these attempts. In GAIM, the mold is only partially filled by

polymer melt. Then compressed gas is injected into the cavity directly or through either nozzle, sprue, or runner. The compressed gas will penetrate through the path of the least resistance, usually toward the melt front through the thickest section of the molded part. As polymer is displaced and forced ahead by the advancing gas, the mold is filled. In GAIM, not only is gas used to assist the filling of the cavity, but also in the packing phase in which the volumetric loss due to cooling is not compensated for by more polymer forced into the cavity, but rather by the expanding gas. This can be observed as gas continues to penetrate inside the molded part after the cavity is filled [6]. The complete cycle of GAIM is illustrated in Figure 1-6.

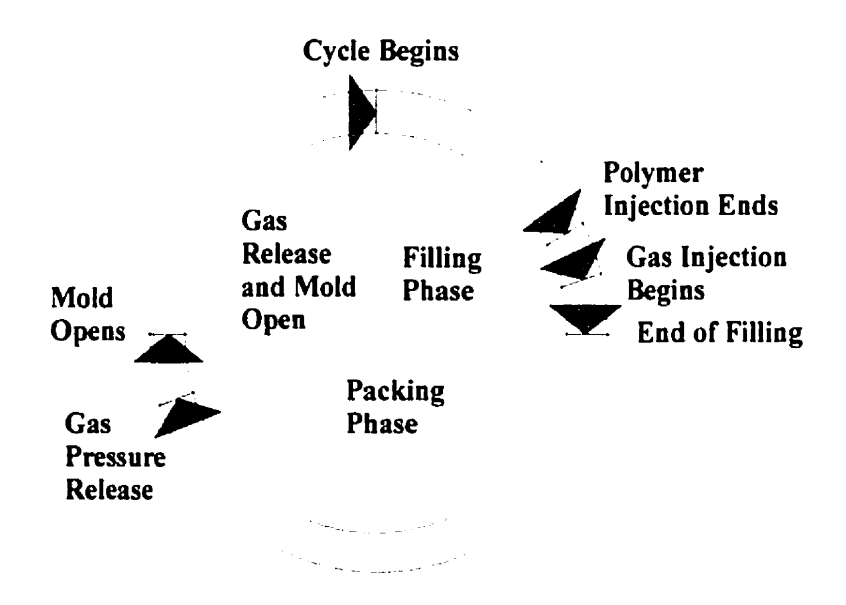


Fig. 1-6: One cycle of gas-assisted injection molding, modified from Fig. 2.3 of [6]

GAIM is being used to provide value in applications demanding higher performance, improved quality, and lower costs. Some more specific advantages of GAIM are: sink marks can be eliminated, dimensional stability is improved, thick and thin sections can be incorporated with less residual stress, clamping force required is reduced, scrap rate is reduced, material used and weight of molded part are reduced, and rigidity of molded part increases [6].

Until now, no reports have been published regarding on-line monitoring of GAIM. Computer simulation using computer-aided engineering (CAE) software is currently used to predict gas penetration and development of the gas channel in the molded part during filling and packing. Some other parameters such as polymer skin thickness, temperature, pressure, stress, part weight, and volumetric shrinkage are also predicted [6]. On the other hand, gas penetration is checked off-line against other process variables such as gas pressure, melt temperature, delay time, and gas injection time. The effect of gas pressure on volumetric fill time is also established [6]. Crawford demonstrated the use of a non-destructive thermal imaging technique using an infrared camera to check the gas penetration and consistency in cooling of gas-assisted injection molded parts [60]. However, this technique is not for on-line process monitoring, but rather applied after the mold opens.

#### 1.5 Thesis content

#### 1.5.1 Objective

The objective of this thesis is to assess the feasibility of using an ultrasonic technique as an on-line monitoring device for conventional and gas-assisted injection molding processes. If successful, this could lead to a process control algorithm to ultimately improve product quality, cost, energy consumption, and production cycle time in these processes.

#### 1.5.2 Content

In chapter 2, advances in ultrasonic on-line monitoring of the injection molding process are discussed. A box is injection molded on a 150-ton Engel co-injection molding machine using high density polyethylene (HDPE). Cavity pressure and plunger position are recorded and utilized in assisting the understanding of the process and verifying the

results of ultrasonic monitoring. From the reflection coefficient plot alone, detection of local polymer melt arrival is demonstrated. Moreover, on-line detection of the end of filling (or completeness of the molded part) and the pressure overshoot due to late switch-over are presented. Temperature and pressure of the molded part can also be determined under certain conditions, by using the tripartite relationship among pressure, ultrasonic wave velocity, and temperature of the molded part. A potential method for determining the local melt front speed using one ultrasonic transducer is proposed. The solidification of the molded part is monitored on-line. The development of solidified and liquid layers are determined. Temperature information inferred from the solidification information is discussed. From the reflection coefficient plot, detachments of the molded part from both external and internal molds are identified. Impacts of the part detachment and the plunger retraction on the reflection coefficient are also discussed. In summary, on-line monitoring of the injection molding process using reflection coefficients from pulse/echo method is presented, and finally ultrasonic sensors are compared with pressure sensor in monitoring the injection molding process.

In chapter 3, gas-assisted injection molding and co-injection molding are monitored with ultrasonic techniques. Gas-assisted injection molding is monitored online using a 400-ton Husky injection molding machine and a Cinpres 2-cylinder gas injection unit. A discussion of cavity pressure, and principles of ultrasonic monitoring, are presented. The capability to monitor on-line the arrival and penetration of gas using ultrasound is demonstrated. Moreover, melt arrival, the start and the end of gas injection, the end of gas-assisted filling, and the effect of variations in gas pressure and gas blow-through on ultrasonic signals are all discussed.

Off-line monitoring of co-injected parts is also presented. Co-injected plates with different amounts of pure acrylonitrile-butadiene-styrene copolymer (ABS) and ABS mixed with 2% carbon (as the core material) are immersed and examined in water. The objective of the measurement is to study the feasibility of ultrasonic techniques in monitoring the interfaces between the two different materials during co-injection process.

In chapter 4, temperature measurement using ultrasonic techniques is presented. Common ultrasonic techniques are first discussed. Then two types of ultrasonic temperature probes are fabricated. The probes consist of a buffer rod used as a wave guide, cooling lines to reduce the temperature on the transducer side of the buffer rod, and a conventional ultrasonic transducer. Principles of determining temperature by creating two discontinuities on the buffer rod are demonstrated. The ultrasonic probes are then calibrated using a high precision (0.01°C) oil bath and a platinum resistance temperature detector (PRTD). The calibration is carried out in both steady and transient states; the transient state here means inserting the ultrasonic probe cooled to room temperature into the oil bath at preset temperatures. One calibrated ultrasonic probe and Dynisco temperature probes are then installed onto the die ring of a co-extrusion blow molding machine, to monitor the temperature during the extrusion process. A real-time Kalman filter is applied in processing the ultrasonic signals to obtain the temperature. The readings from both ultrasonic and Dynisco temperature probes are presented. Finally the ultrasonic and Dynisco temperature probes are compared as to their performance and capabilities.

In chapter 5, results from previous chapters are summarized, original contributions from this study are stated, and future work is proposed.

#### Chapter 2:

## **Advances in On-line Ultrasonic Monitoring of Injection Molding Process**

#### 2.1 Introduction

Polymer injection molding has been widely used due to its mass production capabilities. In order to further improve product quality and reduce the cost, we investigate on-line ultrasonic monitoring of this process. Parameters monitored include filling, flow front speed, temperature, pressure, variation in elastic properties, solidification, shrinkage, *etc*.

In this chapter, cavity pressure is studied and utilized to support the understanding of the whole process monitored on-line with ultrasonic techniques. Advancement in the sensing configuration to obtain information such as end of filling, pressure overshoot, the growth of solidified layers, and detachment of the molded part from the mold cavity walls are all discussed. A potential method of determining flow front speed using a single ultrasonic transducer is proposed. Finally, a comparison between ultrasonic and pressure transducers in process monitoring is presented.

#### 2.2 Experimental setup

#### 2.2.1 Setup and the sample

A 150-ton Engel co-injection molding machine used in the experiments is shown in Figure 2-1. Although this machine can co-inject two different materials, the second

barrel was not activated, and hence single material injection molding is mainly investigated here.

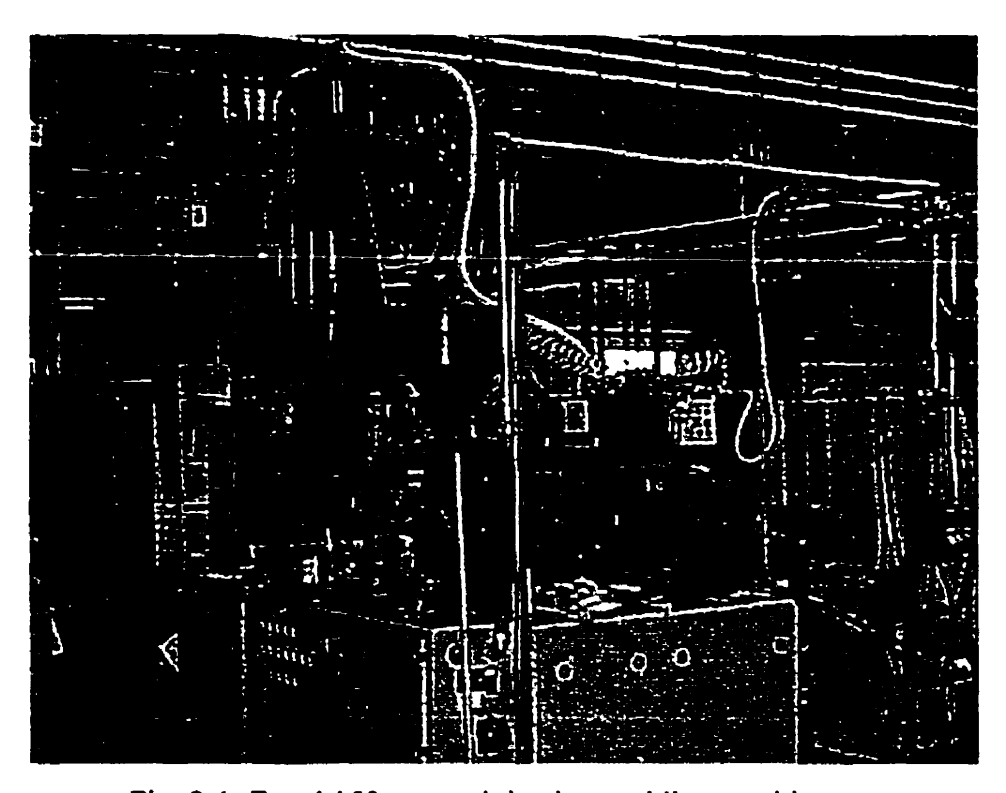


Fig. 2-1: Engel 150-ton co-injection molding machine

Boxes with dimensions specified in Figure 2-2 were molded. The inside surface of the molded part is inclined at a 5° angle so that the molded part can be ejected more easily. It is also noted that the thickness of the molded part is not uniform. At the thin (upper) part of the box, the inside and outside surfaces are parallel to each other, and therefore the thickness is uniform. At the thick (lower) part of the box, the inclined angle on the outside surface is less than the inclined angle on the inside surface, so that the thickness is larger near the bottom of the box. Figure 2-3 shows a section cut out from a molded box; the side view of the cutout part illustrates the non-uniformity in thickness at the lower part of the molded box. HDPE (high density polyethylene) is the material.

In all fields of monitoring, two Panametrics 6.35 mm (¼ inch) diameter, 5 MHz longitudinal ultrasonic transducers (UTs) were used. The two UTs were attached to the

outside of the external (stationary) mold wall, as shown in Figure 2-4. One UT was to monitor the molding process close to the top edge (120 mm from the gate) and the other UT for the process close to the bottom edge (70 mm from the gate). Pulse/echo method was used throughout the monitoring presented in this chapter.

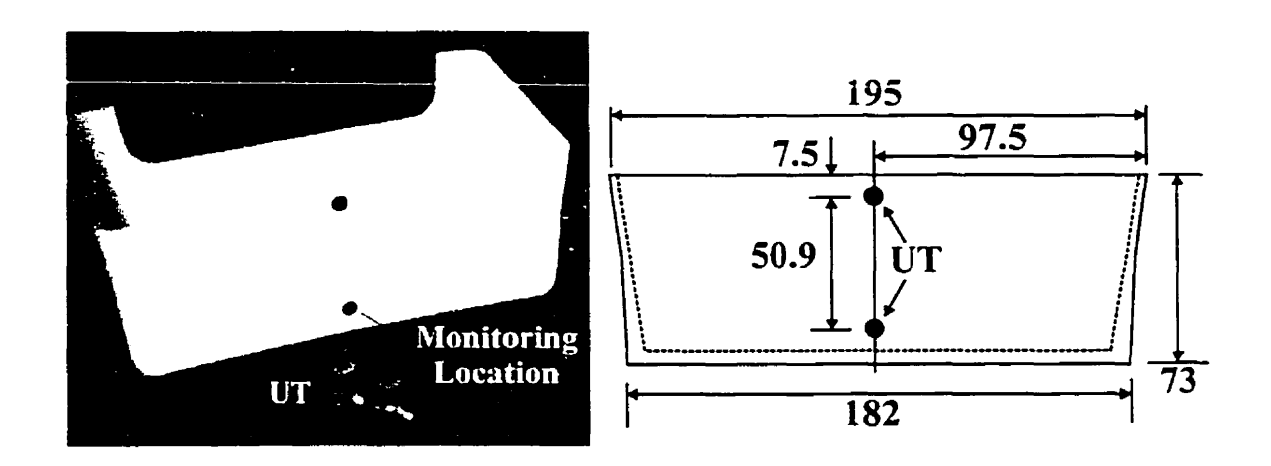


Fig. 2-2: Molded box and its dimensions (in mm)

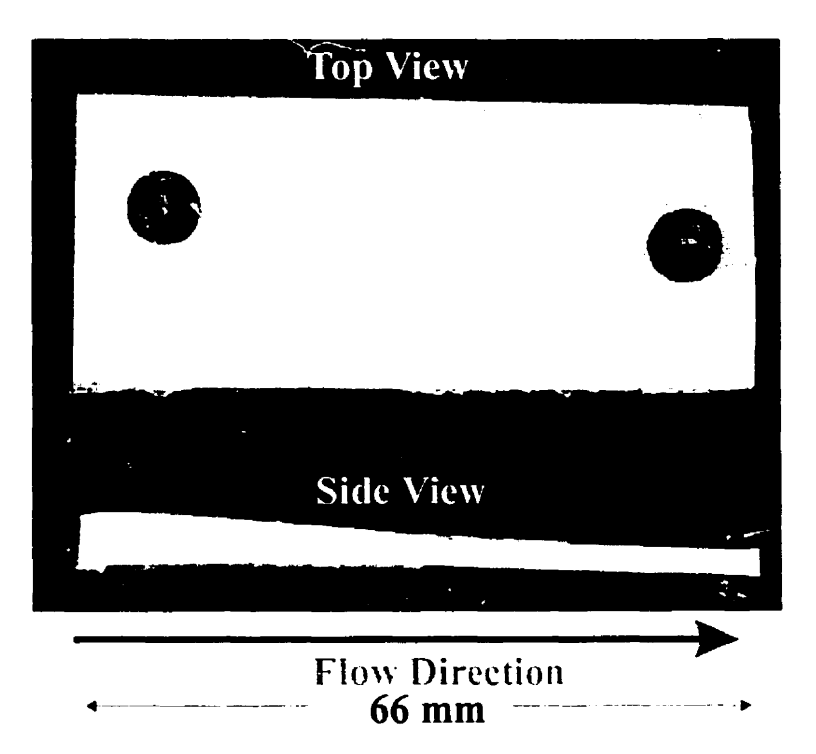


Fig. 2-3: Top and side views of cross-section

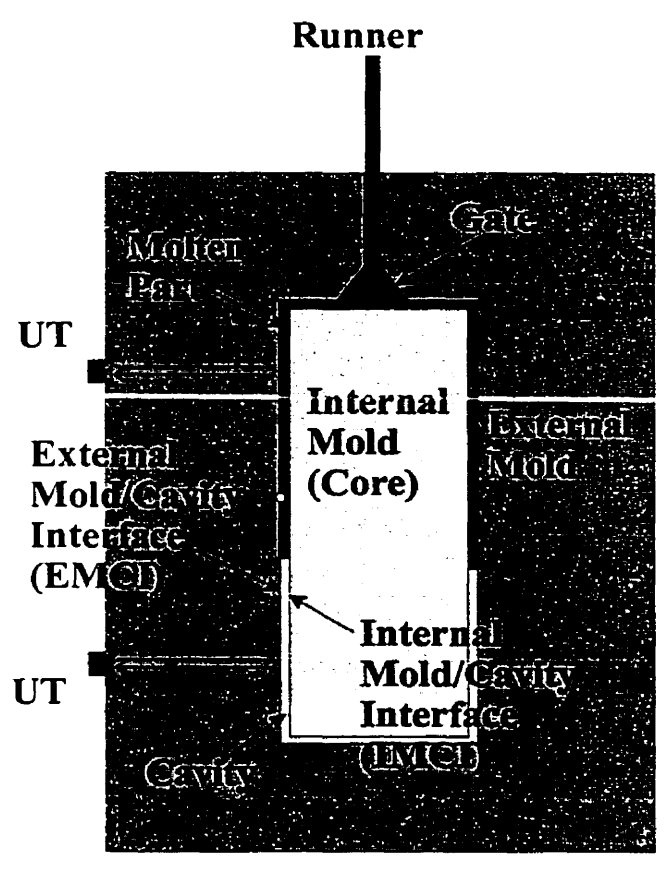


Fig. 2-4: Installation of UTs onto the outside surface of the external mold

#### 2.2.2 Operating conditions

The molding conditions used in this study are summarized in Table 2-1. All molding conditions were held constant except the injection speed.

Table 2-1: Operating conditions for injection molding

Mold Temperature	35.0°C
Melt Temperature	220°C
Injection Plunger Speed	20, 40, or 80 mm/sec
Process Control	Stroke dependent
Stroke Cut-off Point	20.0 mm
Holding Time	10.0 sec
Cooling Time	50.0 sec

#### 2.3 Cavity pressure

Several process parameters influence the final properties of a molded part [27], including pressure. When the term "injection pressure" is used, it often refers to the hydraulic pressure measured at the position behind the plunger. Most hydraulic injection molding machines in the industry use hydraulic pressure measurement for pressure control in both the filling and holding stages of injection molding. Early research indicated that hydraulic pressure is a reliable indicator of raw material variation such as viscosity [50,61,62]. This is why hydraulic pressure measurement is so commonly used for closed-loop velocity control for injection molding machines.

However, hydraulic pressure rarely gives any information about the cavity pressure (pressure inside the mold cavity) in either filling or holding stage [27]. In contrast to raw material variation, cavity pressure affects directly the material property and characteristics of molded parts. Material properties such as viscosity, crystallinity, and molecular orientation, and part characteristics such as surface finish, weight, dimensions, flash formation, and sink marks, have a more direct relationship with cavity pressure than with hydraulic pressure [27]. Therefore, cavity pressure measurement is of greater interest in improving product quality than hydraulic pressure measurement.

A typical cavity pressure curve throughout an injection molding process can be found in a reference [27]. One cavity pressure curve is reproduced in Figure 2-5. This curve shows the cavity pressure monitored at different points inside the cavity. Positions A and B correspond to points closer to the gate (molten polymer arrives earlier) and farther from the gate (molten polymer arrives late), respectively.

Before molten polymer arrives locally, a pressure sensor measures zero gage pressure. After molten polymer arrives, pressure starts to build up proportionally to the distance between the monitoring point and the flow front. Therefore, a pressure sensor

can indicate local flow front arrival. t<sub>A</sub> and t<sub>B</sub> in Figure 2-5 indicate the flow front arrival times at monitoring points A and B, respectively. This pressure buildup process continues until the cavity is completely filled, *i.e.*, the end of filling.

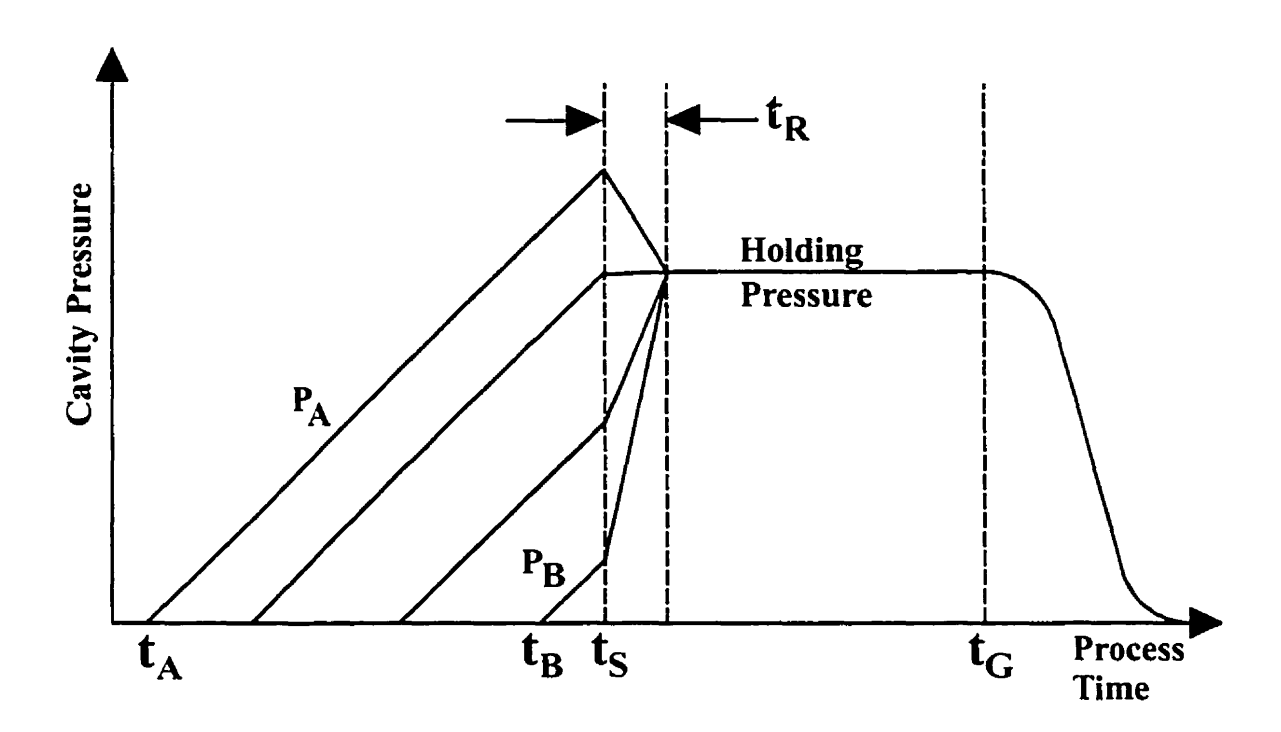


Fig. 2-5: Characteristic cavity pressure curve in injection molding

At the end of filling flow front advancement stops, and as the plunger continues to force material into the mold cavity, the molten polymer is compressed. This is the compression (transition) stage between filling and holding. If pressure is switched over  $(t_S)$  from injection to holding levels as soon as the end of filling occurs, cavity pressure at different monitoring points will follow different paths and converge to the cavity holding pressure within a certain response time  $(t_R)$ . If pressure loss along the flow path is small, cavity holding pressure will be nearly constant from place to place inside the cavity.

The holding stage is a constant pressure stage in which shrinkage of the part due to solidification is compensated for by forcing more polymer into the cavity. This constant pressure condition holds until either the gate freezes, or the monitoring point becomes isolated from the pressure source. As solidification goes on, at one point  $(t_G)$  the injection gate will freeze (polymer solidified at the gate). No more material can be forced into the cavity, and thus cavity pressure can no longer be maintained by the hydraulic plunger. As the part continues to cool down, pressure inside the cavity starts to drop. Gate freezing has a global impact on all positions inside the cavity, namely, the pressure will drop simultaneously at all monitoring points.

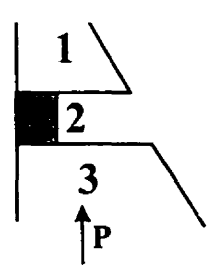


Fig. 2-6: Pressure reduction at section 1 due to isolation from pressure source as section 2 is solidified

Another reason for the failure of the constant pressure condition is local isolation of the monitoring point from pressure waves. Figure 2-6 illustrates this point. When the thin section 2 is solidified, section 1 is isolated from the pressure source. Even though section 3 is still under constant holding pressure, sections 1 and 2 cannot be maintained at constant pressure. Pressure starts to decrease as the part continues to cool down.

### 2.4 Filling monitoring

Due to the increasing use of multiple cavities in injection molding machines to enhance productivity, knowing the completion of the filling in each cavity is vital. In the filling stage, molten polymer is pushed into the mold by the plunger. When the cavity is empty, resistance inside the cavity is little. When the cavity is filled, flow resistance is large. From this point on, the density of the polymer and the cavity pressure start to increase dramatically. High cavity pressure will produce some problems such as flash or non-uniformity in part weight [27]. It is therefore desirable at a certain point to reduce the

hydraulic pressure that is driving the plunger, so that the cavity pressure will not overshoot. This is the switch-over point between the filling and holding stages. Moreover, if the cavity is not completely filled, an incomplete part will be produced. If such a completion of filling can be monitored in high precision timing, an efficient switching from injection to packing pressure may be achieved so as to save energy and to ensure the quality of the parts produced.

It can be seen from Figure 2-4 that when the injection molding process starts, the mold cavity does not contain any molten polymer. The ultrasonic echo received is reflected from the external mold/cavity interface. The energy of the reflected ultrasonic signal depends on the reflection coefficient ( $\Gamma$ ) at the interface. The reflection coefficient is in turn a function of the acoustic impedance of the two media on the two sides of the interface [63]. If the acoustic impedances of the two media are very close, this small impedance mismatch leads to a small reflection coefficient; less energy will be reflected back from an interface with a small impedance mismatch than from one with a large impedance mismatch.

The acoustic impedance of air is very small  $(4.45 \times 10^2 \text{ kg/m}^2/\text{s})$  at room temperature) compared to steel  $(4.66 \times 10^7)$ ; therefore nearly all (>99.99%) of the energy hitting the air/steel mold interface will be reflected, and thus a large amplitude for the received echo is observed. The impedance mismatch for lucite  $(3.16 \times 10^6)$  and steel is less; 24% of the energy will transmit into the lucite, and 76% will be reflected from the lucite/steel mold interface.

Therefore when molten polymer arrives at the monitoring point, interface conditions change. The impedance mismatch for the interface becomes smaller, more energy is transmitted into the polymer, and less energy is reflected. Thus the received echo has a smaller amplitude than before the molten polymer arrives. From the plot of amplitude of the received echo *versus* process time, a drop will be observed which indicates the local flow front arrival (FA). If a monitoring point is placed at the end of the

molten polymer flow path, flow front arrival at this point indicates the end of filling. Taking into account the response time for the system feedback and hydraulic actuator, a point a little bit upstream should be chosen, so that sufficient time is left for mechanical switch-over to avoid overshoot.

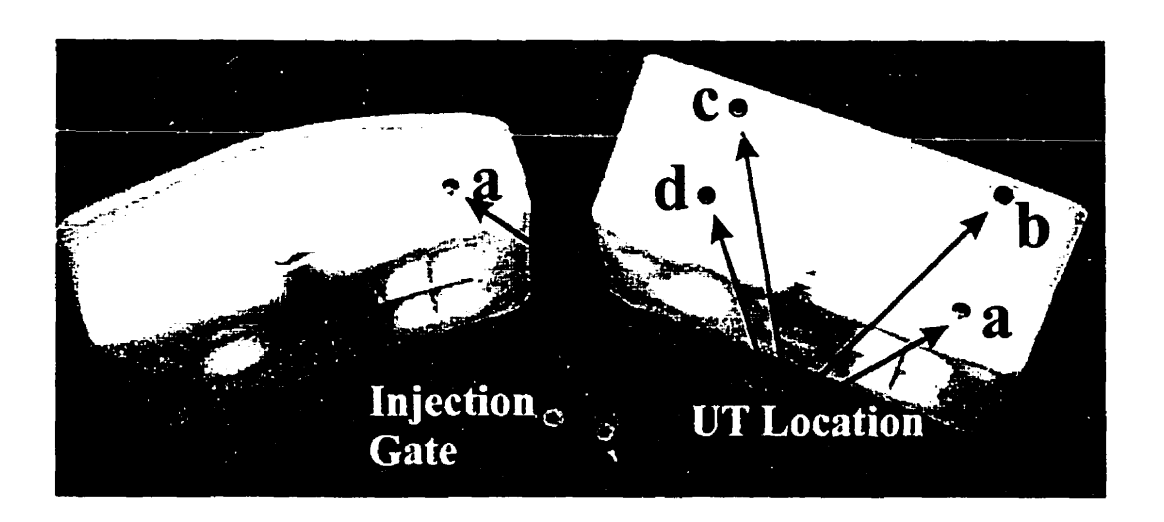


Fig. 2-7: Molded boxes from incomplete and complete cavity filling

Figure 2-7 shows the molded HDPE parts and locations ("a", "b", "c", and "d") of four UTs. The part on the left was the result of incomplete cavity filling, while on the right the cavity was completely filled. Figure 2-8 shows the reflection coefficient,  $\Gamma$ , of the mold/cavity interface echo *versus* injection molding time from two of the UTs (locations "a" and "b") for twelve runs. Note that the 4<sup>th</sup> to the 9<sup>th</sup> runs produced incomplete parts, as shown in Figure 2-7. During the molding of six complete parts, the reduction of  $\Gamma$  was obvious at both locations "a" and "b". However, for incomplete parts not only was there no reduction in  $\Gamma$  at location "b", but also only a small reduction at position "a".

The reason for this discrepancy is that though the molten polymer did arrive at location "a", it only contacted partially with the mold. This was confirmed by the fact that the surface of the incompletely molded part was very rough as seen in Figure 2-7. Such a partial contact led to a poor ultrasonic coupling, and thus induced only a minor reduction

of  $\Gamma$  at location "a". As seen in Figure 2-8, completion of filling can be monitored with 100% success rate.

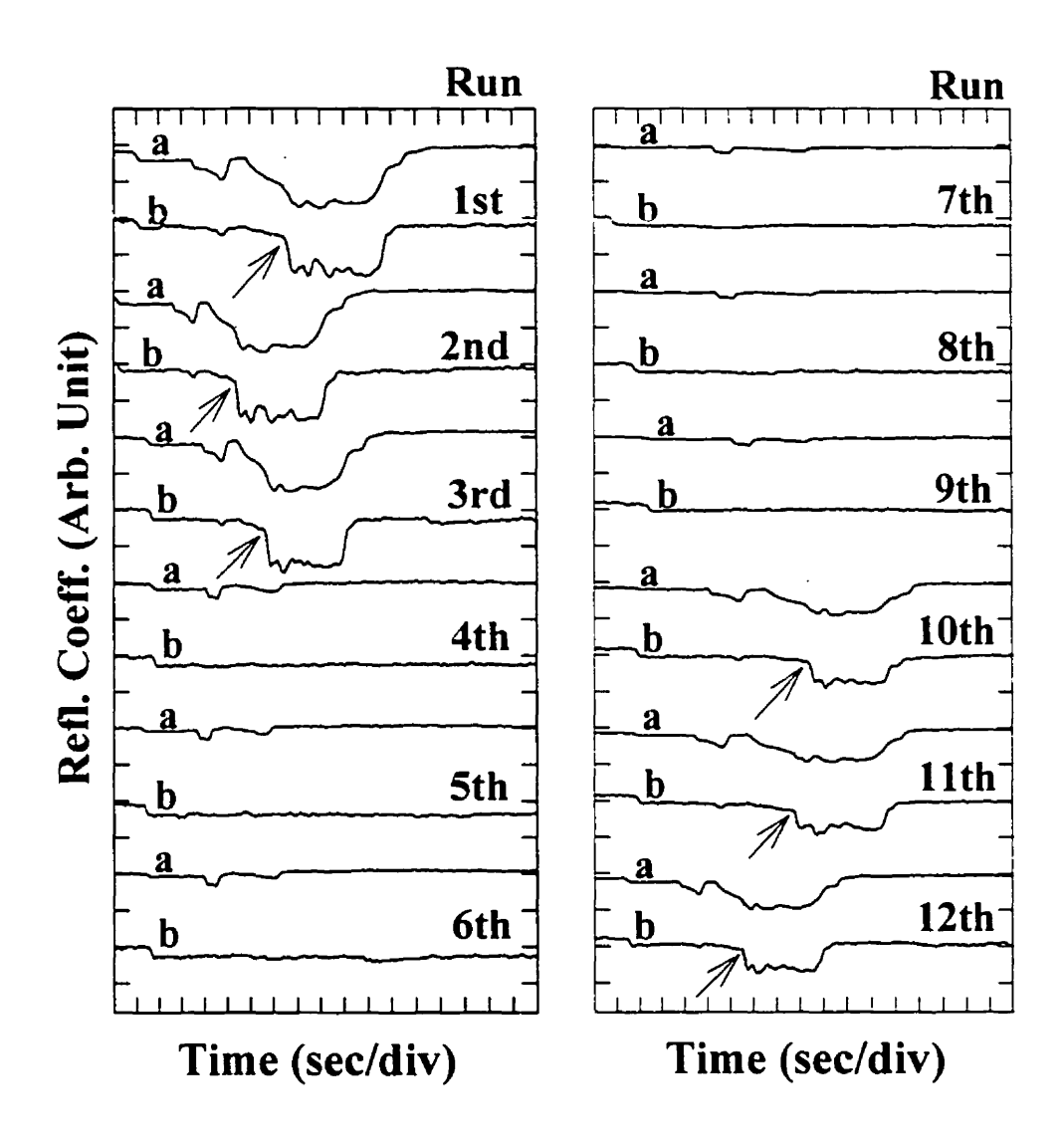


Fig. 2-8: Filling Monitoring for injection molding

In addition, in the 1<sup>st</sup> - 3<sup>rd</sup> runs the amplitude of the second round trip echo traveling in the external mold wall was used for the filling monitoring and in the 10<sup>th</sup> - 12<sup>th</sup> runs that of the first round trip echo was monitored. A higher sensitivity was achieved for the first three runs than the last as demonstrated in previous research [33]. In principle, a higher-order round trip echo has higher sensitivity. However, the spurious

noise coming from the reflection from the grain boundaries, cooling lines, inserts, etc., may significantly reduce the signal-to-noise ratio (SNR) of the desired echoes. An echo selection procedure must therefore be carried out at each sensing location in order to have the best sensitivity.

As demonstrated in section 2.3, cavity pressure undergoes a transition once the end of filling is reached. In the compression stage, increased in pressure will result in increases in both density and stress of the molten polymer, and thus push the molten polymer more firmly against the mold cavity wall. This means that interface condition will improve at the end of filling. Figure 2-9 shows a more detailed plot of reflection coefficient *versus* process time at injection phase monitored at the thin part of the box. As indicated, the transition point where the amplitude starts to exhibit a sharp drop might indicate the end of filling. This phenomenon has been observed consistently. For the six runs producing completely filled parts in Figure 2-8, arrows are placed to indicate this distinct point observed simultaneously, regardless of monitoring locations.

In Figure 2-9, ultrasonic signals were recorded from two locations (Monitoring points "c" and "d" in Figure 2-7). Monitoring point "d" is closer to the gate, and monitoring point "c" is far away from the gate. Also presented are the recorded plunger position and cavity pressure. As marked, both ultrasonic and pressure sensors can monitor local flow front arrival. Furthermore, the distinct feature that  $\Gamma$ s from both monitoring points undergo simultaneous drops is revealed. The discontinuity for density and stress inside the molten polymer, results in the increase in cavity pressure. The end of filling marked by this cavity pressure increase confirms that the reduction of  $\Gamma$  indicates the end of filling. Therefore, both ultrasonic and pressure sensors are capable of monitoring the end of filling (EF). Moreover, possibilities of identifying completion of cavity filling regardless of monitoring locations suggests that the end of filling can be determined using a single UT which is placed not necessarily close to the end of the molten polymer flow path.

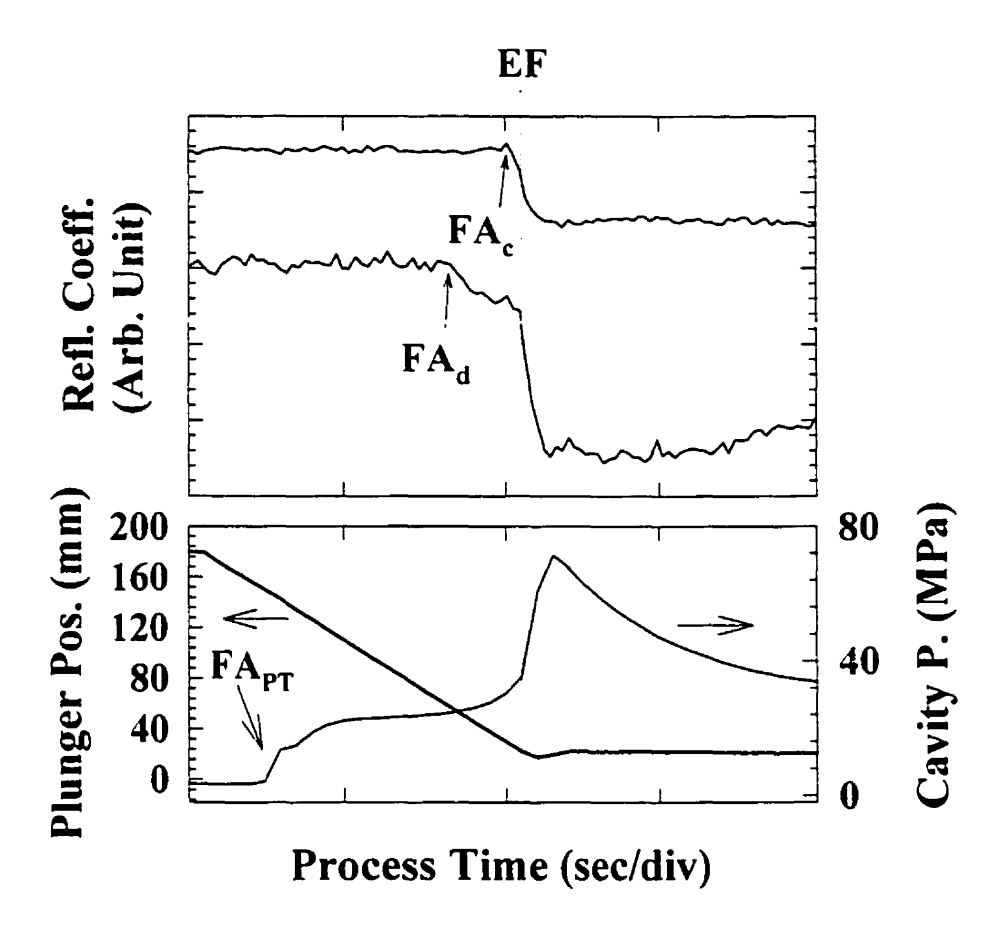


Fig. 2-9: Monitoring the end of filling (EF) using ultrasonic technique. Curves in upper plot are reflection coefficient ( $\Gamma$ ) versus process time plots for echoes ( $L^1$ ) reflected from external mold cavity walls at locations "c" and "d". The thick line in the lower plot is plunger position, while the thin line is the cavity pressure. FA stands for flow front arrival of molten polymer, subscripts "c", "d", and "pt" indicate flow front arrival detected at locations "c", "d" and by the pressure transducer

### 2.5 Effect of Overshoot

If the switching-over from injection to holding phase takes place too late, overshoot occurs. Figure 2-10 shows an injection run with 40 mm/s plunger speed. The

first plot contains two  $\Gamma$ s. The top one was obtained from the echo (L<sup>1</sup>) reflected from the external mold cavity interface (EMCI, as shown in Figure 2-4), while the bottom one was obtained from the echo (L<sub>2</sub>) reflected from the internal mold cavity interface (IMCI, as shown in Figure 2-4), which traveled twice in the molten polymer through the thickness direction. Notice that once molten polymer arrives locally, ultrasound can transmit into the molten polymer and reflect back from IMCI. Therefore, local flow front arrival can also be determined by identifying the appearance of L<sub>2</sub>, as indicated in Figure 2-10. The second plot is the time delay measured between L<sup>1</sup> and L<sub>2</sub>. The third plot is the cavity pressure (thin line) and plunger position (thick line). Recording of ultrasonic signals was not synchronized with the recording of cavity pressure and plunger position. Therefore, the  $\Gamma$  plots are aligned to our best knowledge with the cavity pressure and plunger position plots.

It can be seen from the cavity pressure plot that at switching-over, during the mechanical response time, the plunger is pulled back in preparation for the holding phase. As a result, the cavity pressure drops. Then the cavity pressure picks up again as the plunger advances to keep cavity pressure according to the setting for the holding phase. In the time delay plot, it can be seen that as cavity pressure rise is relatively smooth, the decrease in time delay is also relatively smooth.

Figure 2-11 represents another run at 80 mm/s plunger speed. From the cavity pressure curve, an overshoot occurred during this run. The increase in cavity pressure also implies improvement in coupling between molten polymer and cavity walls. Therefore an overshoot can also be observed from  $\Gamma$  for  $L_2$ , as compared to a smoother  $\Gamma$  for  $L_2$  in the previous case (Figure 2-10). Notice that in the case of overshoot, the time delay between  $L^1$  and  $L_2$  exhibits a fast drop in the beginning, and then the reduction rate turns slow. By comparison with the smoother change in time delay in the case without overshoot, it can be concluded that the fast drop ( $\Delta \tau$ ) in time delay in Figure 2-11 is due to the pressure overshoot ( $\Delta P$ ). However, it is not clear at this point, why after the overshoot, as the cavity pressure is reducing to constant holding pressure, the time delay does not increase

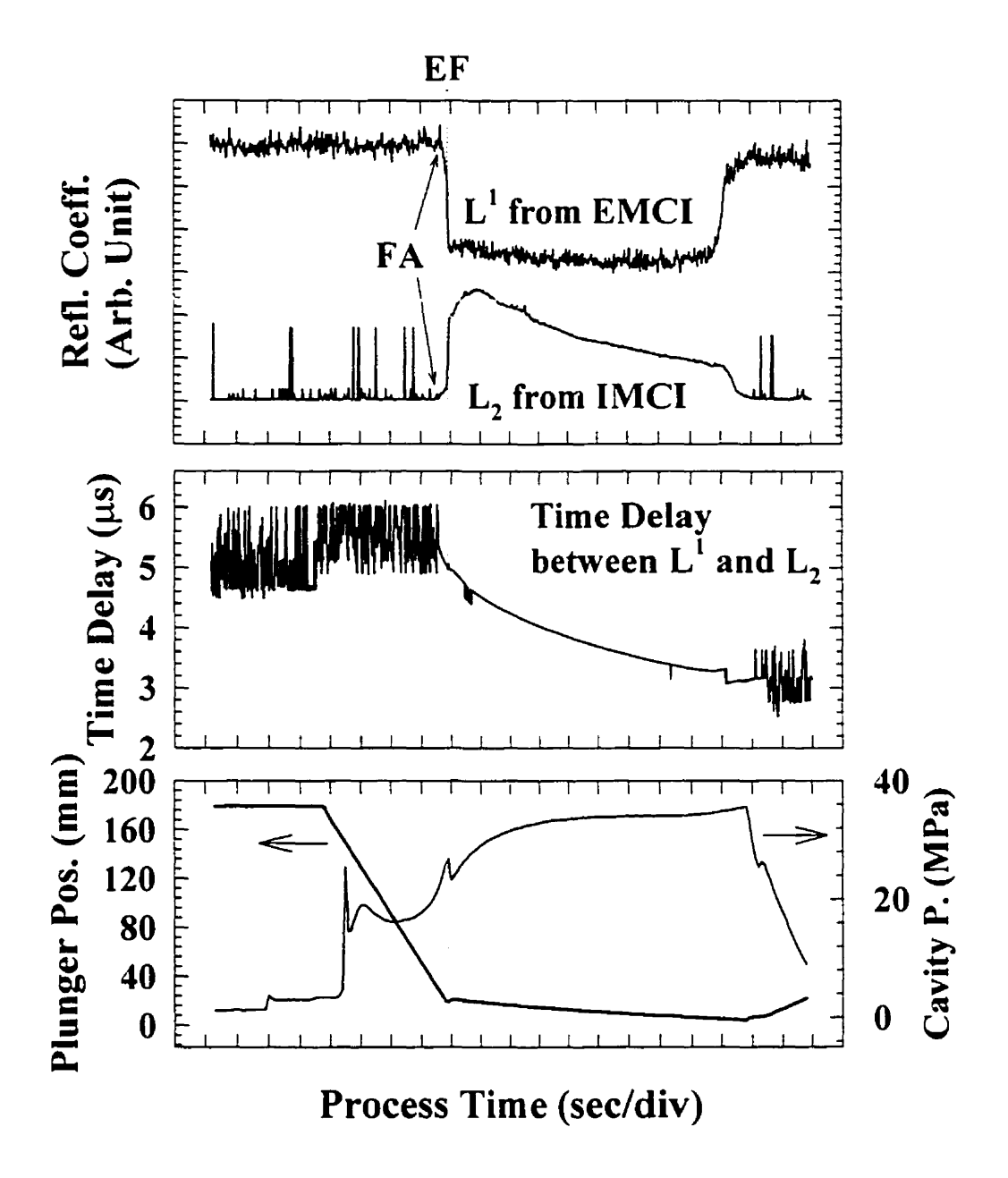


Fig. 2-10: An injection molding run without overshoot.  $\Gamma$  for echoes from external ( $L^1$ ) and internal ( $L_2$ ) mold cavity interfaces, time delay between  $L^1$  and  $L_2$ , plunger position (thick line in bottom plot), and cavity pressure (thin line in bottom plot) *versus* process time plots. EF and FA stand for the end of filling and flow front arrival of molten polymer

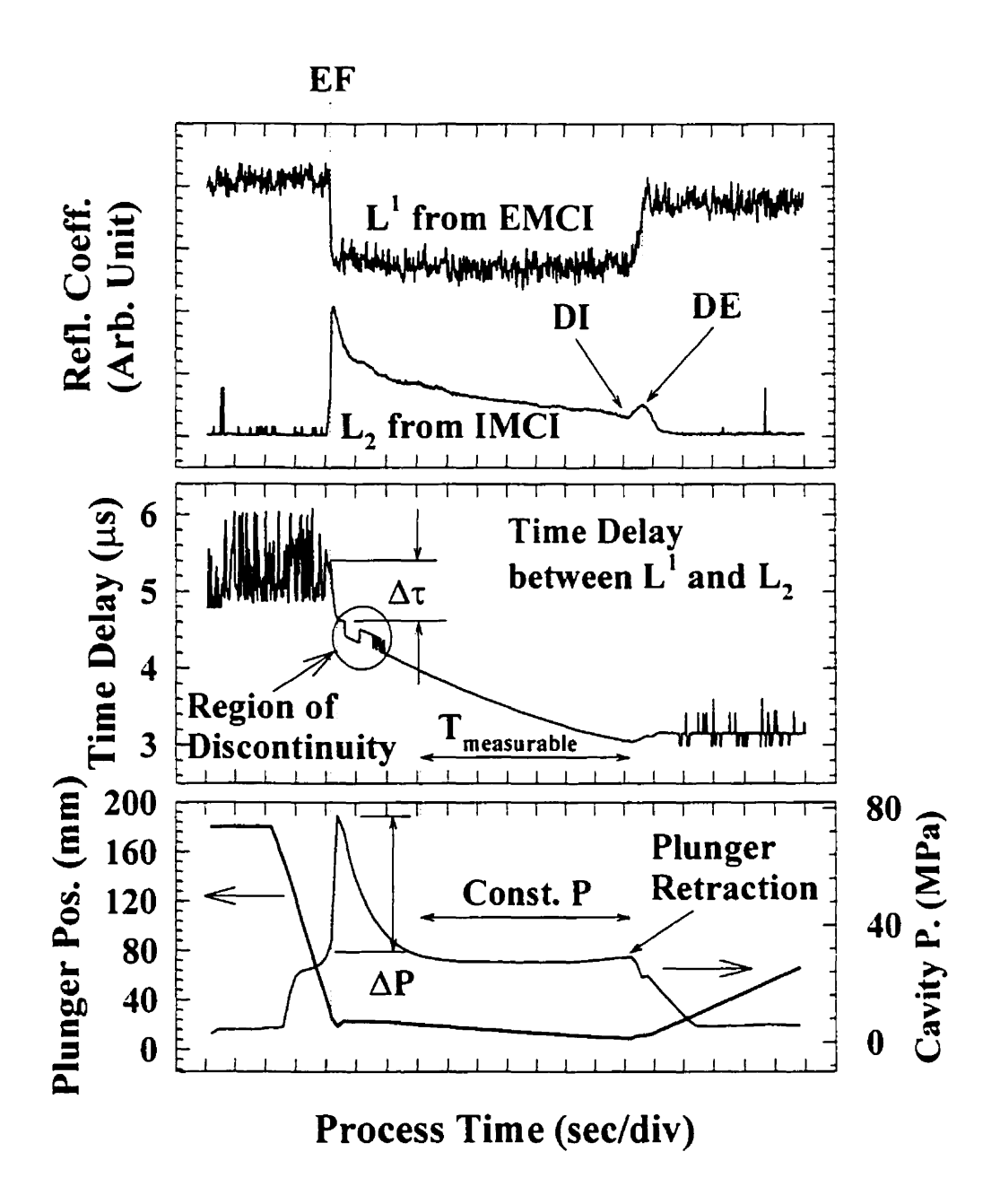


Fig. 2-11: An injection molding run with overshoot.  $\Gamma$  for echoes from external (L¹) and internal (L₂) mold cavity interfaces, time delay between L¹ and L₂, plunger position (thick line in bottom plot), and cavity pressure (thin line in bottom plot) *versus* process time plots. EF, DI, DE,  $\Delta \tau$ , and  $\Delta P$  stand for the end of filling, detachment from internal and external molds, change in time delay, and change in pressure

with the pressure drop. As circled in Figure 2-11, there is a region of discontinuity in the time delay plot. The discontinuity is resulted from the overlapping between L<sub>2</sub> and other noise echoes as L<sub>2</sub> is moving (time delay of L<sub>2</sub> changes). As a result, error occurs in determining the peak of L<sub>2</sub> and in turn, the time delay between L<sup>1</sup> and L<sub>2</sub>. However, the time delay readings before and after the region of discontinuities are accurate. Moreover, the two stages of change in time delay in case of pressure overshoot are verified by other runs which are not presented in this chapter. Therefore the region of discontinuities does not represent any real discontinuity in time delay.

Ultrasonic wave velocity inside a material is dependent on both temperature and pressure. Figure 2-12 illustrates this tripartite relationship taken from one reference [43]. It can be seen that for HDPE (a semi-crystalline material), ultrasonic wave velocity changes dramatically at a temperature around 130°C. This transition represents the crystallization of HDPE. When HDPE is in either solid or liquid states, ultrasonic wave velocity increases with increasing pressure or decreasing temperature.

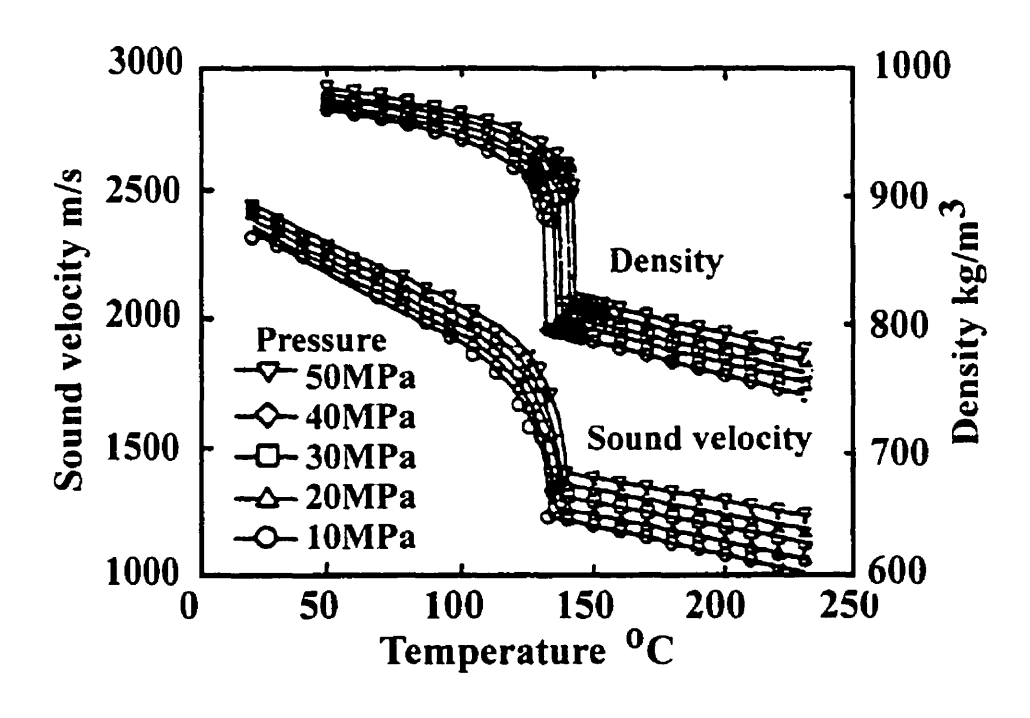


Fig. 2-12: Tripartite (P-V-T) relationship for HDPE from [43]

Since the large increase in pressure due to the overshoot occurs in a very short period of time (less than 0.5 sec), and temperature variation in this short period of time is not large, it can therefore be assumed that the fast drop in time delay results more dominantly from a pressure change than from a change in temperature (cooling). As a result, pressure change inside the polymer can be determined with the assumption that temperature is constant; ultrasonic wave velocity is then dependent only on pressure.

The measured thickness (h<sub>mea</sub>) of the thin part is 2.62 mm. However, with a vertical outside mold wall and a 5° inclined angle on both sides of the cavity walls at the thin part, the effective thickness (h<sub>eff</sub>) of the polymer should be compensated:

$$h_{eff} = h_{mea} / \cos(5^{\circ}) \tag{2.1}$$

The thickness after compensation is therefore 2.63 mm. The ultrasonic wave (V) velocity can be determined by:

$$V = (h_{eff} \times 2) / \tau$$
 (2.2)

where  $\tau$  is the time delay. Within the region of pressure overshoot, the smallest and the largest time delays are 4.58 and 5.17  $\mu$ s, respectively. The ultrasonic wave velocities at high (V<sub>h</sub>) and low pressure (V<sub>l</sub>) are therefore 1148.5 m/s and 1017.4 m/s, respectively.

In Figure 2-11 the injection temperature for HDPE was 220°C. With the assumption that the temperature was constant in the marked region, low pressure (P<sub>I</sub>, before compression) and high pressure (P<sub>h</sub>, after compression) are found, from the tripartite relationship plot with an assumed average temperature of 210°C, to be 3.36 MPa and 26.43 MPa, respectively.

After switching over, the pressure inside the molded part and cavity pressure were held constant during the holding phase. During this constant pressure period, the ultrasonic velocity depends only on temperature. Therefore during the holding phase, the average temperature of the molded part can be determined. The period in which the average temperature is determinable (T<sub>measurable</sub>) is indicated in Figure 2-11. Here the cavity pressure is used as a substitute for pressure inside the molded part. With known constant cavity pressure of 27.58MPa, and the average ultrasonic wave velocity determined by Eqn. 2.2, average temperature of the molded part is determined. Figure 2-13 shows the average ultrasonic wave velocity with pressure and temperature inside the molded part derived whenever they are measurable.

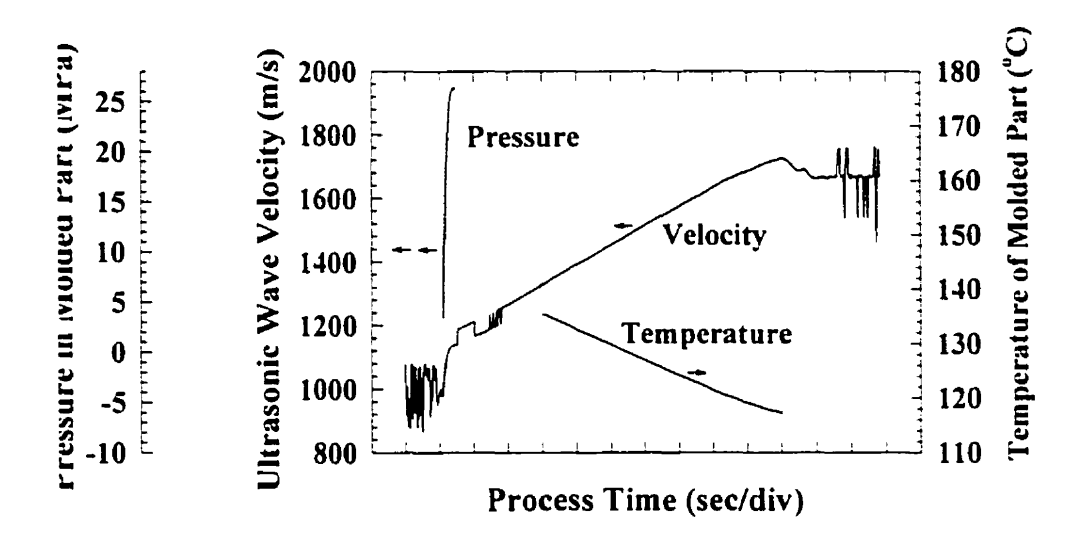


Fig. 2-13: Average ultrasonic wave velocity, pressure, and temperature of the molded part

### 2.6 Flow front speed monitoring

During the filling stage, molten polymer flows inside the cavity. At points inside the cavity where polymer flow fronts from two directions meet, (usually seen as a weld line on molded objects), different degrees of blending of polymers will occur and the strength of the polymer is critical. One important parameter might be of interest is the speed at which the two flow fronts approach each other. Therefore the monitoring of flow front speed is of interest.

Presently, the flow front position is inferred either from plunger position or cavity pressure/temperature sensors. Regardless of recent improvements in machine design, the final product quality is still determined by how efficiently the molten polymer flows into the cavity, which is in turn controlled by the machine setup and controller performance.

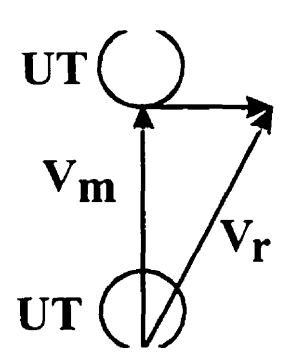


Fig. 2-14: Error in flow front speed measurement with two ultrasonic transducers (UTs).  $V_r$  is the real velocity, and  $V_m$  is the measured velocity

A typical way to determine the flow front speed using ultrasound is by dividing the distance between two monitoring points by the difference of flow front arrival times for those two points [33]. However, flow front speed derived this way is only an average; behind this average is a complex flow path due to the geometry of the molded part. In addition, if the flow direction is not going from monitoring point 1 to point 2, the flow front speed determined is just part of the real flow front speed. This is illustrated in Figure 2-14. As a result, the method using two UTs to determine the flow front speed is valid only when the actual flow path is known, and the velocity is relatively constant between the two monitoring points.

The possibility of determining the flow front speed using only a single UT is explored in this section. Advantages over the two UTs approach are obvious: derived flow front speed is local to the monitoring point, and not an average over a long flow path. Also for a circular UT, determined flow front speed is the same for polymer flows in any direction. In other words, if one UT is able to measure the flow front speed, the flow path needs not be known, and the UT can be placed at any point of interest.

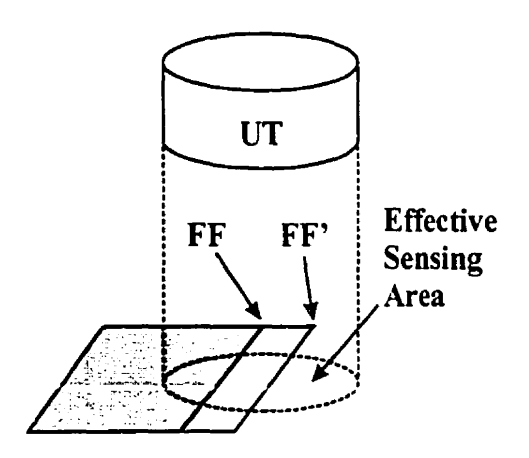


Fig. 2-15: Flow front speed measurement with one ultrasonic transducer (UT). FF and FF' stand for flow front positions at different times

Since for steel, the attenuation, scattering, and dispersion of ultrasonic waves are very small, and the wave is also well bounded when propagating inside the steel mold wall, an effective sensing area on the inside wall of the mold with the same diameter as the UT attached outside the mold can be assumed. When molten polymer flows through this effective sensing area, as stated before in section 2.4, energy will transmit into the molten polymer. As for the remaining part of the effective sensing area, energy is totally reflected from the air/steel interface. Therefore, energy transmission is proportional to the size of the effective sensing area covered. The rate of energy transmission into the molten polymer is thus proportional to the rate of the covering of the effective sensing area by molten polymer. And the rate of the area covered is a function of the flow front speed of the molten polymer. This provides a potential method to determine the flow front speed, as illustrated in Figure 2-15.

When ultrasonic waves propagate inside a medium, the near field (close to the UT) ultrasonic intensity and that in the far field (far from the UT) are very different [31]. Eqn. 2.3 can be used as a criterion to determine the near field length (N) when the diameter of the UT (D) is much larger than the wavelength ( $\lambda$ ):

$$N = \frac{D^2}{4\lambda} \left[ 1 - \left( \frac{\lambda}{D} \right)^2 \right]$$
 (2.3)

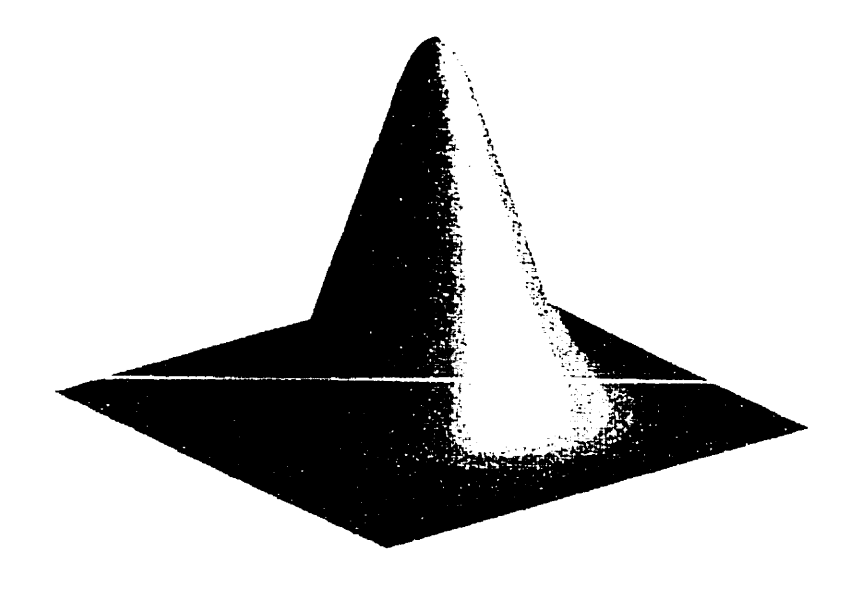
With a 6.35 mm (¼ inch), longitudinal, 5MHz UT, the near field length for ultrasonic waves in steel (wave velocity is 5940m/s) is 8.19 mm. Therefore with UTs attached on the outside wall of the external mold, the ultrasonic intensity at the mold cavity wall is in the far field.

For a plane circular piston UT, the far field ultrasonic intensity distribution is Gaussian. The circular Gaussian function is given by Eqn. 2.4:

$$f(x,y) = \frac{1}{2\pi\sigma^2} e^{-\left[(x-\mu_x)^2 - (y-\mu_y)^2\right]/2\sigma^2}$$
 (2.4)

where  $\mu_x$  and  $\mu_y$  are the means in x and y directions set at the center of the 6.35 mm (¼ inch) diameter UT, and  $\sigma$  is the standard deviation, set at 0.86 mm (0.034 inch) so that the intensity at the boundary of the 6.35 mm diameter monitoring area is close to zero.

Figure 2-16 shows the 3-D Gaussian distributed ultrasonic intensity field and the normalized energy (both transmitted and reflected) over the covered effective sensing area. The energy transmitted is the integration of the intensity above the covered area with the assumption that the flow front is a straight line, as illustrated in Figure 2-15, and the normalized reflected energy is just 1 minus the normalized transmitted energy. Since the amplitude of the received echo is proportional to the energy reflected back from the effective sensing area, a curve similar to the reflected energy curve in Figure 2-16 should exist on the amplitude plot and can be utilized to determine the flow front speed. Correlating the time axis for the section on the amplitude plot and the distance axis in Figure 2-16 will generate the flow front speed as a function of time.



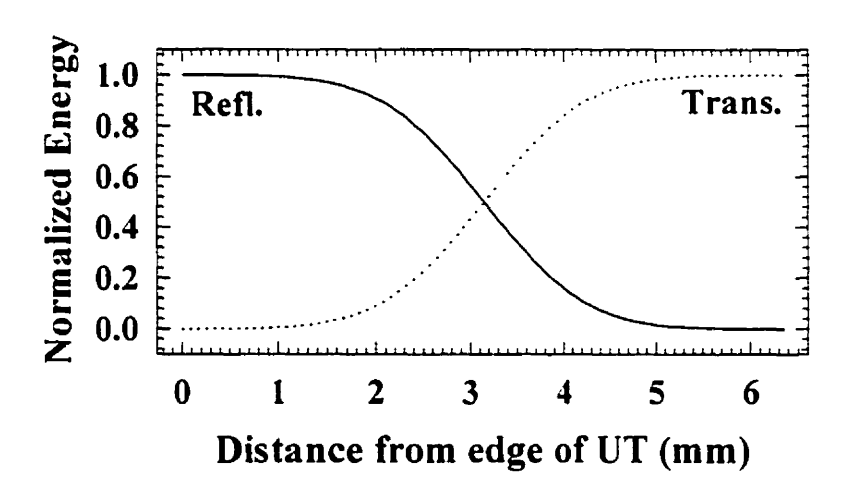


Fig. 2-16: Far field Gaussian distribution of ultrasonic intensity for circular UT and integration (energy transmission) across it. Energy reflection is obtained by subtracting normalized energy transmission from 1

Various plunger speeds (20, 40, and 80 mm/sec) were used in the experiments. Different plunger speeds resulted in different flow front speeds inside the mold cavity. Figure 2-17 aligns the amplitude plot from the two monitoring points during the injection stage for the three different plunger speeds. Note that the time axes for the two monitoring points with each plunger speed are synchronized. Several phenomena are

observed. With flow front arrival aligned for the thick monitoring point, flow front arrived earlier at the thin section in the 80 mm/s case than the 20 mm/s case. From the thin and thick parts monitoring points, the end of filling occurs earlier in the 80 mm/s case than the 20mm/s case. Both of these indicate that flow front speed in the 80 mm/s plunger speed run is faster than that in the 20 mm/s plunger speed run.

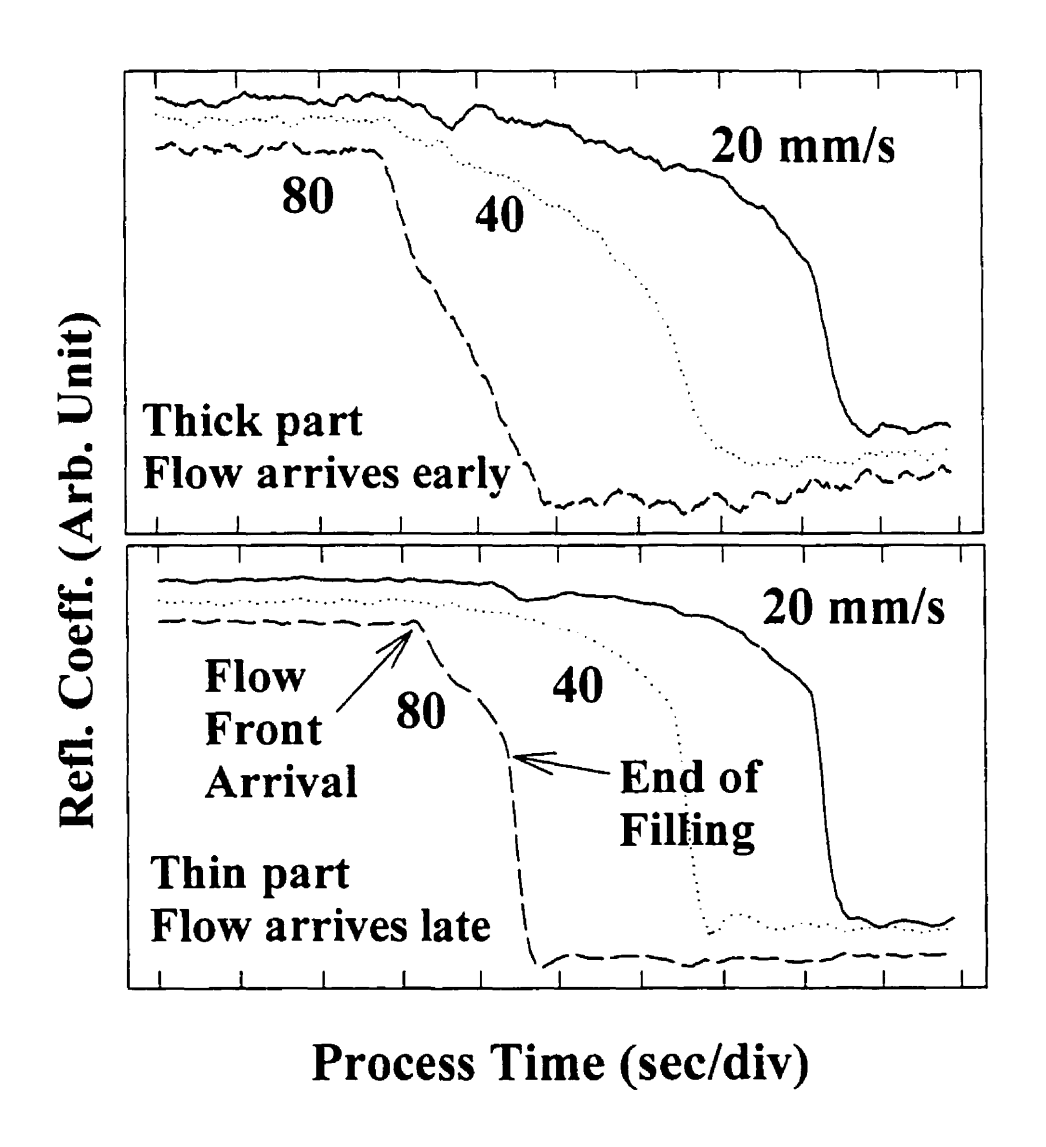


Fig. 2-17: Injection phase in injection molding with different plunger speeds

For the 80mm/s case, there exists a section between the flow front arrival and the end of filling in Figure 2-17 that is similar to the normalized reflected energy curve in Figure 2-16. However, comparing the flow front arrival time for the two monitoring points, the flow front advanced from the thick part monitoring point to the thin part monitoring point in around 0.5 sec. This distance is about seven times the diameter of the circular UT. Therefore, from the beginning to the end of covering the effective sensing area, the time span is around 0.07 sec. The indicated section between the flow front arrival and the end of filling has a time span of around 1.2 sec, and therefore does not represent the covering of the effecting sensing area. With the current data acquisition system, acquiring and saving time for each data point was 0.01 sec, and therefore the resolution was not enough to discern the covering of the effective sensing area.

### 2.7 Solidification monitoring

After molten polymer is injected into the mold cavity, the part starts to cool down as heat is transferred from the part to the mold. When temperature continues to drop, the molten polymer starts to solidify eventually. Depending on the type of material, a transition range exists between liquid and solid states. The development of this transition region indicates the development of the solid/liquid boundary inside the molded part. This is referred to as the solidification behavior. With ultrasonic technique, this solidification behavior can be monitored before detachments from cavity walls occur, provided that the signal-to-noise ratio (SNR) is good. Figure 2-18 shows the waveform plot (series of snapshots of ultrasonic echoes) aligned with Γs, cavity pressure, and plunger position plots. Vertical axes for all three plots are the aligned process time. This reveals the capability of ultrasound in monitoring solidification during the holding phase, while the pressure transducer cannot. Refer to Figure 2-19 for descriptions of echoes shown in the waveform plot.

For semi-crystalline materials like HDPE, characteristics such as density and ultrasonic wave velocity change dramatically from liquid to solid state and vice versa, as

can be seen from the tripartite relationship in Figure 2-12. With acoustic impedance (Z) of a medium defined as the product of density ( $\rho$ ) and wave velocity (V) of that medium, the acoustic impedance for HDPE also undergoes a discontinuity at the crystallization temperature ( $T_c$ ) where both density and ultrasonic wave velocity experience a discontinuity. This significant change in acoustic impedance effectively forms another interface for energy reflection due to impedance mismatch between liquid and solid layers. For HDPE, echoes reflected from such solid/liquid interfaces can be observed. These solid/liquid interfaces are excellent temperature references for  $T_c$  because they are accurate to within  $\pm 5^{\circ}$ C for HDPE.

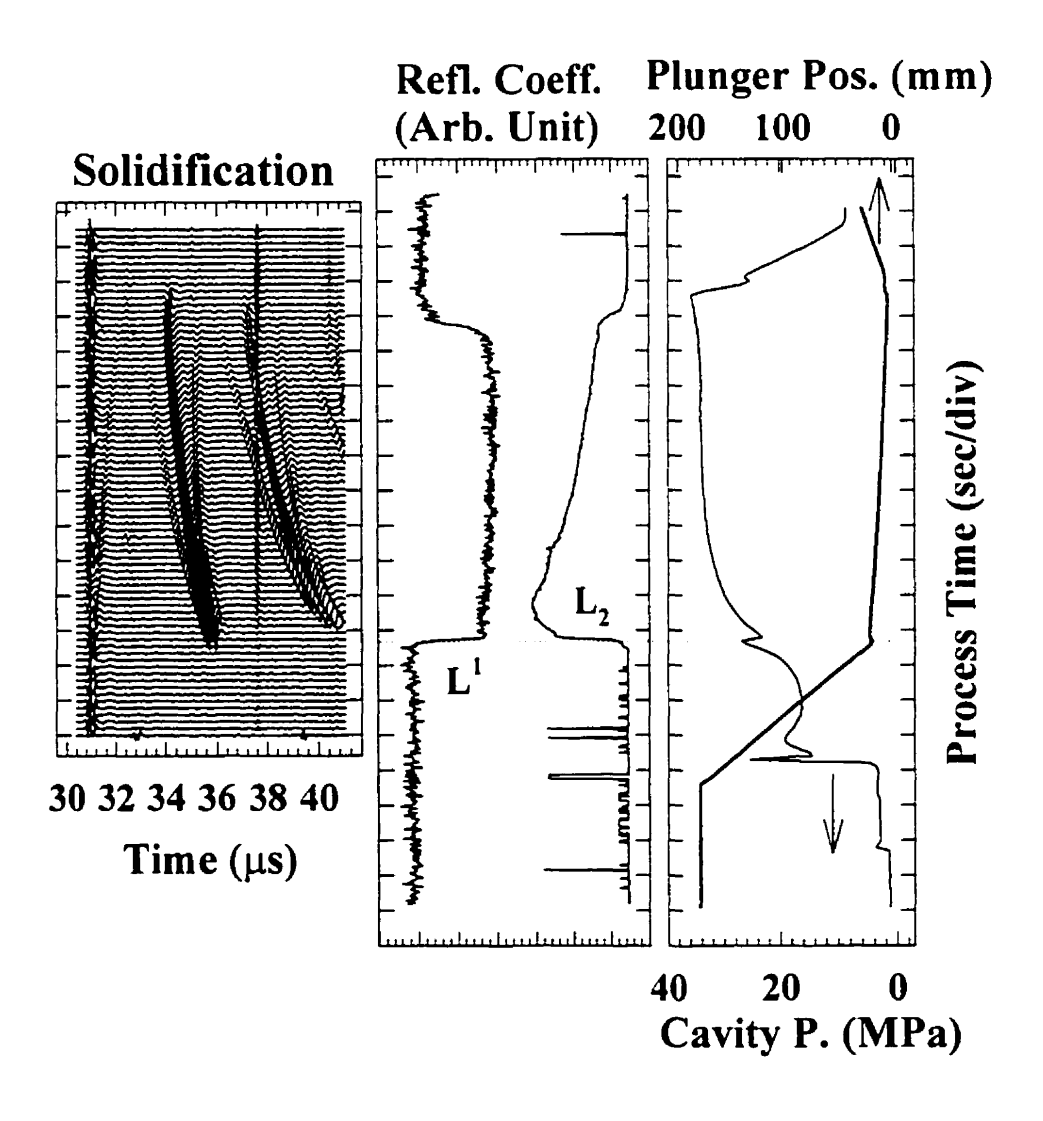


Fig. 2-18: On-line monitoring of solidification

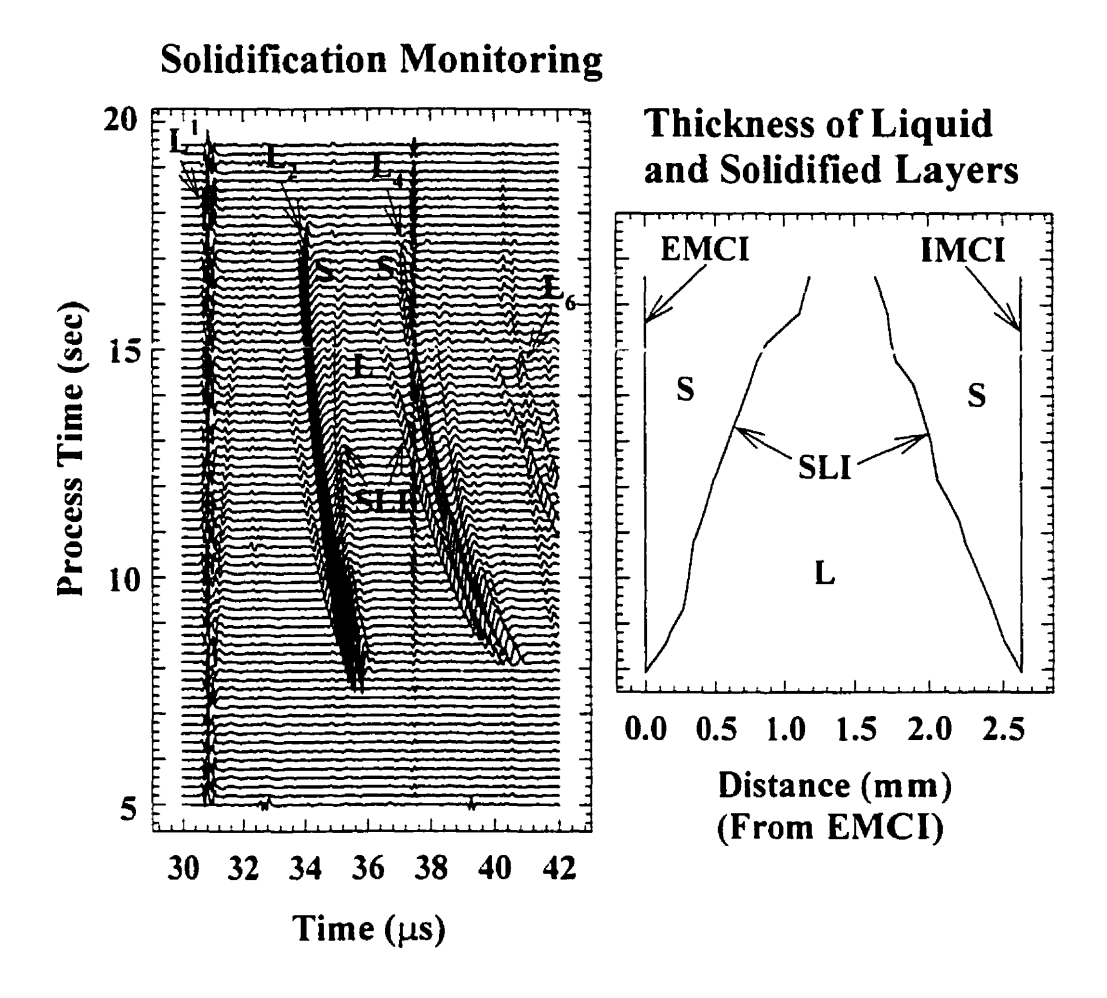


Fig. 2-19: Solidification fronts and thickness of liquid and solid layers.  $L^1$  is the echo reflected from the external mold/cavity interface (EMCI).  $L_2$ ,  $L_4$  and  $L_6$  are the  $1^{st}$ ,  $2^{nd}$ , and  $3^{rd}$  round trip echoes reflected from the internal mold/cavity interface (IMCI). L and S stand for liquid and solid layers. SLI stands for solid/liquid interface

On the left of Figure 2-19 is the ultrasonic waveform plot. The stationary echo on the left is the 1<sup>st</sup> reflected echo (L<sup>1</sup>) from the external mold/cavity interface (EMCI). The moving echoes on the right are the multiple reflected echoes (L<sub>2</sub>, L<sub>4</sub>, and L<sub>6</sub>) from the internal mold/cavity interface (IMCI). It can be seen that two echoes start to develop and move away from the two mold/cavity walls, one on each side. These two echoes are the two solid/liquid interfaces (SLIs). As demonstrated, solidification starts from the two contacting surfaces between hot molten polymer and the molds. And as the whole part is

cooling down, the boundaries marked by the 130°C isotherm move toward the center of the liquid layer. The two advancing SLIs form two solidification fronts approaching each other. In the illustrated case, since detachment from the external mold (to be discussed in the next section) occurs before the two solidification fronts meet, the completion of solidification of molded part was not observed. After identifying the two solid/liquid interfaces, the two solid regions and the one liquid region are therefore identified and marked as in Figure 2-19.

From the four echoes reflected from the four interfaces (EMCI, two SLIs, and IMCI), three time delays are determined. These three time delays represent the times for ultrasonic wave to travel twice the distance inside the external solid layer, the sandwiched liquid layer, and the internal solid layer, respectively. From the tripartite relationship chart, ultrasonic wave velocity is very different in the solid layers than in the liquid layer. Also a temperature gradient exists inside all these three regions, *i.e.*, temperature is not uniform inside any of these three regions. Previous research has shown the feasibility of approximating thickness of these layers with appropriate assumptions [43]. Modified assumptions are made in this thesis in order to approximate more precisely the thickness of each of these three layers.

During the solidification stage, the molded part is assumed to be maintained at constant pressure. From Figure 2-18, the cavity pressure is 33.8 MPa (4900 psi) in the holding stage after compression. Since pressure inside the molded part is not known, cavity pressure reading is taken as the pressure of the molded part. Also from the tripartite relationship, ultrasonic velocity is more sensitive to temperature variation in solid than in liquid state. Therefore an assumption as to average temperature inside the liquid layer is made in order to approximate the thickness of the liquid layer. This average temperature of the liquid layer is taken as the average temperature between the crystallization temperature (130°C) and the temperature at the center of the liquid layer. The temperature at the center of the liquid layer is assumed to be a linear function reduced from the melt temperature at injection (220°C) to the critical boundary temperature (130°C). The

temperature at the center of the liquid layer is assumed to be that of the melt temperature at injection at the beginning of solidification. This is because, as polymer in contact with the mold walls starts to cool down, the hot polymer melt at the center is still advancing to fill the cavity. As a result, the hot material continues to push the melt in the core forward, and thus the center is kept at high temperature. The critical boundary temperature is used as the temperature at the center of the liquid layer at the end of solidification, since when the two solidification fronts meet, the last portion of the liquid layer starts to solidify at this temperature.

With the assumed pressure and average temperature inside the liquid layer, average ultrasonic wave velocity ( $V_{avg}$ ) can be obtained from the tripartite relationship. The thickness of the liquid layer ( $h_l$ ) can be approximated as follows:

$$h_t = \frac{1}{2} \times V_{avg} \times \tau_t \tag{2.5}$$

where  $\tau_l$  is the time delay measured between the two solid/liquid interface echoes. Since temperature of the external and internal molds are controlled by independent temperature control units, it is assumed that the two mold cavity surface temperatures are similar. As a result, temperature profiles and ultrasonic velocity profiles are all similar in the two solid layers. This symmetric assumption is adopted to simplify the approximation of the thickness of the two solid layers. Since the summation of the thickness of the three layers equals the compensated wall thickness from Eqn. 2.1, thicknesses of the two solid layers ( $h_{s-ex}$  and  $h_{s-in}$ ) are obtained by partitioning the difference between the compensated wall thickness and the liquid layer thickness according to travel times inside solid layers ( $\tau_{s-ex}$  and  $\tau_{s-in}$ ), as follows:

$$h_{s-ex} = \frac{\tau_{s-ex}}{\tau_{s-ex} + \tau_{s-ex}} \times \left(h_{eff} - h_{i}\right)$$
 (2.6a)

$$h_{s-in} = \frac{\tau_{s-in}}{\tau_{s-in} + \tau_{s-in}} \times \left(h_{ell} - h_{l}\right)$$
 (2.6b)

Approximate solidification front advancement inside the polymer is therefore derived and shown on the right of Figure 2-19. By taking the derivative of the curvature, which represents the location of the solidification front, the speed of solidification front advancement can be determined. In addition, as mentioned before, ultrasonic technique can identify locations in the molded part at the monitoring point where temperature are at 130±5°C. This good temperature reference can be used to assist in the derivation of a temperature profile across the molded part and verification of temperature inside the part modeled by computer-aided engineering (CAE) software.

### 2.8 Detachment monitoring

After the gate freezes, no more material can be forced into the mold cavity to compensate for the volumetric loss resulting from shrinkage due to cooling. As the part continues to cool down and shrink, the part will start to detach from the mold cavity walls on both sides. Since the cooling of the part is most efficient through conduction when the part is in contact with the mold cavity walls, the cooling becomes less efficient after mold/part detachment. Previous work also demonstrated the effect of the gap on the cooling [33]. Therefore part detachment can potentially be used to determine the time of part ejection, and thus to optimize the cycle time.

Figure 2-20 shows the principle of monitoring part detachments from both the internal (DI) and external (DE) mold. When the part is in good contact with cavity walls on both sides, L<sup>1</sup> is the reflected echo received from interface 1 (external mold/polymer). Part of the ultrasonic wave transmitted into the polymer will be reflected from interface 2 (polymer/internal mold), transmitted through interface 1, and received by the ultrasonic transducer. This first echo from interface 2 is labeled L<sub>2</sub>. Similarly, the second echo from interface 2 is labeled L<sub>4</sub>. Since energy continues to be partitioned into reflected and

transmitted parts at every boundary, ultrasonic energy in echoes received after more trips will be weaker than echoes received after fewer trips inside the polymer. In other words, energy and amplitude of the received echo for  $L^1$  will be larger than that for  $L_2$ . And similarly energy and amplitude of the received echo for  $L_2$  will be larger than that for  $L_4$ .

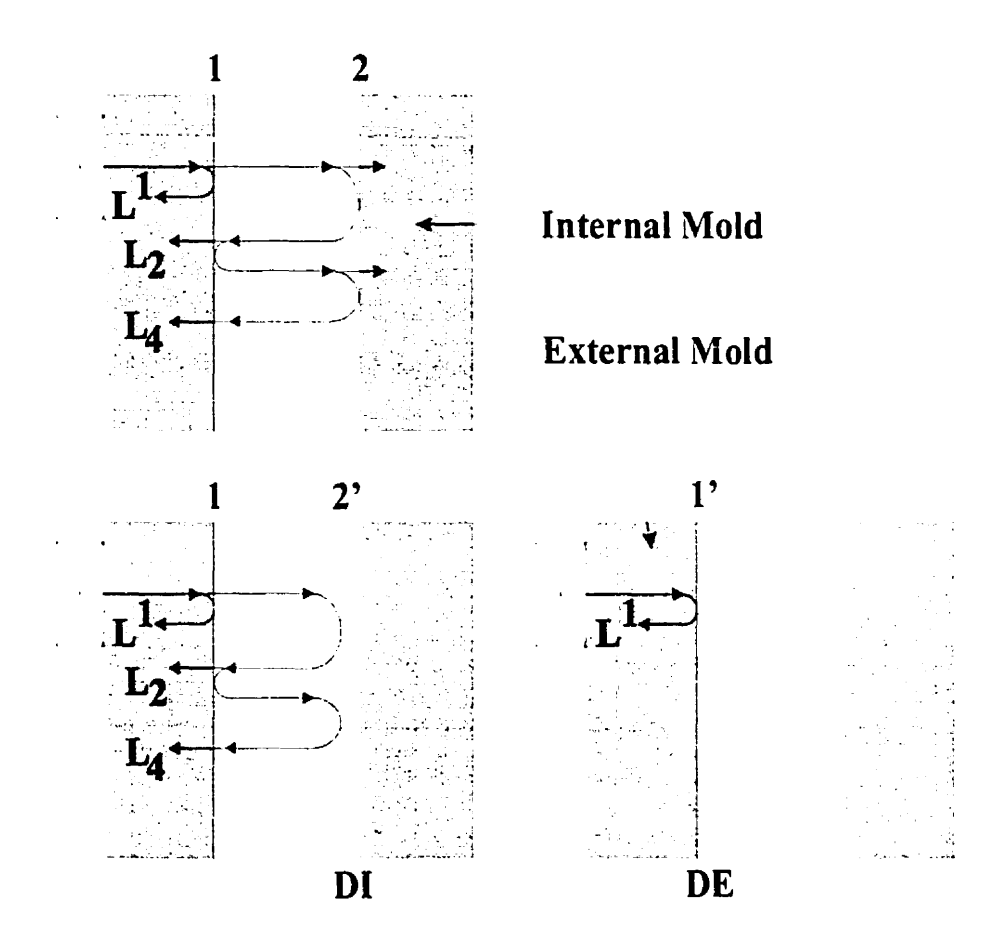


Fig. 2-20: Detachment mechanism from internal (DI) mold/cavity interface (interface 2 and 2' after detachment) and external (DE) mold/cavity interface (interface 1 and 1' after detachment) and echoes received from these interfaces

When DI occurs, the interface 2 changes from polymer/internal mold to polymer/air (interface 2'). Since the ultrasonic wave is totally (if the gap is larger than  $1\mu m$ ) reflected at the polymer/air interface, due to large impedance mismatch, no energy will be transmitted into the air. As a result, the energy and amplitude of the received echoes  $L_2$  and  $L_4$  will increase. Moreover, the phase of the reflected echoes from interface

2' is reversed (180° different) compared with the echo from interface 2 [43]. This is because at interface 2, the ultrasonic wave is striking a medium with greater acoustic impedance than polymer, while at interface 2', the ultrasonic wave is striking a medium with lower acoustic impedance than polymer.

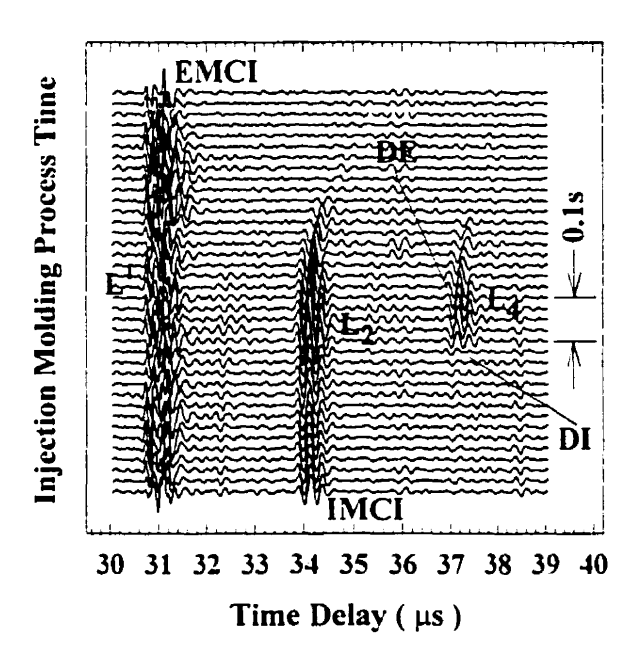


Fig. 2-21: On-line monitoring of detachment from internal mold (DI) and external mold (DE)

Figure 2-21 is the waveform plot for one run near the end of the holding stage, with  $L^1$ ,  $L_2$ , and  $L_4$  labeled. The increases in amplitudes for  $L_2$  and  $L_4$  are observed, especially when  $L_4$  suddenly becomes much more visible. Therefore, the detachment from the internal mold is effectively monitored. Similarly in the run shown in Figure 2-11, DI is also identified from the changes in  $\Gamma$  for  $L_2$ .

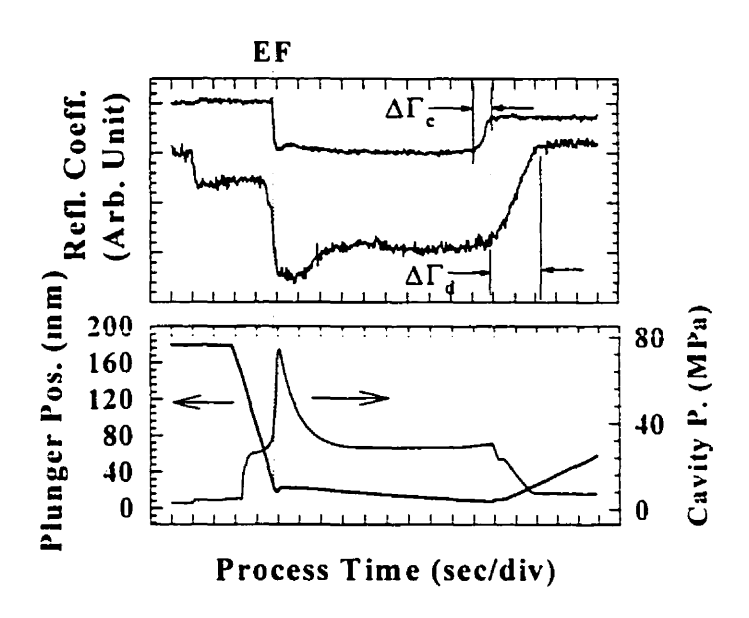
When the part starts to detach from the external mold, interface 1 (external mold/polymer) changes to interface 1' (external mold/air). No ultrasonic energy will be transmitted into the polymer, and as a result, no information about the material can be detected by ultrasound anymore. This means no echo is received from within the polymer.

On the other hand, since all energy is totally reflected from interface 1', the amplitude of  $L^1$  increases to maximum. The run shown in Figure 2-10 illustrates this case. Since DE occurs first, the  $\Gamma$  for  $L_2$  does not increase but rather decreases. In Figure 2-11, DE is also marked when the  $\Gamma$  for  $L_2$  start to diminish.

However, more attention must be paid in interpreting the changes in  $\Gamma$  at the end of the holding phase. Figure 2-22(a) shows one run monitored from locations "c" and "d" in Figure 2-7. Location "d" is close to the gate, while point "c" is far from the gate.  $\Gamma$ s monitored at both locations return to maximum at the end of the cycle. However, there is a difference in the pattern by which  $\Gamma$ s return to their maximum value. At monitoring location "c", the increase occurs gradually (slow in the beginning) while at monitoring location "d", a sudden linear increase is observed.

From cavity pressure plot, it can be seen that the plunger starts to retract at around 15 sec into the monitoring. The retraction of the plunger causes pressure inside the molded part to drop. The coupling between the part and cavity walls will reduce. And as a result, amplitude of reflected echo will increase, and  $\Gamma$  in turn, will increase. As identified in Figure 2-22(a), the linear increase in  $\Gamma$  at location "d" occurs simultaneously at the same time plunger starts to retract. Therefore, it can be inferred that there were still polymer in molten state at center of the molded part at location "d". As the plunger retracts, pressure inside the molded part also reduces. And the change in  $\Gamma$  at location "d" ( $\Delta\Gamma_d$ ) is in fact due to the change in pressure because of the plunger retraction. Since the gate has not froze and the plunger has not retracted, the gradual increase in  $\Gamma$  seen at point "c" is resulted from the gradual detachment of the part from cavity wall.

The effect on  $\Gamma$  due to both detachment and plunger retraction can occur at the same time. Figure 2-22(b) illustrates this case. Again at monitoring location "c", increase in  $\Gamma$  ( $\Delta\Gamma_c$ ) is due to local detachment of the molded part. However, at location "d", effects from both detachment (gradual) and reduction in pressure (sudden) were present, with the former overrun later by the latter.



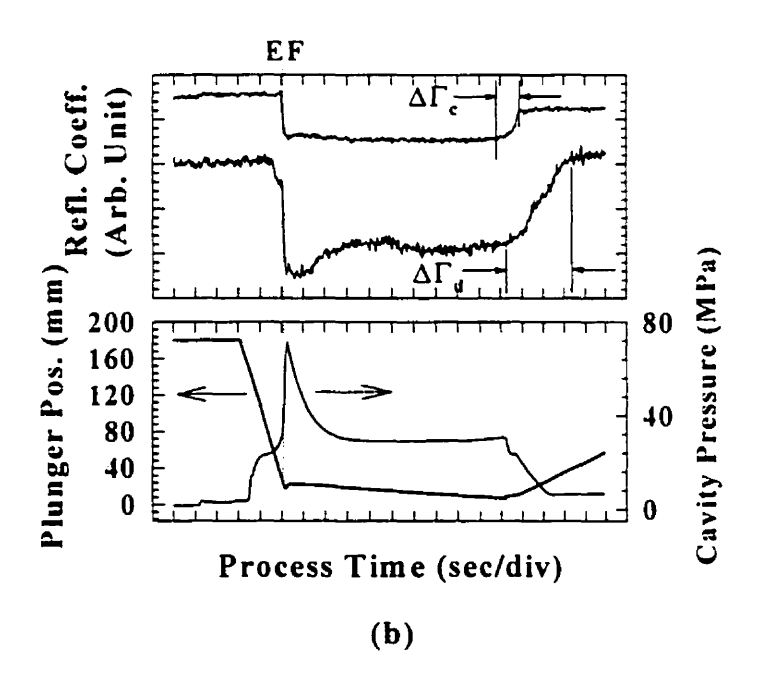


Fig. 2-22: Effect on  $\Gamma$  due to detachment and plunger retraction. a) Effect of plunger retraction on  $\Gamma$  at location "d". b) Effect of both detachment and plunger retraction on  $\Gamma$  at location "d". Upper plots contain reflection coefficients ( $\Gamma$ s) monitored from locations "c" and "d". Lower plots show corresponding cavity pressure (thin line) and plunger position (thick line)

### 2.9 Summary

The injection molding of an HDPE box was monitored on-line using an ultrasonic technique. By attaching a conventional ultrasonic transducer (UT) to the outside surface of the mold, echoes received by a simple pulse/echo method were used to monitor the injection molding process on-line. The normalized reflection coefficient ( $\Gamma$ ) is utilized as a simple technique for monitoring. Figure 2-23 shows a pair of representative curves to summarize this technique. The  $\Gamma$  curve on the top was monitored from a thin and flat section of the molded box, while the  $\Gamma$  curve at the bottom was from a thick and curved section.

Points 1 in Figure 2-23, where  $\Gamma$ s start to reduce indicate the arrival of melt front at the monitoring points locally. When cavity walls on both sides are flat and parallel, resolution of local melt front arrival is better than when cavity walls are non-parallel and curved. A potential method to determine local flow front speed using a single UT is also proposed. However, in order to identify regions 2 representing the process of covering effective sensing area, higher acquisition speed than the current setup (86 ms per acquisition) is required.

Points 3 in Figure 2-23, where  $\Gamma$ s start to undergo a sharp change, indicate the end of cavity filling. This information can be used to check the completeness of the molded part. In order to provide a signal to switch over pressure from injection pressure to holding pressure, allowance for mechanical response time must be included. As a result, a sensor should be placed a little bit upstream from the predetermined (from simulation) latest flow arrival point.

Points 4, where  $\Gamma$ s start to bounce gradually back to their maximum, indicate either local part detachment, plunger retraction, or gate freezing. If the gradual increase does not occur simultaneously at different positions, it represents the start of local part detachment. If the gradual increase is monitored simultaneously at many locations, it

represents pressure reduction due to gate freezing. On the other hand, if a sudden and linear increase occurs, it comes from the reduction of pressure due to plunger retraction. Therefore sections 5 in Figure 2-23 represent the change of  $\Gamma$ s due to abrupt pressure reduction from plunger retraction. Effects from these three sources can occur at the same time.

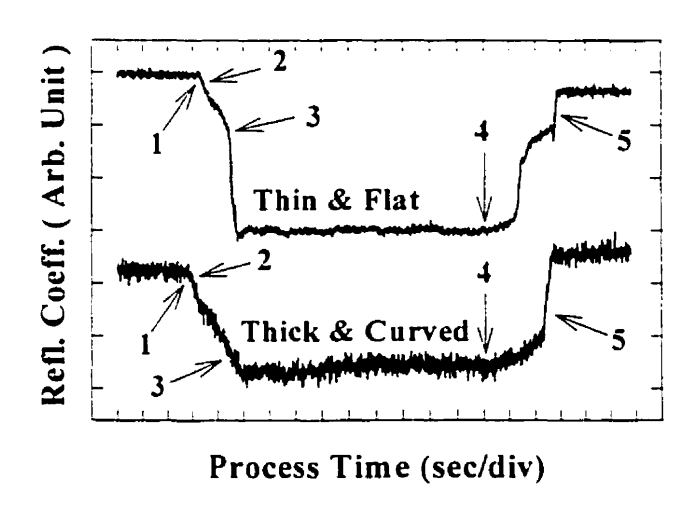


Fig. 2-23: Summary of on-line monitoring of injection molding using  $\Gamma$  plots: 1) Flow front arrival, 2) Covering of effective sensing area, 3) End of filling, 4) Part detachment or gate freezing, 5) Effect of plunger retraction

As  $\Gamma$  bounces back, it does not return to its original value from either monitoring location, as shown in Figure 2-23. This deviation results from the change in ultrasonic coupling due to temperature effect; it can be compensated for easily, and is not considered in this study.

Moreover, on-line monitoring of solidification was also demonstrated. The development of the two solid-liquid interfaces were observed. Thicknesses of solid and liquid layers were determined. In addition, the solid/liquid interface echo indicated the locations within the molded part where temperature were at 130°C (crystallization temperature) with high accuracy (±5°C). This is a good temperature reference to assist the derivation of temperature profile inside the molded part and the verification of

temperature modeled by CAE software. Average temperature and pressure inside the molded part can also be determined under certain conditions. From results demonstrated in this chapter, Table 2-2 is to summarize the comparison between conventional ultrasonic and pressure sensors for injection molding process monitoring.

Table 2-2: Comparison between ultrasonic and pressure sensors in on-line monitoring of injection molding process

Conventional Ultrasonic Sensor	Conventional Pressure Probe	
Non-intrusive	Intrusive	
Array configuration can be easily	Array configuration difficult to	
implemented	implement	
Capable of monitoring flow front	Capable of monitoring flow front arrival	
arrival (sec. 2.4)		
Capable of monitoring completion	Capable of monitoring completion of	
of filling (sec. 2.4)	filling	
Measures pressure inside molded part	Measures cavity pressure at all time	
under certain conditions (sec 2.5)		
Indirect pressure monitoring	Direct pressure monitoring	
Capable of monitoring solidification	No such capability	
at the same position (sec 2.7)		
Measures temperature of molded part	No such capability	
under certain conditions (sec 2.5)		
Capable of monitoring part	Capable of monitoring part detachment	
detachment (sec 2.8)		
Capable of monitoring material	No such capability	
properties		

## Chapter 3:

# On-line Ultrasonic Monitoring of Gasassisted Injection Molding and Off-line Measurement for Co-injection Molding

#### 3.1 Introduction

Due to the difficulty of fabricating special and complicated design features with high quality using conventional injection molding methods, numerous attempts such as gas-assisted injection molding (GAIM) have been developed in the past two decades [6]. Currently the most crucial parameters affecting gas penetration and volumetric filling time in controlling GAIM are gas pressure, delay time (time between the stop of polymer injection and the start of gas injection), gas-injection time, inlet melt temperature, and polymer volume fraction prefilled in the cavity [6].

In this chapter, previous knowledge of on-line monitoring of conventional injection molding process is adopted to monitor GAIM on-line. Results from on-line monitoring of the local polymer melt arrival, gas injection, end of cavity filling, gas penetration, gas blow-through, and their potential uses are presented. Difficulties in wall thickness measurement and the effect of change in gas pressure are also discussed. Finally, off-line thickness measurement for co-injected plates is presented.

### 3.2 Gas-assisted injection molding

# 3.2.1 Experimental setup and the sample

Ultrasonic monitoring of GAIM was done on a 400-ton Husky injection molding machine and a two-cylinder gas injection unit from Cinpres, as shown in Figure 3-1. Two 6.35 mm (¼ inch) diameter, 5MHz, longitudinal wave ultrasonic transducers (UTs) were installed on the external surface of the mold for process monitoring. Since the temperature of the external surface of the mold during GAIM was below 50°C, conventional broadband UTs and couplants at room temperatures were sufficient. Plexiglass plates were screwed onto the outside of the mold wall to hold the springs that press UTs firmly against the mold at desired monitoring locations. Figure 3-2 shows the installation of the two UTs.



Fig. 3-1: Husky injection molding machine and Cinpres 2-cylinder gas injection unit

HDPE (high density polyethylene) was the material used in the GAIM presented in this chapter. Figures 3-3(a) and (b) show the molded sample. "A" and "B" are the two

locations monitored simultaneously by a two-channel monitoring system. The gas channel inside the stem is revealed from the cross-section of the sample shown in Figure 3-3(b).

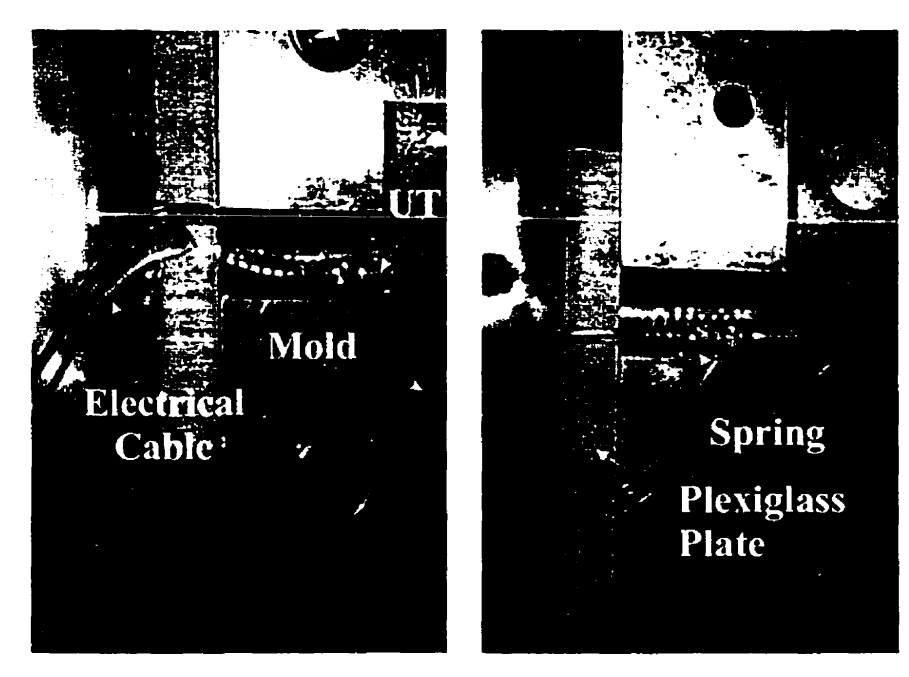


Fig. 3-2: Installation of UTs on the external mold wall

### 3.2.2 Operating conditions of the injection molding machine

The molding conditions used in this study are summarized in Table 3-1. All molding conditions were held constant except the percentage of polymer fill and the gas pressure.

Table 3-	1: Operati:	ng conditions	for GAIM
----------	-------------	---------------	----------

Polymer injection time	3.0 sec
Total cycle time	55 sec
Gas injection time	30.5 sec
Gas pressure	$2.5 - 5.0 \times 10^4 \text{ KN/m}^2$
Mold temperature	40°C
Melt temperature	250°C
Polymer fill percentage	85 - 95 %

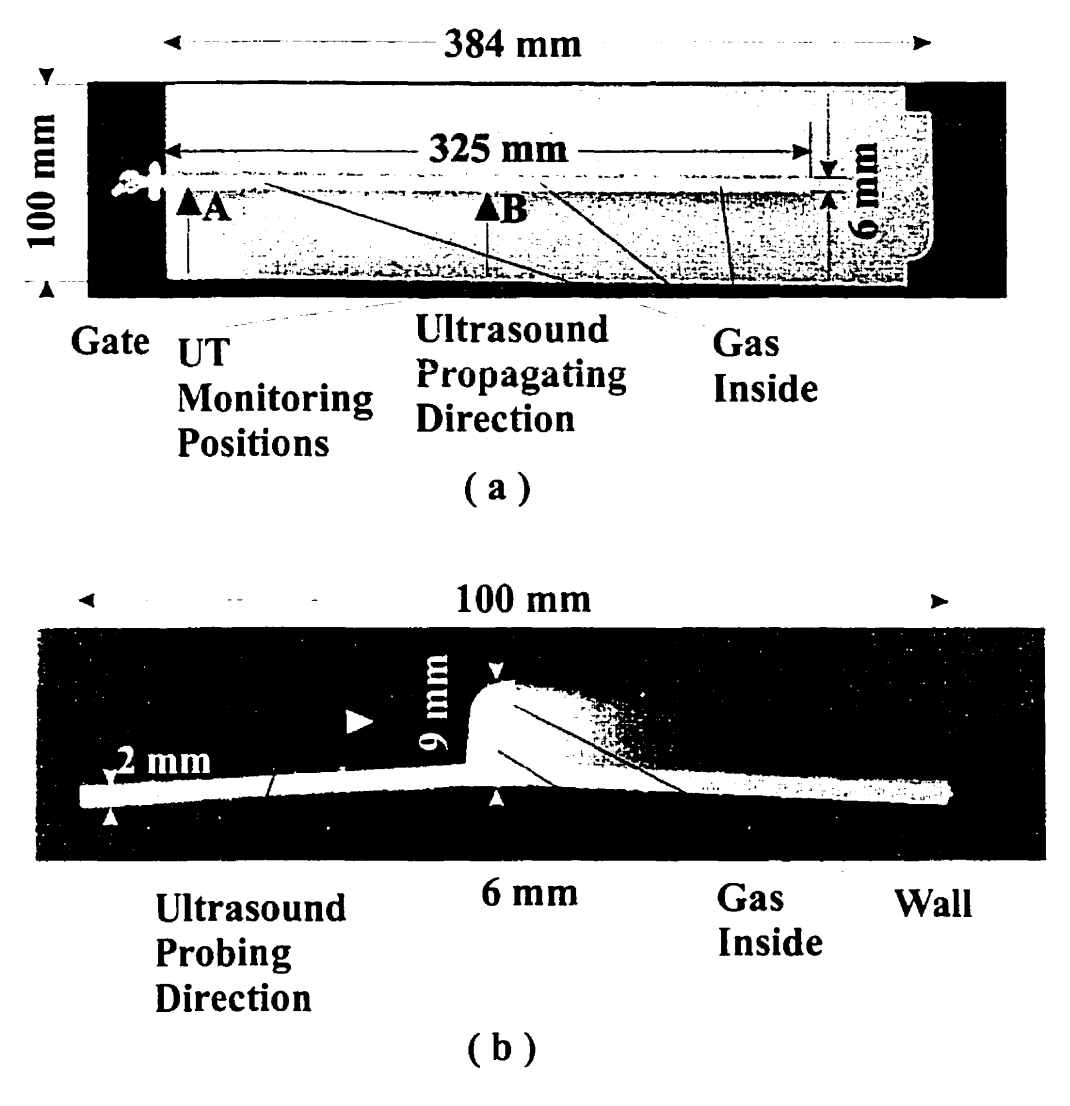


Fig. 3-3: HDPE sample made by GAIM: (a) Top view and dimensions of molded part with UT monitoring points, and (b) cross-section view of the molded part revealing the gas channel inside

### 3.2.3 Cavity pressure

Cavity pressure for GAIM is discussed in this section to enhance the understanding of the GAIM process. It has been demonstrated in section 2.3 that local cavity pressure in injection molding increases proportionally to the polymer flow length (length of polymer between the monitoring point and the polymer flow front) beyond the monitoring point. As a result, a high injection pressure is needed for polymer flow front advancement far from the gate. On the other hand, in GAIM, inert gases such as nitrogen are injected into the cavity to assist cavity filling. When polymer melt is pushed by gas to

fill up the cavity, polymer melt (more viscous) is displaced by gas, and the amount of polymer in front of the gas flow front reduces as more melt is deposited on cavity walls. As a result, gas pressure required to keep the polymer melt front advancing at the same speed reduces with time. So the pressure requirement for the GAIM process is lower than for conventional injection molding [6]. Therefore, cavity pressure in GAIM is generally lower than in conventional injection molding.

Moreover, since gas has negligible viscosity, gas pressure can be considered uniform. As a result, pressure exerted on the polymer by gas from inside is uniform in magnitude, and the cavity pressure is therefore more uniform across the molded part than with conventional injection molding. This lower and more uniform cavity pressure distribution in GAIM produces lower and more uniform residual stress in the molded part, resulting in less warpage. Furthermore, less clamping force is required for GAIM [6].

The gas injection unit used in the GAIM presented in this chapter uses discontinuous pressure generation. In this approach, nitrogen inside a cylinder is compressed to a preset pressure level. Then the gas is released and injected into the cavity. In this kind of system, high pressure in the cooling stage normally cannot be maintained [6]. A typical gas pressure for GAIM from this kind of gas generation system is shown in Figure 3-4.

Figure 3-5 shows typical cavity and gas pressure curves for a GAIM. A time delay exists between polymer and gas injection. When polymer melt pressure is as high as the gas pressure in the gas generation unit, gas can be injected. Since gas pressure cannot be maintained in discontinuous types of gas generation system, pressure will drop as time passes. When the end of cavity filling is reached, as demonstrated in section 2.3, pressure inside the melt will rise to the gas pressure set for holding phase. Since in the GAIM system used for experiment, melt and gas enter from the same gate, and since there is no other gate to prevent gas from penetrating back into the barrel, constant holding pressure

could not be maintained. Therefore, for our experiment, no constant holding pressure was anticipated.

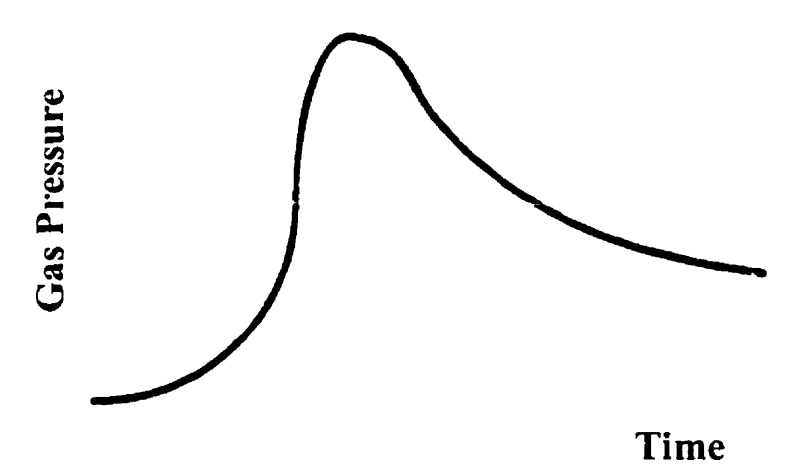


Fig. 3-4: Gas pressure by discontinuous gas generation unit [6]

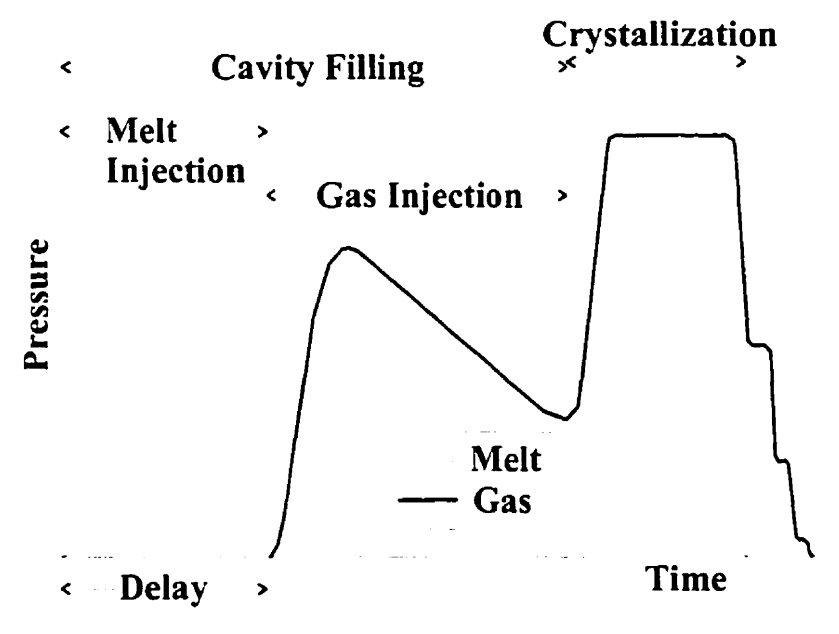


Fig. 3-5: Typical polymer melt and gas pressure curves in GAIM [modified from 6]

# 3.2.4 Principle of on-line monitoring of GAIM

Figures 3-6(a) to 3-6(d) represent different circumstances during the whole GAIM process monitored by ultrasonic technique. As presented in section 2.4, before melt arrives locally at a monitoring point, only echoes reflected from the external mold/cavity

interface (EMCI) are observed. Figure 3-6(a) illustrates this circumstance, and shows the first return trip echo ( $L^1$ ) from EMCI. After melt arrives, part of the ultrasonic energy penetrates into the melt, and the first return trip echo ( $L_2$ ) reflected from the internal mold/cavity interface (IMCI) is received by the UT. Meanwhile, the amplitude and the reflection coefficient ( $\Gamma$ ) of  $L^1$  reduce. This circumstance is illustrated by Figure 3-6(b).

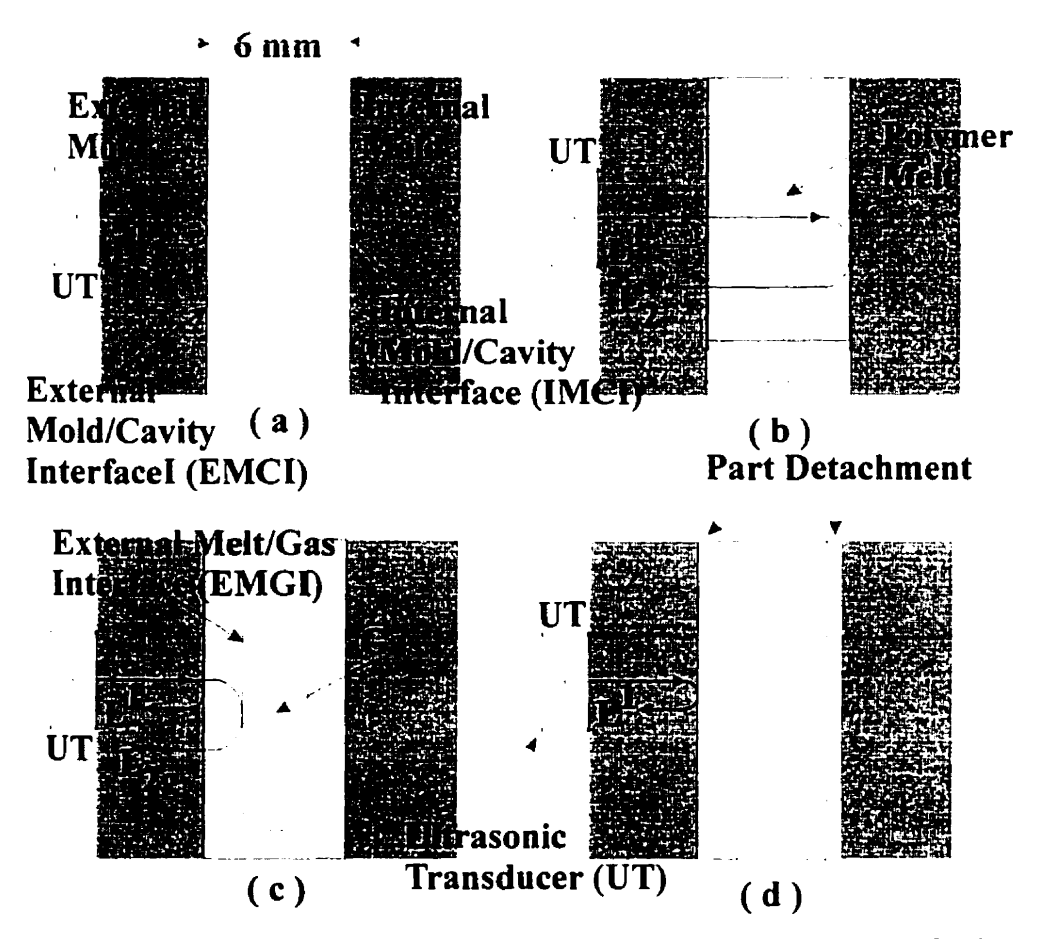


Fig. 3-6: Principle of ultrasonic on-line monitoring of GAIM: Before arrival of polymer melt (a), after polymer melt arrival (b), after gas arrival (c), after detachment (d), and echoes reflected from EMCI ( $L^1$ ), IMCI ( $L_2$ ), and EMGI ( $L_{2g}$ )

Figure 3-6(c) illustrates the arrival of the gas flow front. Because of the additional layer of gas inside the polymer melt, two (one on each side) melt/gas interfaces are formed. Since the ultrasonic wave is totally reflected at the melt/gas interface, information cannot be obtained beyond the external melt/gas interface (EMGI). As a

result, as the gas flow front arrives at the local monitoring point,  $L_2$  from IMCI will diminish and disappear after the ultrasonic wave passage to IMCI is completely blocked by the gas layer. On the other hand, the first return trip echo ( $L_{2g}$ ) reflected from EMGI is observed. These two echoes ( $L_2$  and  $L_{2g}$ ) can be distinguished from the time delay information.  $L_{2g}$  should be later than  $L^1$ , and earlier than  $L_2$ . Finally, in Figure 3-6(d), after the detachment of the solidified part from the EMCI, the ultrasonic wave is totally reflected from the EMCI, the process can no longer be monitored. This is when  $\Gamma$  measured at EMCI returns to its maximum, as demonstrated in section 2.8.

#### 3.2.5 Results

Figure 3-7 shows seven snap shots during one run of GAIM monitored from location "A". Arrows indicate the first reflected echo ( $L_{2g}$ ) from EMGI. This demonstrates that  $L_{2g}$  can be monitored on-line with ultrasonic technique. Using the same technique as in section 2.4, the gas flow front arrival was monitored by identifying the development of  $L_{2g}$ . Even though the time delay between  $L_{2g}$  and  $L^1$  (the first echo on the left side) was obtained, the melt layer thickness, which later on became the wall thickness of the molded part, was not easy to obtain. The reason is that in addition to time delay, ultrasonic wave velocity is also needed in order to obtain the thickness of the melt layer. From the tripartite relationship, it is difficult to determine ultrasonic wave velocity with both pressure and temperature changing simultaneously. Therefore, with a discontinuous gas generation system it is difficult to monitor the wall thickness.

Figure 3-8 shows, from top to bottom, the time delay between EMGI and EMCI  $(\tau_m)$ , amplitude of  $L_{2g}$ , amplitude of  $L_2$ , and time delay between IMCI and EMCI  $(\tau_g)$ . The arrival of polymer melt was indicated by noting the appearing of  $L_2$ . Since for GAIM, the cavity was not filled up by injection pressure, but rather by the gas injected later, polymer melt pressure increase inside the cavity was not high, and was not maintained as melt started to cool down after being injected into the cavity.

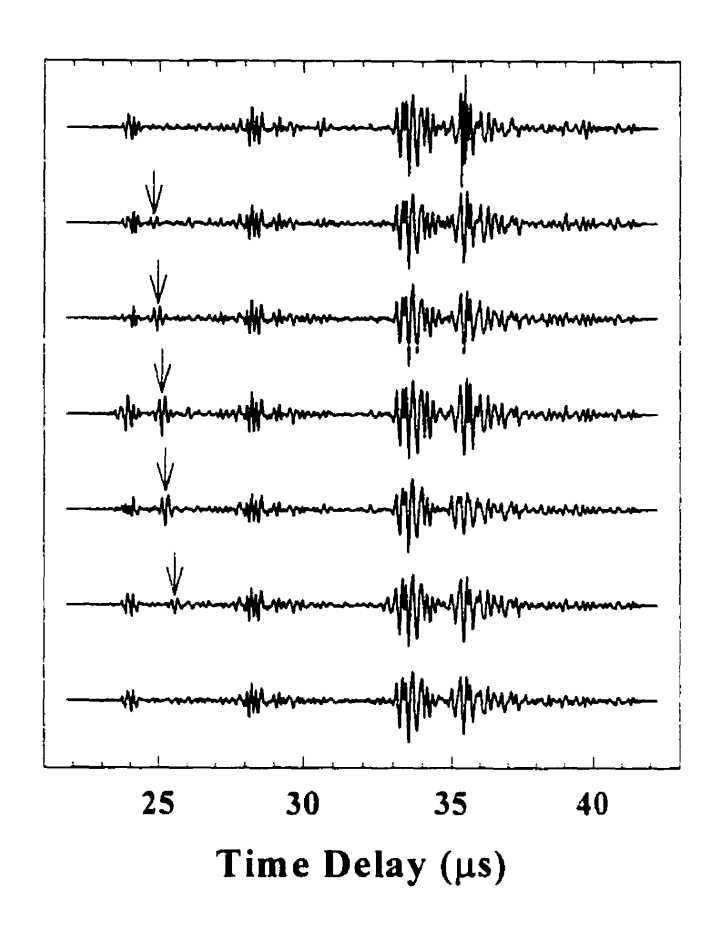


Fig. 3-7: Echo (L<sub>2g</sub>) (indicated by arrows) reflected from external melt/gas interface (EMGI)

When  $L_2$  became visible, polymer melt has wetted EMCI. This meant that the melt has arrived locally at the monitoring point. About 3 seconds after polymer arrival, one local maximum was reached for  $L_2$ . This was identified as the start of gas injection which caused a sudden rise in melt pressure. This pressure rise improved the wetting with EMCI (increase in amplitude) and increased ultrasonic velocity (decrease in time delay). This sudden increase in pressure was confirmed from the time delay ( $\tau_m$ ) plot, where a sharp drop occurred. After this point, the stage of gas-assisted cavity filling started until the cavity was filled. As gas pressure started to drop, as shown in Figure 3-4, the amplitude of  $L_2$  also reduced. Meanwhile, the cooling down of the molded part was observed from the reduction of  $\tau_m$ .

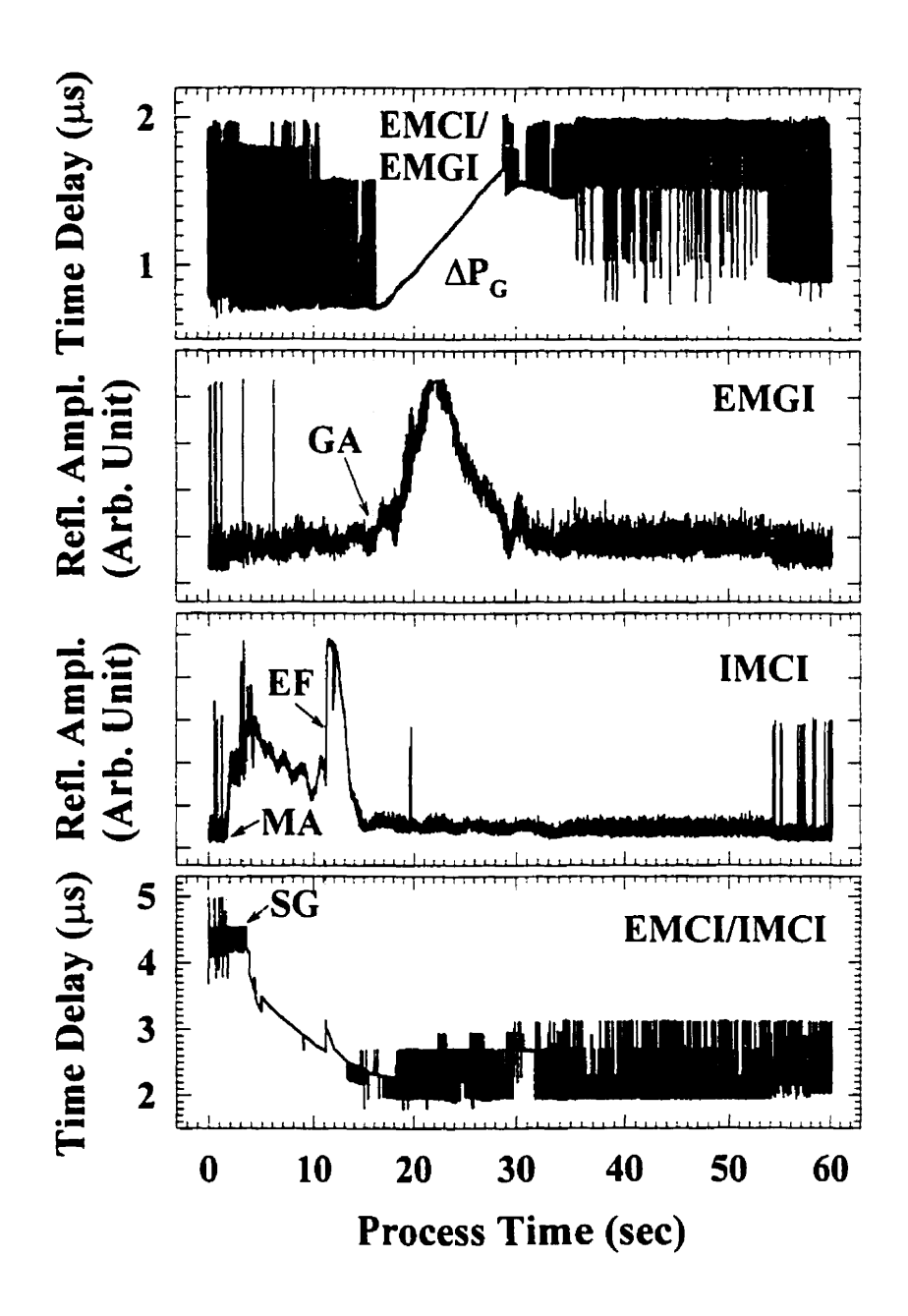


Fig. 3-8: Ultrasonic on-line monitoring of GAIM: Reflection coefficient ( $\Gamma$ ) plots for the echo ( $L_{2g}$ ) from the external melt/gas interface (EMGI) and the echo ( $L_{2}$ ) from the internal mold cavity (IMCI) interface and time delay plots between these echoes and the echo ( $L^{1}$ ) reflected from external mold cavity interface (EMCI). Also marked: Melt arrival (MA), start of gas injection (SG), end of filling (EF), local gas front arrival (GA), and change in gas pressure ( $\Delta P_{G}$ )

At around 10 seconds into monitoring, the amplitude of  $L_2$  underwent a sharp increase again. As understood in section 2.4, this discontinuity indicates the end of filling. It has been demonstrated in section 3.2.3 that at the end of filling, the GAIM process goes from injection stage into compression stage, in which pressure increases. However, it is not clear at this point why  $\tau_g$  also increased, since both increase in pressure and cooling down in temperature should result in an increase in ultrasonic wave velocity. By identifying the end of filling, insufficient filling, if occurs, can be detected during GAIM.

In GAIM, gas is not only used to assist in filling the cavity, but also in packing the part. In other words, as the molded part starts to cool down, shrinkage occurs. The loss in volume due to cooling is compensated for by the injected gas. Therefore, after the end of filling, a gas channel continues to develop, and the gas flow front continues to advance. As the gas flow front reaches the monitoring point, the EMGI will prevent the transmission of the ultrasonic wave, and L<sub>2</sub> disappears. The impact of gas flow front arrival is shown in Figure 3-9. Since the ultrasonic wave reflects in the direction normal to an interface, reflected ultrasonic waves from curved melt/gas interface will be directed in various directions. As a result, during the transition period in which the gas flow front passed the monitoring point, L<sub>2</sub> continued to diminish in amplitude, while L<sub>2g</sub> continued to develop in amplitude. After the EMGI was well developed (parallel to EMCI), L<sub>2</sub> disappeared, as can be seen from Figures 3-8 and 3-9.

As the gas continued to penetrate inside the polymer, the amplitude of  $L_{2g}$  increased as the development in EMGI started to stabilize. Later on, the effect of the pressure drop started to take over, and the amplitude of  $L_{2g}$  started to reduce. The pressure drop in the melt was confirmed from the time delay ( $\tau_g$ ) plot. Since molded part temperature was continuously dropping, which should result in an increase in ultrasonic velocity, this increase in  $\tau_g$  was therefore attributed to the drop in melt pressure. As mentioned before, the holding pressure cannot be maintained since the gas injection unit is a discontinuous type gas generation system.

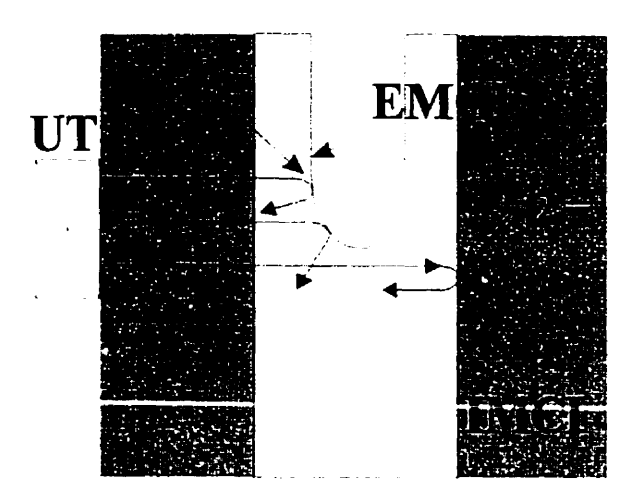


Fig. 3-9: Diminishing of echo ( $L_2$ ) reflected from internal mold/cavity interface (IMCI) and developing of echo ( $L_{2g}$ ) reflected from external melt/gas interface (EMGI)

In order to verify the end of filling, another run of GAIM was carried out. In this run, three cavity pressures and one plunger position were recorded simultaneously with ultrasonic signals. Figure 3-10 shows the monitoring result. Cavity pressures and plunger position are shown in the top plot. The middle plot is the reflection coefficient ( $\Gamma$ ) for L<sup>1</sup>, and the bottom plot shows  $\Gamma$  for L<sub>2</sub>. The setup for the new run was not identical with the previous one. As can be seen from Figure 3-10, polymer injection stopped as around 4 seconds into monitoring. Gas injection then started at 5.4 seconds, and gas holding was released at 12 seconds, a much shorter gas holding time than in the previous setup (30.5 sec).

From the cavity pressure curves, the end of filling and the gas release were identified. From reflection coefficient plots, both the end of filling and the gas release were identified from  $\Gamma$  of  $L_2$ , while from  $\Gamma$  for  $L^1$ , the above information is not observed clearly. But the purpose of confirming the previous claim that the end of filling was identified with  $\Gamma$  of  $L_2$  was achieved. Since cavity pressure dropped significantly once gas holding was released, neither the ultrasonic nor the pressure sensor provided more information about the process. As a result, no gas/melt interface echo was observed with the new setup.

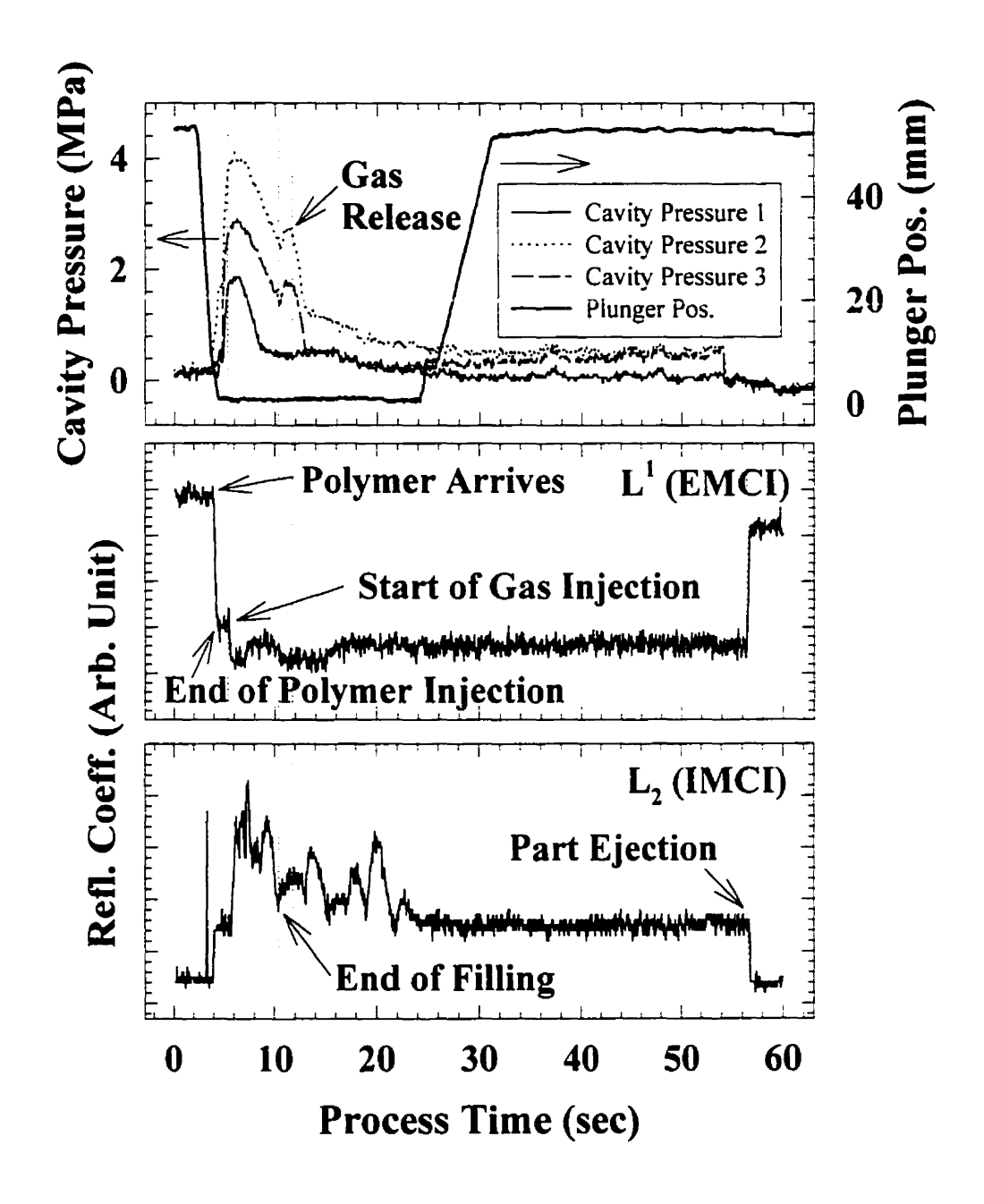


Fig. 3-10: Ultrasonic on-line monitoring of GAIM - A complete part, monitored from location "B": Top: Cavity pressures and plunger position. Middle: Reflection coefficient ( $\Gamma$ ) for the echo ( $L^1$ ) from external mold cavity (EMCI). Bottom: Reflection coefficient ( $\Gamma$ ) for the echo ( $L_2$ ) from internal mold cavity (IMCI)

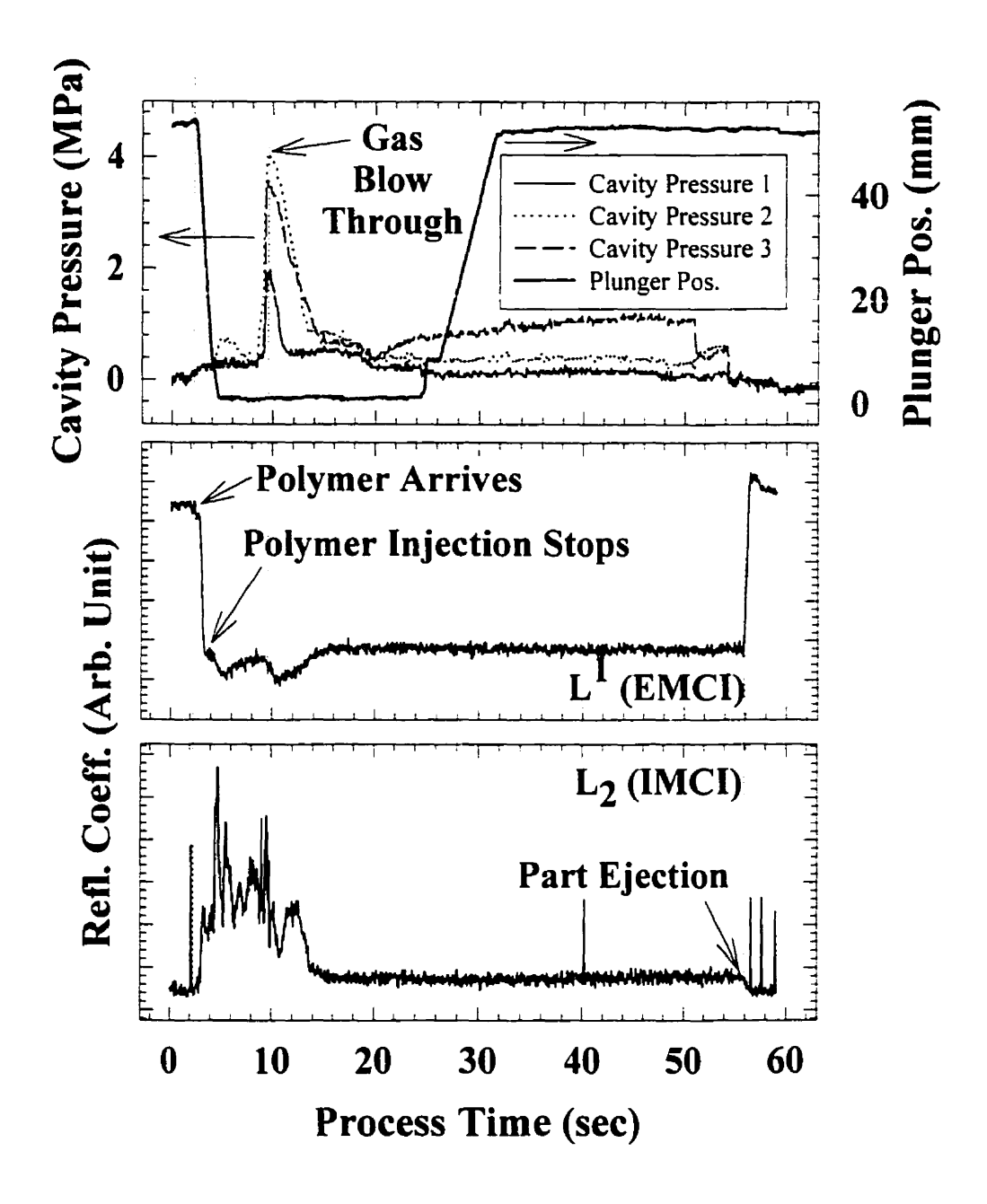


Fig. 3-11: Ultrasonic on-line monitoring of GAIM - Gas blow-through case, monitored from location "A": Top: Cavity pressures and plunger position. Middle: Reflection coefficient ( $\Gamma$ ) for the echo ( $L^1$ ) from external mold cavity (EMCI). Bottom: Reflection coefficient ( $\Gamma$ ) for the echo ( $L_2$ ) from internal mold cavity (IMCI)

Gas pressure was also varied under the new setup. In the run producing complete parts, the maximum gas pressure was set to 20.68 MPa. In another run, the maximum gas pressure was raised to above 31.03 MPa. As a result, gas blew through the molded part. Figure 3-11 shows the recorded cavity pressures, plunger position, and ultrasonic signals for this gas blow-through case. It can be seen that pressure sensors clearly identified the time when gas blow-through occurred. This was confirmed by observing sudden drops in both gas and cavity pressures. Meanwhile, from the reflection coefficient of L<sup>1</sup>, the effect of gas blow-through (an increase due to pressure drop) was also observed, as identified in Figure 3-11.

#### 3.3 Co-injection molding

In GAIM, echoes reflected from the external melt/gas interface can be seen since ultrasound is totally reflected at the melt/gas interface. In co-injection molding, rather than gas, another material is injected simultaneously or sequentially into the cavity. As a result, impedance mismatch exists at the interface between the co-injected materials. However, since the impedance mismatch between these two materials cannot be as large as that between melt and gas interface in GAIM, the amplitude of the echo reflected from the material interface in co-injection molded parts is small. Even though the amplitude is small, the interface and surface on the other side of the sample are still observable with ultrasound. Magda, *et al.* have demonstrated the detectability of interfaces in such co-injection molded part using ultrasonic techniques [64].

In this section, the co-injection molding process is not monitored on-line. Rather, the technique used by Magda is applied. Several molded parts with different proportions of two materials were used to study off-line the visibility of the interfaces, in an immersion tank. Figure 3-12 shows the top and bottom views of the co-injected part made by a 150-ton Engel co-injection machine shown in Figure 2-1. Materials used were acrylonitrile-butadiene-styrene copolymer (ABS) and ABS mixed with 2.8 % carbon (referred as mixed ABS from now). Different volumes of ABS were first injected, and

then mixed ABS was injected later. As a result, penetration of mixed ABS inside pure ABS was of different degrees. Figure 3-13 shows the cross-section of co-injected plates under study. These plates were chosen because when aligned from top to bottom, these plates represented different stages in a co-injection process. On-line monitoring of the co-injection process is possible if interfaces in such plates with different thicknesses of ABS layers can be identified.

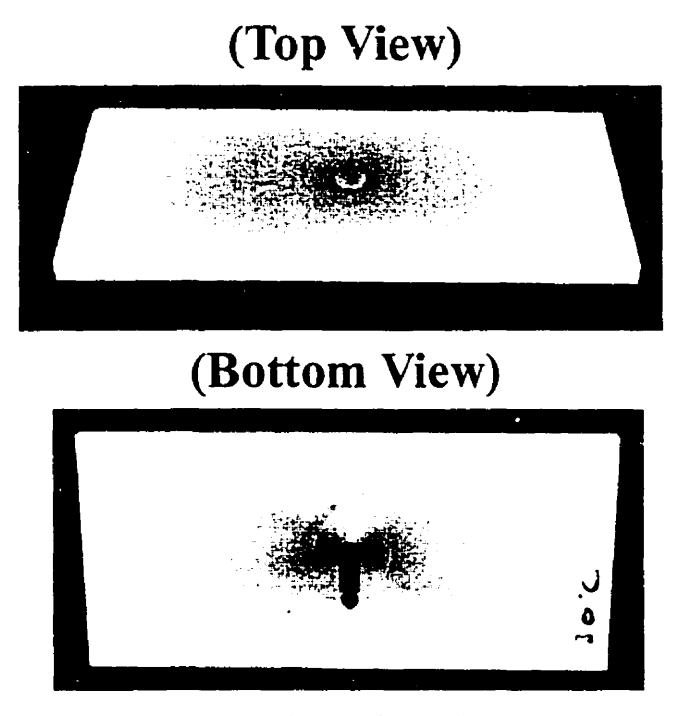


Fig. 3-12: Top and bottom views of co-injected plate under study

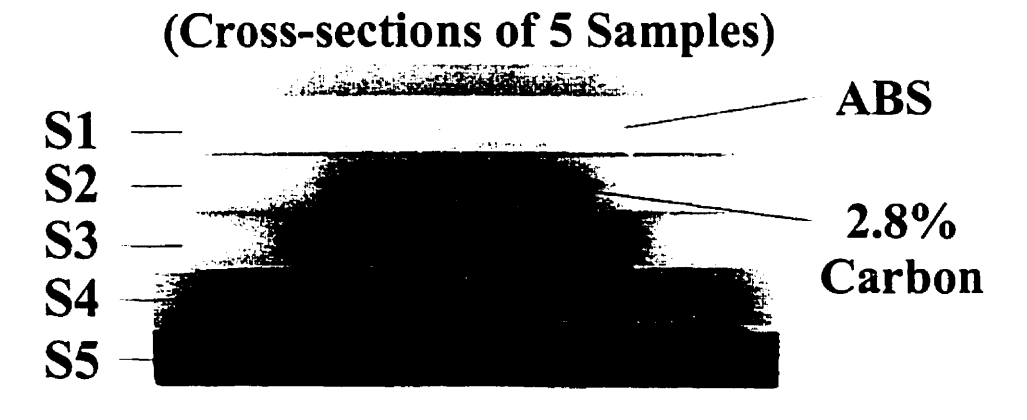


Fig. 3-13: Five co-injected samples (\$1~\$5) co-injected with different amounts of ABS and mixed ABS

Since no mixed ABS was present in S1, no interface echoes were expected. Similarly for S5, no interface echoes were expected. For S2, S3, and S4, two interfaces (one on top and one at bottom) were physically visible. From S2 to S4, mixed ABS occupied more volume, and therefore pure ABS was thinner in S4 than in S2. The off-line ultrasonic measurement was carried out using the immersion method (water was used as the couplant). Two (one from the top, and the other from the bottom) ultrasonic transducers (UTs) were used to detect the interfaces with the pulse/echo method. The setup is shown in Figure 3-14.

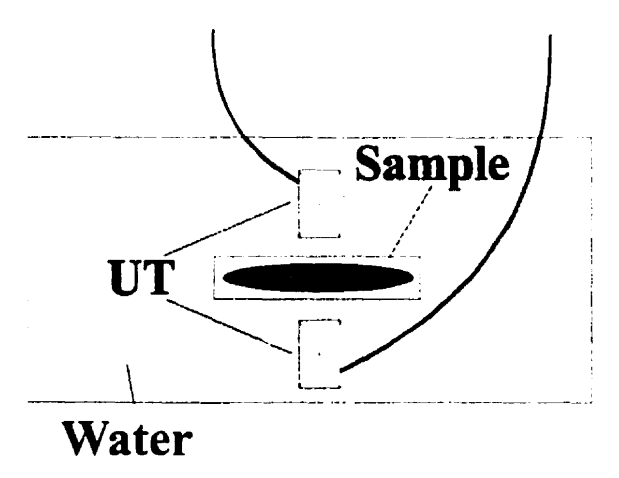


Fig. 3-14: Sample and ultrasonic transducers (UT) setup in immersion tank for interface measurement of co-injected plates

Figure 3-15 shows the result of off-line interface monitoring of co-injected plates by UTs from both the top and the bottom surfaces. Notice that not only the surface from the UT side was observed but also the echo reflected back from the surface on the other side of the sample. This means that, unlike GAIM in which polymer on the other side of gas layer cannot be monitored, in co-injection molding, UT installed on one side can monitor through the whole thickness of the molded part.

As for echoes from both interfaces, the interface echo close to the UT was monitored since UT was best aligned with this interface. If the interface on the far side is not parallel with the interface on the near side, echoes reflected from the interface on the far side might not be received. This means firstly that though amplitude from the interface

on the far side might not be strong, this echo can be detected by installing another UT on the other side of the mold. Secondly, this off-line observation indicates that in on-line monitoring when the interface is not parallel with the surface (cavity wall when inside the mold), the interface on the far side is difficult to monitor. However, if the interface is well developed (close to parallel), the echo from the far interface is observable, such as S4 examined from the bottom surface and illustrated in Figure 3-15.

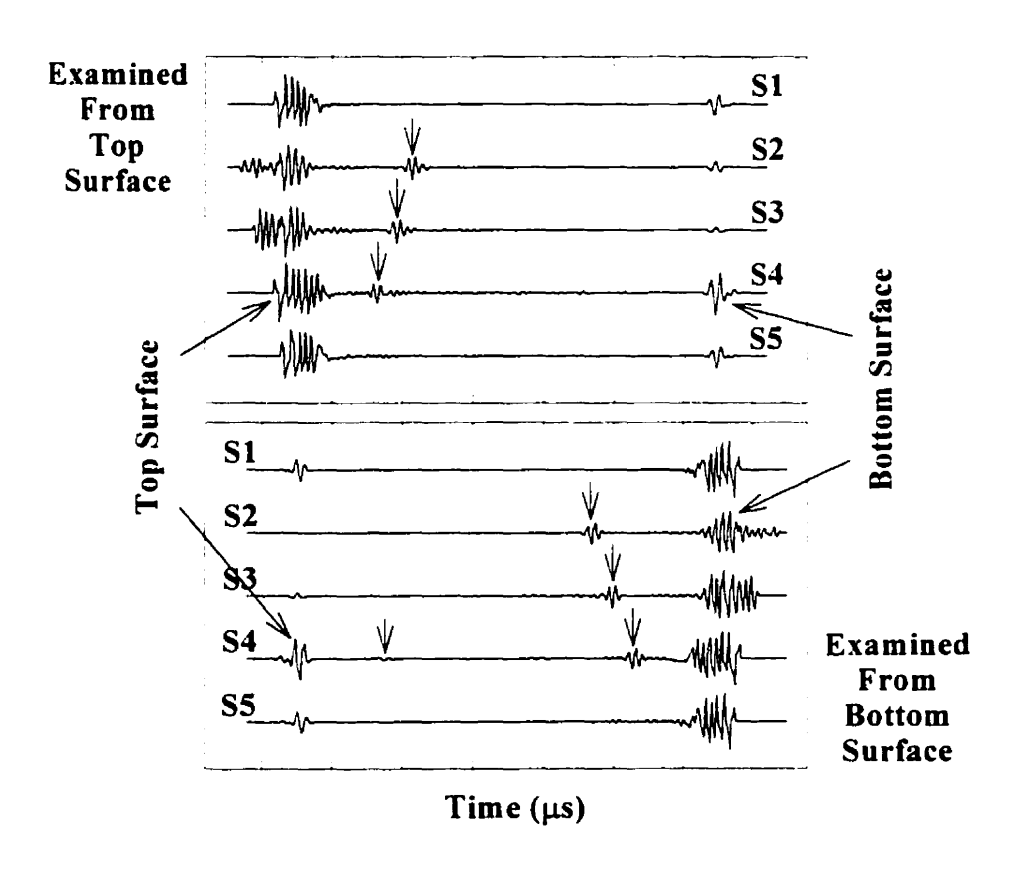


Fig. 3-15: Interface echoes (marked by arrows) observed in co-injected plates from both top and bottom surfaces

#### 3.4 Summary

In this chapter, attempts were made to monitor on-line gas-assisted injection molding using ultrasonic techniques. From knowledge of on-line monitoring of the conventional injection molding process presented in chapter 2, several features during the GAIM process were monitored with reflection coefficient ( $\Gamma$ ) plots of echoes reflected from different interfaces. Figure 3-16 shows, from top to bottom, the  $\Gamma$  plot of echoes from EMCI, IMCI, and EMGI.

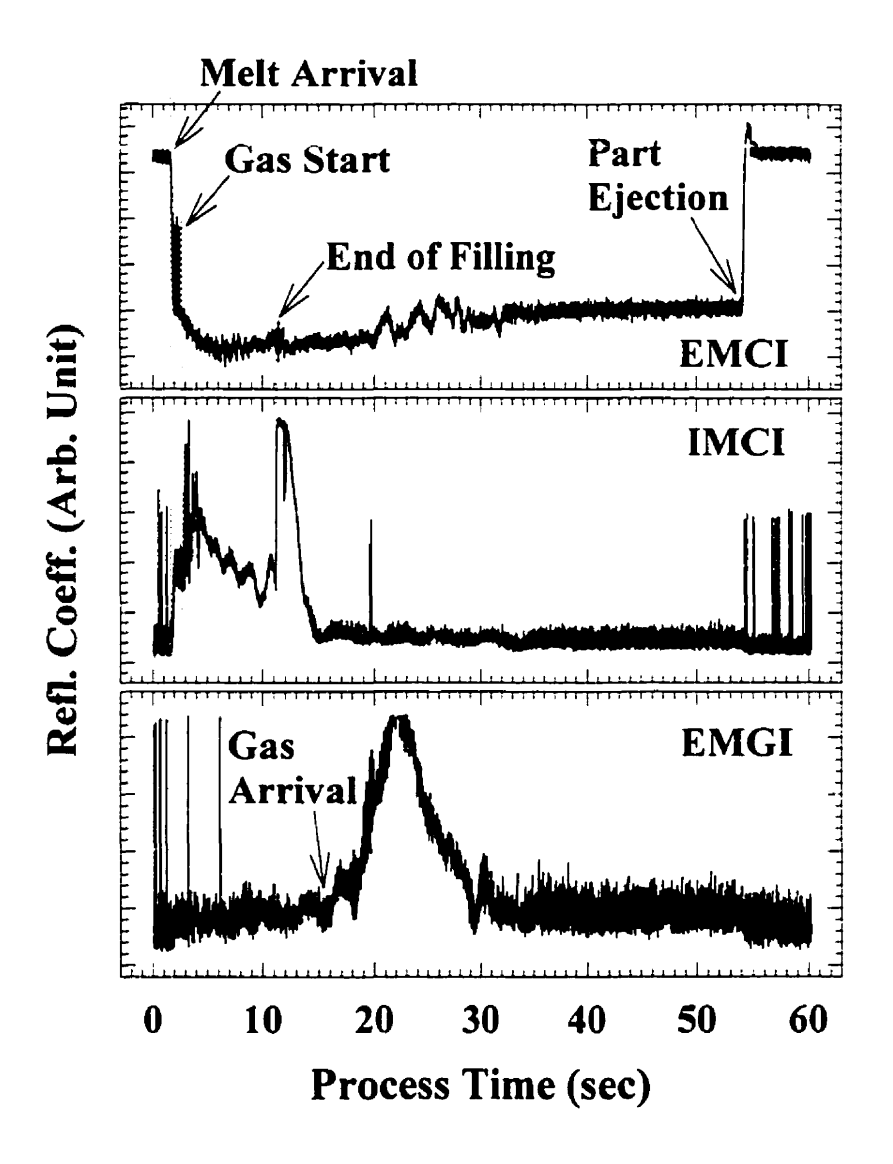


Fig. 3-16: Summary of on-line monitoring of GAIM using reflection coefficient  $(\Gamma)$  plots. The three  $\Gamma$  plots are for echoes  $(L^1, L_2, L_{2g})$  reflected from the external mold/cavity interface (EMCI), the internal mold/cavity interface (IMCI), and the external melt/gas interface (EMGI)

From such  $\Gamma$  plots, polymer melt arrival, start of gas injection, end of gas-assisted cavity filling, gas arrival and part ejection were monitored on-line using ultrasonic techniques. Since gas pressure could not be controlled with our discontinuous gas generation unit, gas pressure dropped during the process. The drop in gas pressure was inferred from the reduction in  $\Gamma$  for echoes from IMCI and EMGI, and the increase in  $\Gamma$  for the echo reflected from EMCI. With a short gas holding time, release of gas pressure was also observed. Detection of gas blow-through using ultrasonic techniques was also demonstrated.

Due to the non-invasive nature of ultrasonic techniques, array implementation to monitor local gas arrival can be used to monitor gas penetration inside the molded part. Insufficient filling can also be detected, if the end of filling is not observed. If neither pressure nor temperature information of the polymer is known, the wall thickness is difficult to determine.

The capability of ultrasound to monitor off-line the interface between different materials in co-injected parts has also been demonstrated. Though parallelism of the interfaces with cavity walls on both sides is an issue. UTs can be installed on both internal and external molds to monitor interfaces from both sides.

### Chapter 4:

# Ultrasonic Temperature Measurement

#### 4.1 Introduction

The temperatures of the melt and the mold are very important in controlling properties and dimensions of molded parts in the injection molding process. Thermodynamic properties, *e.g.*, viscosity and density, of the molten polymer change with melt temperature. On the other hand, mold temperature is very important in determining part dimensions, part quality, the cooling time, and economy of the process [27]. Therefore, the cavity wall temperature and temperature (average and profile) of the molded part are of great interest.

In this chapter, the application of ultrasonic techniques in temperature measurements is discussed. Two types of ultrasonic temperature probes are calibrated and used to perform temperature measurement. It is noted that the focus here is not the development of the probe, but rather its application in temperature measurement. Surface temperature of the ultrasonic probe, which has close relation to the temperature of the adjacent molten polymer in the extrusion process, is measured with the calibrated probe and compared with conventional temperature sensors used in injection molding machines. Finally, a comparison of performance between ultrasonic and conventional temperature probes is presented.

### 4.2 Ultrasonic techniques in temperature measurement

Ultrasonic techniques have been used in measuring the average melt temperature inside nozzle, barrel, and die during extrusion [35~37]. The tripartite (P-V-T) relationship

of the part inside the melt is again used. With known dimensions of the barrel and time delay for round trip ultrasonic propagation, average (over the path of the ultrasonic wave) ultrasonic velocity inside the polymer melt is obtained. If the pressure is also monitored, from the tripartite relationship, the average (over the path of the ultrasonic wave) temperature of polymer melt inside the barrel can be determined. The temperature thus derived is satisfactory when the temperature and, in turn, ultrasonic wave velocity inside the polymer melt are quite uniform.

Meanwhile, most commercially available and high performance (high electromechanical coupling contact and broad bandwidth) piezoelectric-type UTs cannot sustain temperatures higher than 50°C for long periods of time (e.g. hours or days). If an ultrasonic temperature probe is to be used in monitoring temperature not only at low but also at elevated temperatures, either a new type of transducer is needed [36, 65] or means must be developed to isolate the transducer from these harsh conditions [66]. Due to the current unavailability of convenient, high performance UTs and couplants, a classic approach was adopted by inserting a metallic ultrasonic waveguide (buffer rod) between the UT and the measuring point [32]. Advantages of the clad buffer rod include significantly improved signal-to-noise ratio (SNR), elimination of trailing echoes by cladding, good ultrasonic energy guidance, easy fabrication, and machinability [67~70]. After wrapping air cooling pipes at the end where the UT is installed, temperature can be brought down to within 50°C so that the above-mentioned conventional UT and couplant can be used. This technique has been demonstrated in monitoring the die casting and graphite/epoxy composite curing processes [69,70]. The buffer rod (referred to as ultrasonic probe from now on) is modified in this study to demonstrate another application for measuring temperature.

Lynnworth and others have demonstrated the feasibility in measuring temperature using multizone ultrasonic waveguides [71~73]. In those approaches, either multi-discontinuities were created, or simply both ends of a sensing element were used for reflection of ultrasound. In this study, in order to measure the temperature of the molten

polymer in extrusion, small discontinuities were created close to the end of the ultrasonic probe, which was flush with the molten polymer. Figure 4-1 shows the schematic drawing with the ultrasonic probe installed inside the extrusion die. "a" and "b" were the two discontinuities created (450 µm width slots as shown in Figure 4-2). Figure 4-2 shows the location of the two discontinuities and the ultrasonic probe after machining. The machinability of the cladding makes it possible to fabricate an ultrasonic probe with the same geometry as other conventional temperature and pressure probes. Figure 4-3 shows a machined ultrasonic probe together with a Dynisco pressure probe PT462E-5M and a Dynisco temperature and pressure probe TPT463E-1M. The two commonly used conventional probes can therefore be replaced easily by the new ultrasonic probe.

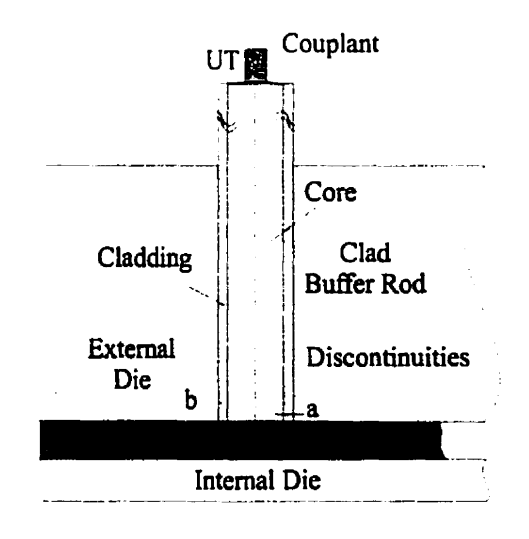


Fig. 4-1: Slot ultrasonic probe with two discontinuities inside the die

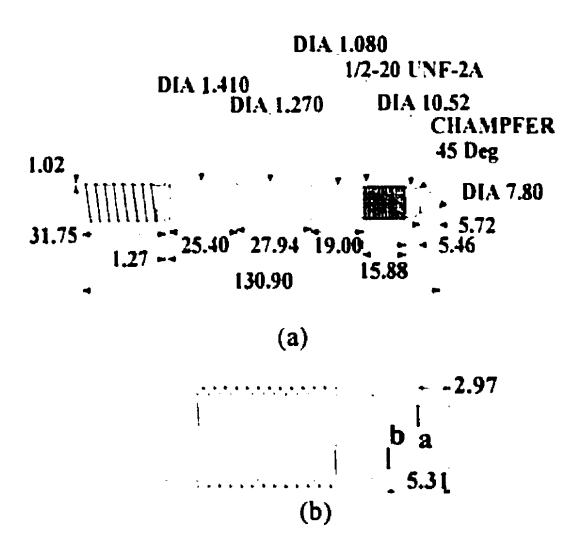


Fig. 4-2: Dimensions of the slot probe and discontinuities "a" and "b"(in mm)

It has been demonstrated in section 2.5 that ultrasonic wave velocity depends on both temperature and pressure (the tripartite relationship) of the polymer melt. Provided that the pressure does not change very much during extrusion, ultrasonic wave velocity depends only on the temperature of the material. The ultrasonic wave property in metal is no exception. Since the distances between the probing end and discontinuity "a" and between the two discontinuities ("a" and "b") are short (a couple of mm's), a linear temperature distribution is assumed:

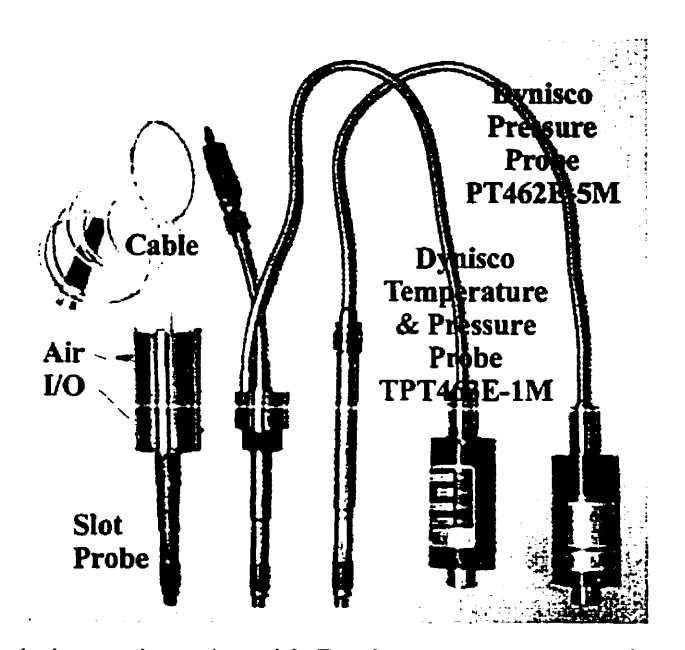


Fig. 4-3: Machined ultrasonic probe with Dynisco temperature and pressure sensors

$$T(x) = Ax + B \tag{4.1}$$

where B is the surface temperature at the probing end of the probe and A is the temperature gradient along the distance x from the probing end. As a result, the measured time delay  $\tau_1$  (between the echo reflected from the first discontinuity,  $L_a$ , and the echo reflected from the end of the ultrasonic probe,  $L^1$ ) and  $\tau_2$  (between the echo reflected from the first discontinuity,  $L_a$ , and the echo reflected from the second discontinuity,  $L_b$ ) are given by:

$$\tau_1 = 2 \times \int_0^{d_1} \frac{dx}{V(T)}$$

$$\tau_2 = 2 \times \int_{d_1}^{d_2} \frac{dx}{V(T)}$$
(4.2)

where  $d_1$  is the distance between the probing end of the ultrasonic probe and the first discontinuity, and  $d_2$  is the distance between the first and the second discontinuities. Time delays  $\tau_1$  and  $\tau_2$  can be used to obtain the surface temperature (i.e., coefficient B in

Equation 4.1) and heat flux (i.e., coefficient A in Equation 4.1) at the contacting surface of the ultrasonic temperature probe.

Another type of ultrasonic probe with modified discontinuities is shown in Figure 4-4. Instead of making slots into the core, the core is made with two steps on the probing end of this new ultrasonic probe. This new ultrasonic probe (referred from now on as the step ultrasonic probe) has the following advantage over the previous one (referred from now on as the slot ultrasonic probe): Since the slots cut into the core in the slot ultrasonic probe create asymmetry in the probe, the probe under thermal expansion might be distorted unpredictably. As a result, the distance between discontinuities is difficult to determine. At the same time, some ultrasonic wave will be reflected back and forth between discontinuities, and thus create more noise in reflected echoes.

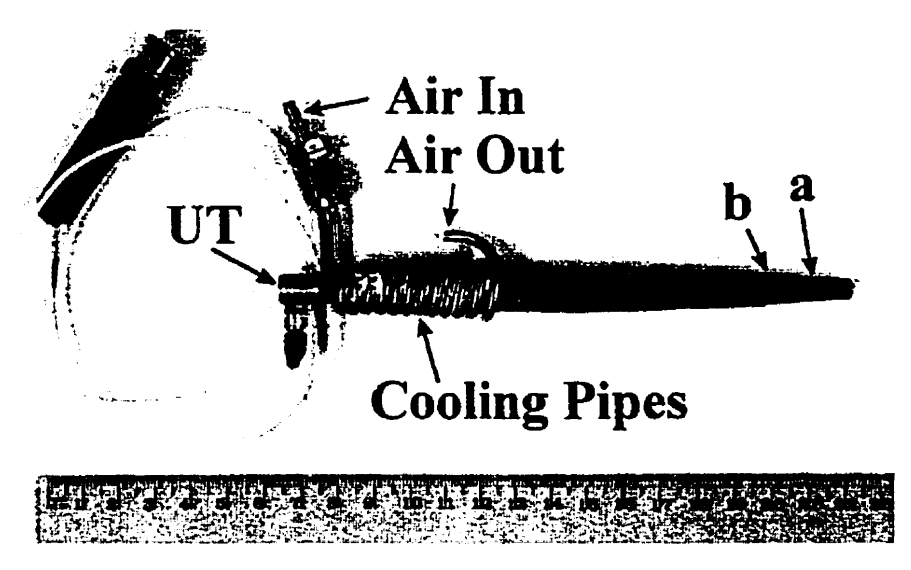


Fig. 4-4: Step ultrasonic probe with discontinuities "a" and "b"

On the other hand, the step ultrasonic probe is more symmetric in geometry, and as a result, a more symmetric deformation under thermal expansion is expected. The distance between the steps can be clearly defined, and leads to an improved measurement accuracy. Figure 4-5 shows the recorded echoes from the probing end  $(L^1)$  and the two steps  $(L_a$  and  $L_b)$  with both the uncladded and the cladded step buffer rod. It can be seen

first that the signal-to-noise ratio, SNR, as claimed before, is significantly improved due to the cladding. Trailing echoes are also significantly reduced.

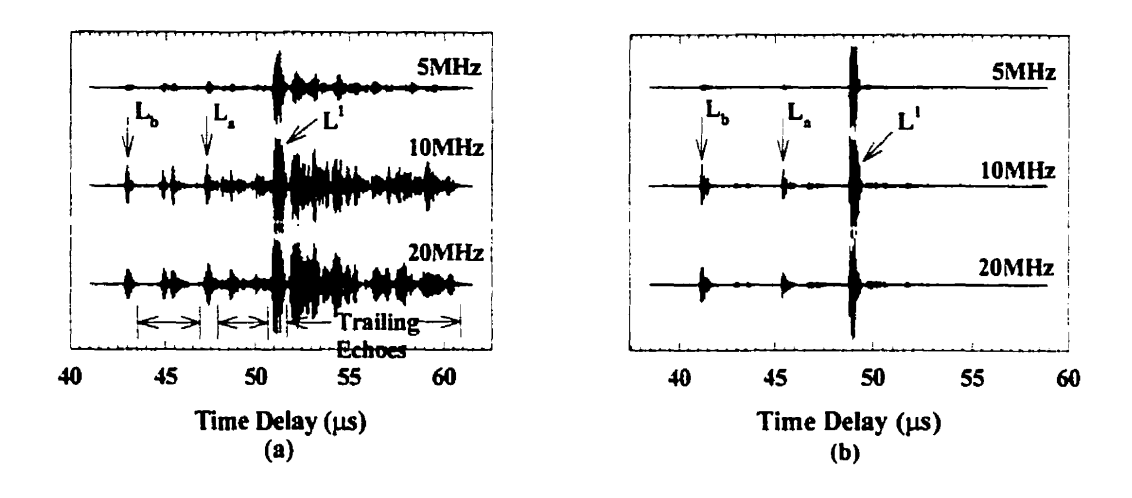


Fig. 4-5: L<sup>1</sup>, L<sub>a</sub>, and L<sub>b</sub> from (a) uncladded and (b) cladded step probe using UTs with different central frequencies

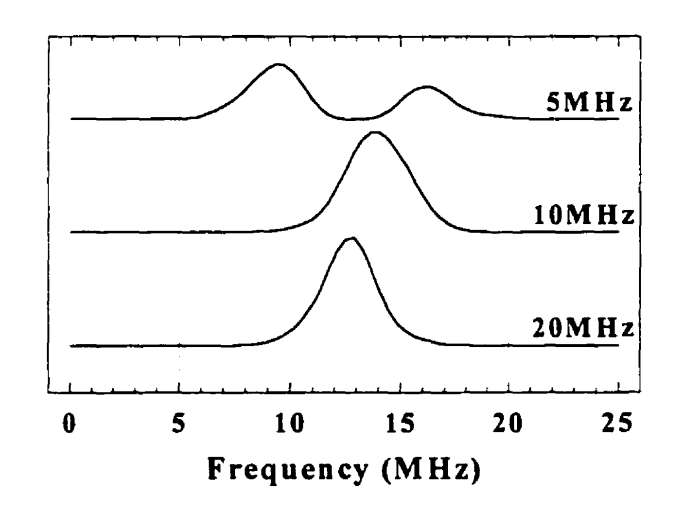


Fig. 4-6: Frequency spectrum of  $L^1$  with cladded step probe

Another thing worthy of notice is that the resolution of L<sub>a</sub> and L<sub>b</sub> obtained by a 5MHz longitudinal wave UT is not good. The reason is that the buffer rod itself functions like a band pass filter. Signals with either high or low frequencies may be attenuated. Figure 4-6 shows the frequency spectrum of L<sup>1</sup> obtained with UTs of different central

frequency, applied to the step probe shown in Figure 4-4. It can be seen that with 5 and 20 MHz longitudinal UT, signals with the central frequency are attenuated very much. Therefore, the optimal UT suitable for this step ultrasonic probe should be 10 MHz UTs.

#### 4.3 Calibration of ultrasonic probe

In order to determine the temperature with high accuracy, the ultrasonic probe must be calibrated. Since in the extrusion die, the pressure was not significantly different from atmospheric pressure, the calibration done in this study was only at atmospheric pressure. Therefore, the calibration process was to produce a calibration curve between ultrasonic velocity and temperature for the specific ultrasonic probe. Since the ultrasonic probe is composed of a core and an outside cladding of different material, the thermal conductivity for the joint entity as a whole cannot be the same as either the core or the cladding material alone. Therefore the calibration curve must not be interpreted as a material property of either the core or the cladding material, but rather the property of the ultrasonic probe under calibration.

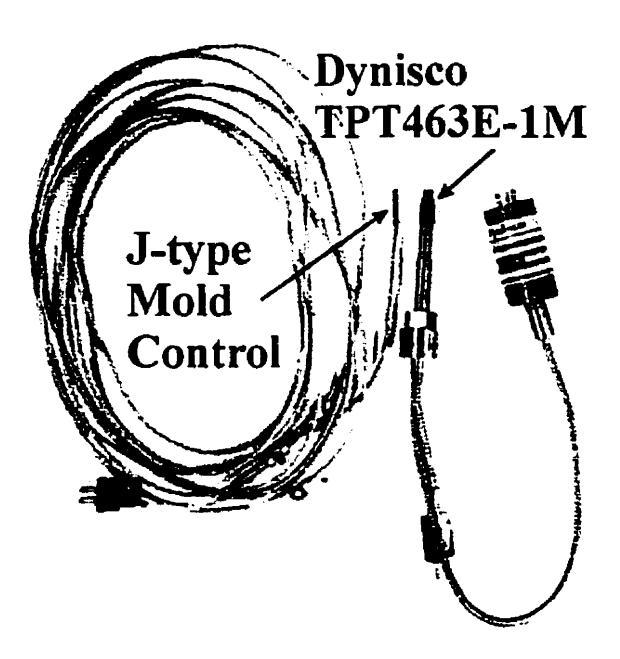


Fig. 4-7: Two conventional temperature sensors used in injection molding machines

At the same time, two other temperature measurement devices (thermocouples) used in industrial machines were also calibrated with the two ultrasonic probes. Figure 4-7 shows the two temperature probes. On the right is a Dynisco TPT463E-1M temperature probe, and on the left is another J-type thermocouple (referred to as 'mold control' from now on) manufactured by Ri Ka Industrial Co., Ltd., used in controlling mold temperature for a PLACO co-extrusion blow molding machine. These two J-type-thermocouple outputs were not read by high precision multi-meters, but rather by the same temperature display used in the extrusion machines. This was done so that the thermocouple was not calibrated alone, but with the display device.

#### 4.3.1 Setup

The calibration of the ultrasonic probes was carried out at the Institute for National Measurement Standards, National Research Council (INMS-NRC). To calibrate a temperature measuring device, a reference thermometer to indicate temperatures on a standard scale is necessary. The temperature probe under calibration and the reference thermometer are placed in a controlled environment in which the temperature probe and the reference thermometer can be brought to the same temperature [74]. At INMS-NRC, the reference thermometer was a 100 $\Omega$  platinum resistance temperature detector (PRTD), and the controlled environments were stirred water and oil baths. For temperatures under 100°C, the water bath was used. For temperatures between 100°C and 280°C, the oil bath was used as the controlled environment. With the combination of the PRTD and the specifically designed high performance oil bath, the accuracy of the overall system was better than 0.01°C (0.02°F). The means to record the signal from the ultrasonic probe was a data acquisition system. Figure 4-8 shows the water and oil baths, with the acquisition system for ultrasonic probes in the front. Figure 4-9 shows the setup with both the slot ultrasonic probe and PRTD inside the oil bath. Though not shown, the step ultrasonic probe and the two other thermocouples were calibrated the same way as the slot ultrasonic probe.

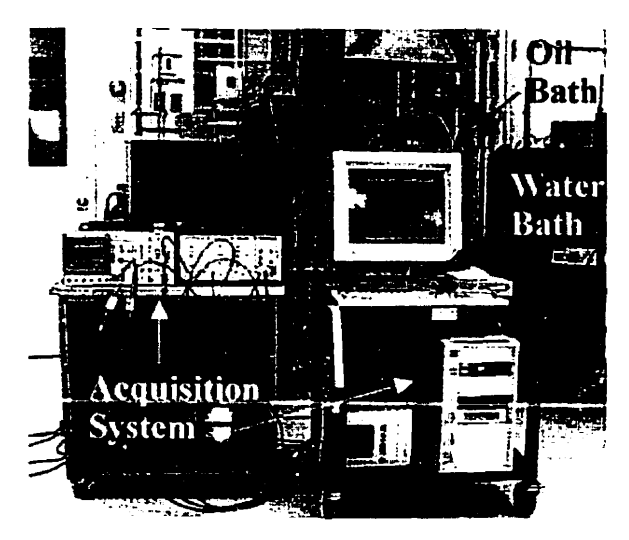


Fig. 4-8: Water and oil bath at INMS-NRC with acquisition system used in calibration of temperature probes

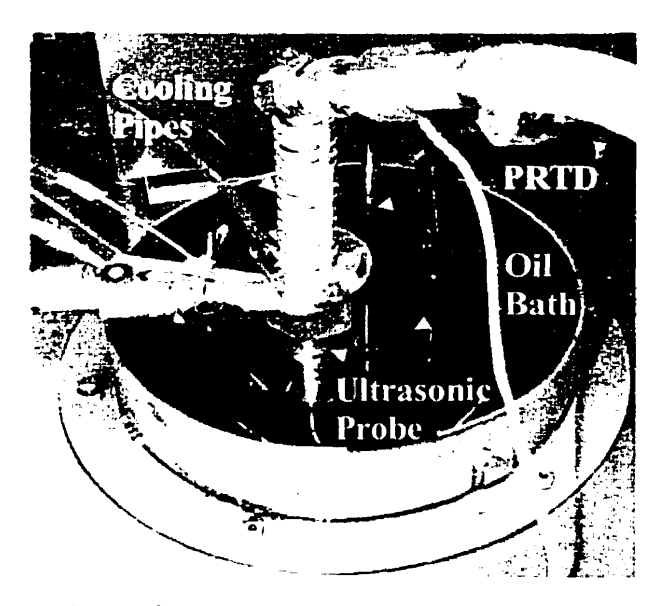


Fig. 4-9: Setup for calibration of ultrasonic temperature probe

### 4.3.2 Steady state calibration

The calibration curve was obtained in steady state, *i.e.*, sufficient time was allowed for water bath, oil bath, ultrasonic probes, PRTD, and the two J-type-thermocouples to reach a steady state. Ultrasonic probes and PRTD readings were taken when the readings from the PRTD did not drift more than 0.02°C per minute. To obtain

the calibration curve between ultrasonic wave velocity and temperature, echoes from the ultrasonic probes and temperature readings indicated by the PRTD were recorded.

Figure 4-10 shows the calibrated readings from the two conventional thermocouples under steady state conditions. The mold control J-type thermocouple readings were very close to PRTD readings. The difference between the two were less than 1.1%. On the other hand, readings from the Dynisco temperature probe deviated more from the PRTD readings. The differences in readings from Dynisco and PRTD were less than 2.8%. Even though a deviation was observed, the error was still within 4% accuracy in temperature measurement, a typical accuracy level for thermocouples.

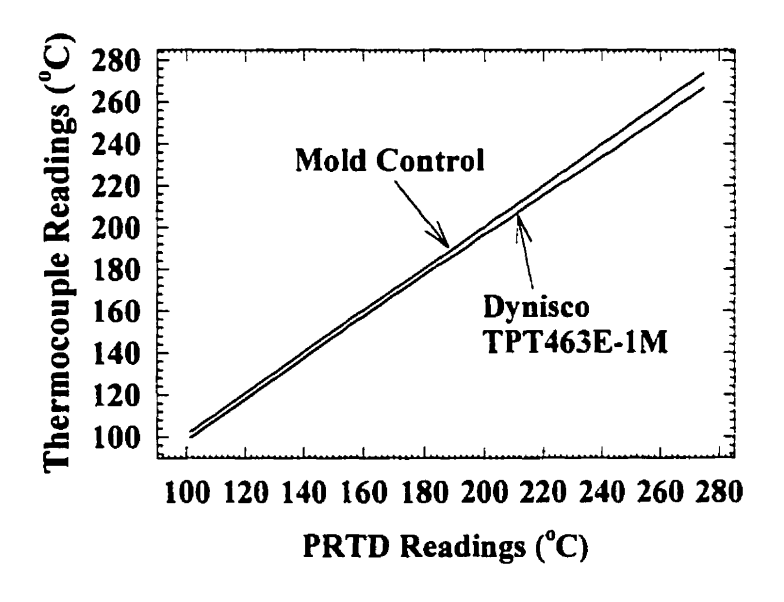


Fig. 4-10: Calibration curves for the two conventional temperature sensors (Dynisco TPT463E-1M and J-type mold control thermocouple)

Figure 4-11 shows the calibrated ultrasonic wave velocity *versus* PRTD temperature readings using UTs with central frequencies of 5, 10, and 20 MHz for slot ultrasonic probe. The calibration was concentrated around 200°C, since the slot ultrasonic probe was later used in temperature monitoring in an extrusion process in which the polymer melt temperature was around 200°C.

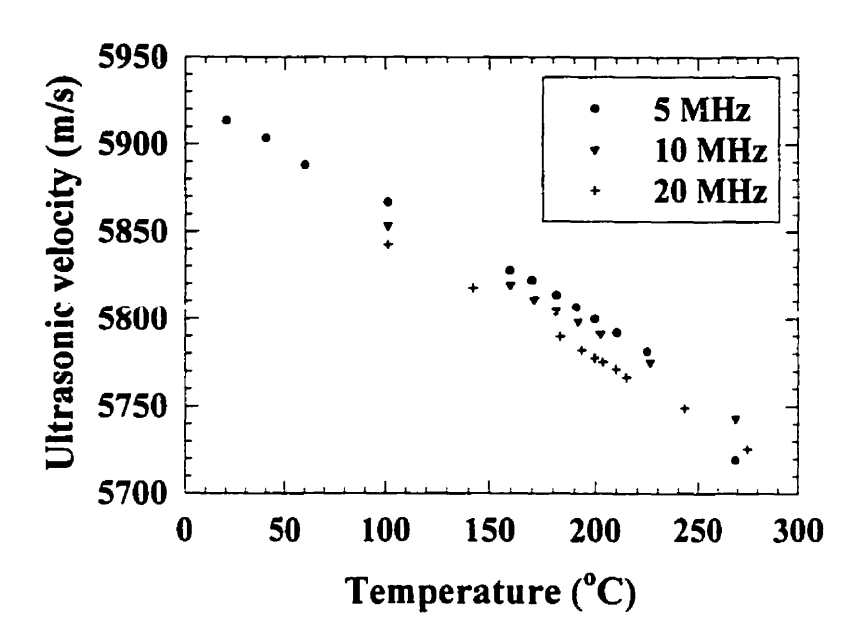


Fig. 4-11: Calibrated ultrasonic wave velocity inside the slot ultrasonic probe versus PRTD temperature readings, using ultrasonic transducers (UTs) of different central frequencies

A linear relationship between the ultrasonic wave velocity and temperature was expected. As can be seen in Figure 4-11, the calibrated curve was most linear using the 20 MHz UT, while the curve obtained using 5 MHz UT was least linear. Since ultrasonic wave velocity was obtained through time delay, and accuracy in determining time delay was affected by the SNR as addressed in section 4.2, as recommended there, broadband UTs should be used in temperature measurement.

### 4.3.3 Temperature measurement in fluids

Another set of tests was carried out by inserting the cooled ultrasonic probes and the two thermocouples into the stabilized oil bath. This is commonly referred to as temperature measurement in fluids. In this test, the step ultrasonic probe was tied together with the Dynisco thermocouple, and the slot ultrasonic probe was tied with the mold control thermocouple. Figure 4-12 shows the results when the oil bath was set to 100°C. It can be noticed that the mold control thermocouple stabilized faster than the Dynisco thermocouple, since the diameter was smaller (referred to Figure 4-7).

Since no instrument responds instantly to a change in its environment, it is common to characterize the response of a temperature sensor by a first order thermal response time  $\alpha$ . If an element is inserted into a constant temperature environment, which is the case of the test demonstrated in this section,  $\alpha$  is the time required for the temperature difference between the environment and the element to be reduced to 1/e of the initial difference. Response time can therefore be defined as the time required for temperature sensor readings to reach 63.2% of the steady state value [74]. Response times were determined for all four temperature probes. Table 4-1 shows the response times for temperature measurement in fluids for the four temperature probes. However, care must be taken in interpreting the response times derived from this test.

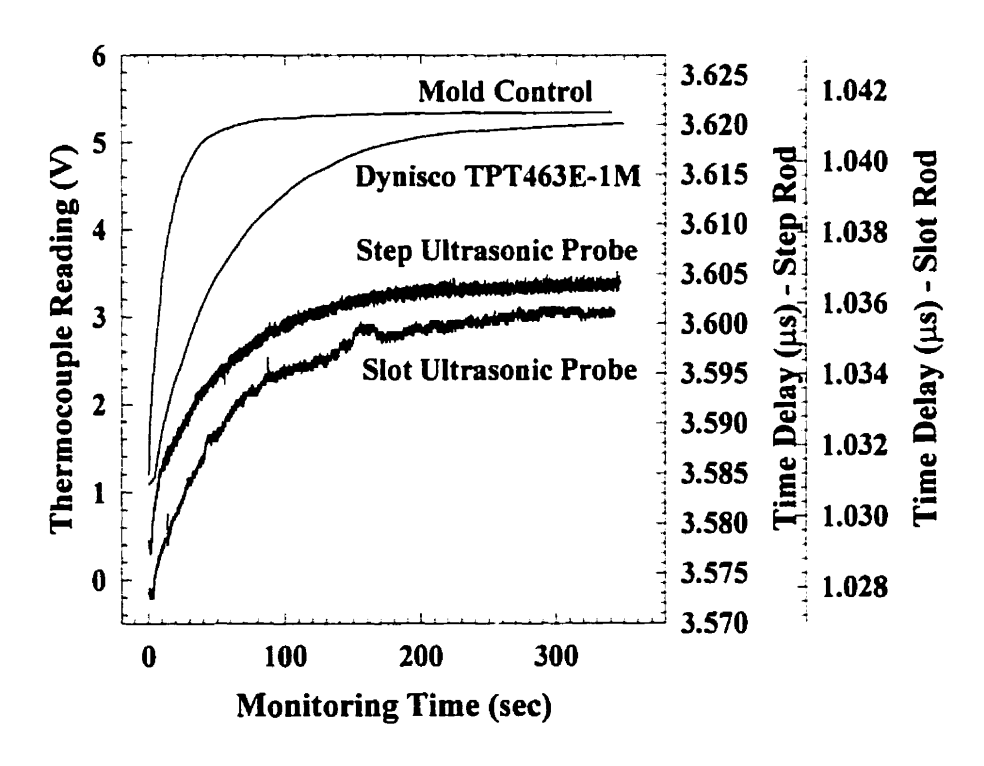


Fig. 4-12: Response to step temperature change for all temperature sensors

Table 4-1: Response times for various temperature probes in fluid temperature measurement

Temperature Sensor	Response Time (sec)
J-type Mold Temperature Control	12.68
Dynisco TPT463E-1M	58.28
Step Ultrasonic Probe	44.45
Slot Ultrasonic Probe	56.47

Though the response was transient, temperature measurement in fluids was not the same as the transient surface temperature measurement. For transient surface temperature measurement, heat is conducted into temperature probes from the contacting surface alone. However, for the test demonstrated here, temperature probes were inserted into an environment at uniform temperature, and heat was conducted not only from the probing end of temperature probes, but also from all sides embedded in the constant temperature environment. Therefore, the response time derived from Figure 4-12 should not be interpreted as the response time for transient surface temperature measurement for any of the four thermocouples.

Similarly for ultrasonic probes, the result only verifies that like thermocouples, when an ultrasonic probe is inserted into an environment of different temperature, the transient effect is considerable. In the demonstrated case, the time for the ultrasonic signal to settle  $(5\alpha)$  was 3.7 minutes for the step probe and 4.7 minutes for the slot probe. This is reasonable, since the step probe has a smaller diameter than the slot probe. This result implies that the settling time in transient surface temperature measurement might also be several minutes.

Another observation is that the response of the step probe was more stable than the slot probe. The instability in time delay measured from the slot probe might result from the aforementioned asymmetry in probe geometry. The asymmetry caused the nonuniform thermal expansion at the tip of the slot probe. As for the step probe, more stable time delays were observed due to its symmetry in geometry.

# 4.4 Temperature measurement in polymer extrusion

The calibrated slot ultrasonic probe with 5 MHz UT, and the Dynisco temperature probe (TPT463E-1M), together with the Dynisco pressure probe (PT462E-5M), were installed in the extrusion die on a PLACO co-extrusion blow molding machine. These probes were installed at symmetric positions in order to compare temperature readings from the Dynisco temperature probe and the slot ultrasonic probe. The setup is shown in Figure 4-13.

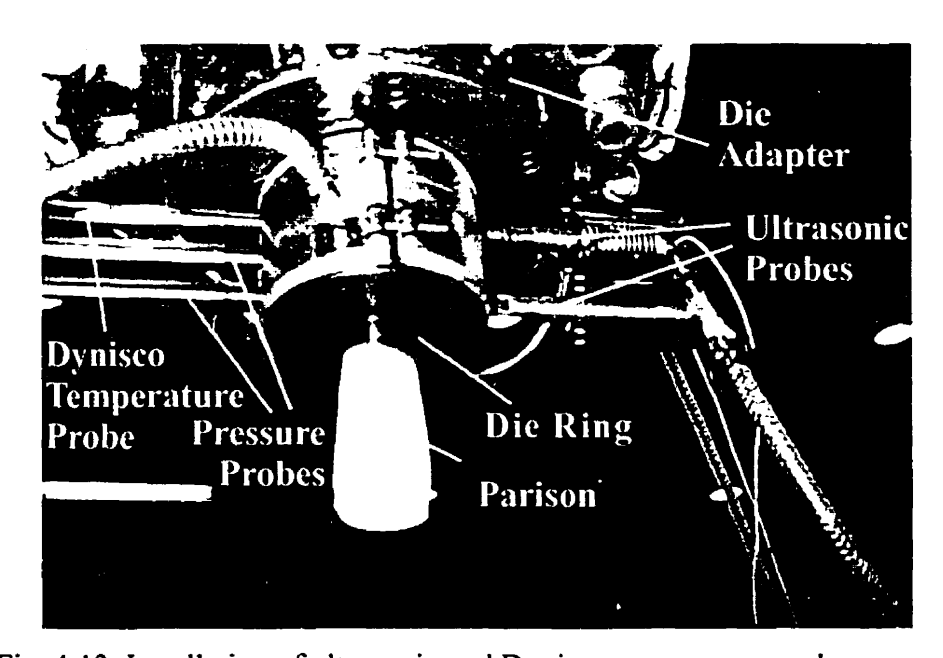


Fig. 4-13: Installation of ultrasonic and Dynisco temperature and pressure probes in the die of the extruder on a PLACO co-extrusion blow molding machine

Figure 4-14(a) and (b) show the ultrasonic signal received before and after (with  $L^1$  saturated) the molten polymer arrived at the monitoring point.  $L^1$  was the echo reflected from the probing end of the slot ultrasonic probe.  $L_a$  and  $L_b$  were echoes

reflected from, respectively, the  $1^{st}$  and  $2^{nd}$  discontinuities. Time delay between  $L^1$  and  $L_a$  was used to determine the surface temperature at the probing end of the ultrasonic probe. With additional time delay between  $L_a$  and  $L_b$ , another temperature and in turn the heat flux can be determined and used to inversely calculate the temperature profile inside the polymer. The determination of the temperature profile inside the polymer using an inversion algorithm is the subject of another study. After molten polymer arrives, the time delay between  $L^1$  and  $L_2$  ( $1^{st}$  round trip echo reflected from the other side of die wall), or  $L_2$  and  $L_4$  and so on, can be used to determine the average temperature of the molten polymer.

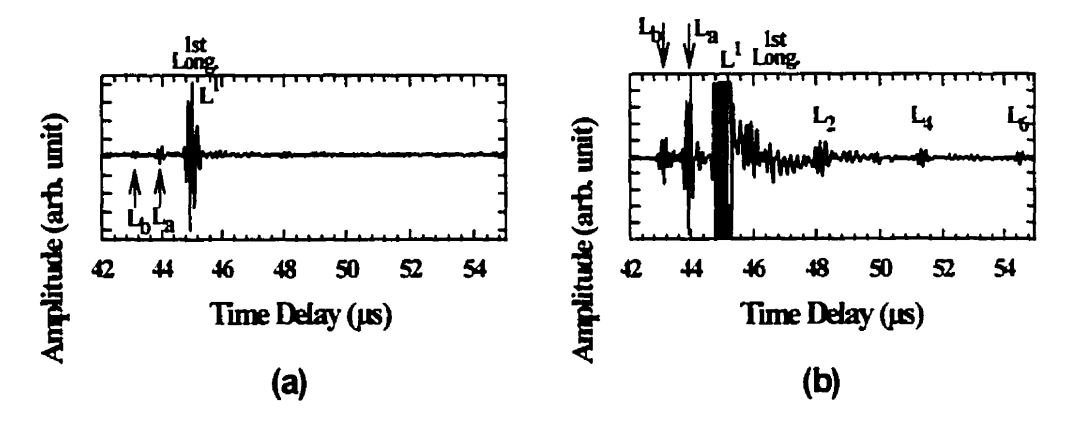


Fig. 4-14: Ultrasonic signals received (a) before and (b) after molten polymer arrives at the monitoring point using slot ultrasonic probe

The Dynisco temperature readings has a shift bias of 2.5 to 4.0°C, as shown in Figure 4-10. A digital compensator is introduced to compensate for the Dynisco temperature shift bias as follow [77]:

DCR=
$$1.163570299 \times 10^{-5} \times DR^{5} - 1.150703853 \times 10^{-2} \times DR^{4}$$
  
+ $4.548466541 \times DR^{3} - 8.98261 \times 10^{2} \times DR^{2}$  (4.3)  
+ $8.862907195 \times 10^{4} \times DR - 3.49508296 \times 10^{6}$ 

where DCR (°C) is the corrected Dynisco temperature reading, and DR (°C) is the original reading read by the thermocouple. The range of application for this digital compensator is between 190 and 205°C.

With the calibrated ultrasonic wave velocity and temperature curve shown in Figure 4-11, the surface temperature at the probing end of the slot ultrasonic probe could be determined. The time delay obtained from the ultrasonic probe was smoothed out by a real-time Kalman filter [75,76], and Equations 4.2 were solved to yield the surface temperature at the probing end. A shift bias of 32.5 °C was observed in the ultrasonic temperature reading. This bias might be caused by the electronics, the thermal expansion of the discontinuities (the slots), and the size (both width and depth) of the slots. After correcting the shift bias, ultrasonic temperature readings are in good agreement with corrected Dynisco temperature readings. Figure 4-15 shows the temperature measured by both the slot ultrasonic probe and the Dynisco temperature probe.

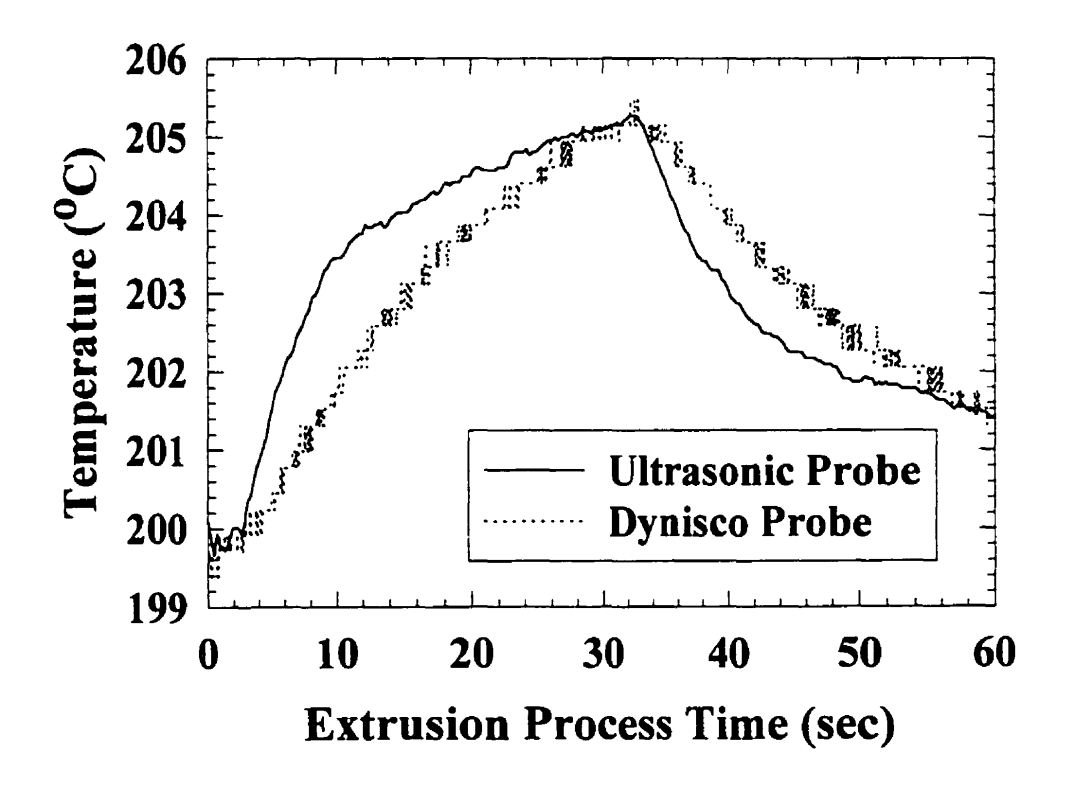


Fig. 4-15: Temperature readings from slot ultrasonic probe and Dynisco TPT463E-1M temperature probe during polymer extrusion process

It can be seen from Figure 4-15 that after extrusion started, both the slot ultrasonic probe and the Dynisco temperature probe detected a rise in temperature. This rise in

temperature was due to the arrival of hot polymer melt at the die ring. As polymer passed the die ring in the beginning, viscous dissipation resulted in a fast rise in temperature as detected by the ultrasonic probe. As steady state was approached, the viscous dissipation also leveled out, and the temperature rise slowed down. It can be seen that the ultrasonic probe is more sensitive to the heat flow (rate of temperature change) than the Dynisco temperature probe. This might indicate a faster response time to temperature change for the slot ultrasonic probe than the Dynisco temperature probe. Similarly, at around 30 seconds into the monitoring, when extrusion stopped, the slot ultrasonic probe showed more sensitivity in detecting the rate of temperature drop (to controlled die temperature) than the Dynisco temperature probe.

#### 4.5 Summary

In this chapter, an ultrasonic wave guide was adopted to be an ultrasonic temperature probe that could be used at elevated temperatures. It was machined so that it could be used to replace commercially available temperature probes (such as the Dynisco TPT462E-1M). After ultrasonic wave velocity was calibrated with a high-accuracy oil bath and platinum resistance temperature detector (PRTD), an ultrasonic wave velocity versus PRTD temperature readings calibration curve was established for the specific ultrasonic probe.

The calibrated ultrasonic probe was used together with the calibrated conventional temperature probe to monitor the surface temperature at the probe end during the polymer extrusion process. This temperature should be close to the surface temperature of the die ring. Though the true temperature of the wall of the die ring was not known, temperature readings from the ultrasonic probe were comparable to readings from the Dynisco temperature probe. Based on the knowledge of this chapter, a comparison between ultrasonic and conventional (Dynisco TPT463E-1M) temperature probes is summarized in Table 4-2.

Table 4-2: Comparison between ultrasonic and Dynisco TPT463E-1M temperature probes in temperature measurement

Slot Ultrasonic Probe	Dynisco TPT463E-1M
Intrusive	Intrusive
Easy to install and remove	Easy to install and remove
Difficult to calibrate	Easy to calibrate
Indirect temperature measurement	Direct temperature measurement
Fast response to temperature	Slow response to temperature
change	change
More sensitive to heat flow (rate	Less sensitive to heat flow
of temperature change)	
Capable of determining the	No such capability
average temperature of the	
polymer	
Capable of determining	No such capability
temperature profile in polymer	
(between cavity walls)	
Capable of monitoring elastic	No such capability
properties of polymers	

### Chapter 5:

### **Conclusions**

#### 5.1 Thesis summary

Ultrasonic techniques have been investigated in this thesis with the objective of developing new, fast, non-intrusive, and non-destructive sensors. These sensors performed on-line ultrasonic monitoring of the injection molding process in order to improve product quality, reduce energy consumption, costs and production cycle time, and verify the computer simulation. In particular, on-line monitoring of conventional and gas-assisted injection moldings were presented. All monitorings were carried out simply by attaching conventional ultrasonic transducers to the external mold wall and utilizing the pulse/echo technique. Ultrasonic signals after digitization were acquired and processed by various programs (virtual instruments) created under the LabView environment.

On-line monitoring of the injection molding process was discussed in chapter 2. The monitoring was carried out on a 150-ton Engel co-injection molding machine, and the material used was high-density polyethylene (HDPE). We placed ultrasonic transducers at locations where polymer melt were expected to arrive near the end of the injection phase. The detection of flow arrival at these locations can be used not only as an indicator for part completeness, but also a potential signal to control the switching-over of the injection molding process from injection to holding phase. The detection of flow front arrival is based on the change of the interface at the cavity walls. After material arrives, part of the ultrasonic energy is transmitted into the polymer. As a result, the reflection coefficient of the reflected interface echo reduces. By identifying the drop in reflection

coefficient of the reflected interface echo, local flow front arrival at the sensing location can be identified. The monitoring of part completeness has been demonstrated to be 100% successful using this technique.

Moreover, once the cavity is completely filled, cavity pressure starts to converge to the preset holding pressure, provided that switching-over is proper. This means pressures everywhere inside the cavity will experience a simultaneous change, though of different magnitudes. At locations far from the injection gate, the pressure increase is very large, while at points close to the gate, the change might be small. It has been demonstrated that such a distinct pressure change can be identified using ultrasonic techniques. This was verified by comparing the ultrasonic signals with the readings from a pressure sensor which was installed flush with the internal cavity wall. The results indicate that placing only one ultrasonic transducer far from the injection gate is sufficient to determine the completeness of the molded part.

If the injection molding process is not switched over from injection to holding phase in time, the high injection pressure will result in a pressure overshoot inside the cavity. When polymer is present inside the cavity, the ultrasonic wave is not only reflected from the external mold cavity wall, but also the transmitted part is reflected from the internal mold cavity wall. It has been demonstrated that, similar to the overshoot observed by pressure transducers, the reflection coefficient of the echo reflected from the internal mold cavity wall after traveling through the part also underwent an overshoot, as shown in Figure 2-11. Moreover, the overshoot indicated that not only the cavity pressure, but also the pressure of the molded part, experienced a sudden and dramatic change in a short (<0.3 sec) time period. Increased pressure in the polymer resulted in an increase in ultrasonic velocity. As a result, the time required for ultrasound to travel one round trip between cavity walls reduced. A smooth change in this time delay was observed for an injection molding run without overshoot. But the time delay for an injection molding run with overshoot consisted of two clear stages. The first stage was more dominantly influenced by the pressure rise due to the overshoot than by the cooling

of the part. The second stage was more dominantly influenced by the temperature drop due to cooling, as pressure was kept constant in the holding phase. Using the tripartite relationship shown in Figure 2-12, with determined average ultrasonic wave velocity and constant temperature in the short time period known, the average pressure overshoot in the molded part was found to be 23.1 MPa.

It was proposed in chapter 2 to measure the flow front speed using only one UT. Since ultrasonic energy is guided inside the steel mold, an effective sensing area can be assumed on the cavity wall. As the polymer flow front gradually advances and covers up the effective sensing area of the transducer, more and more energy (proportional to the size of the area covered) is transmitted into the polymer. As a result, the reflection coefficient for the echo reflected from the cavity wall will also reduce gradually. By identifying in the early section where the reflection coefficient drops, theoretically the flow front speed can be determined. However, the dimension of the effective sensing area was small (6.35 mm in diameter), and covered in 0.07 sec at 80 mm plunger speed. Limited by the acquisition time of 0.01 sec per acquisition, the current acquisition system does not provide adequate resolution to derive the flow front speed as proposed.

After injected into the mold, molten polymer is cooled down and solidified as heat is taken out through the mold walls, which are in turn cooled by cooling pipes. As solidification occurs, a region of mixed solid and liquid phases polymers exists. This region is at the critical temperature of crystallization. For semi-crystalline materials like HDPE, both density and ultrasonic wave velocity undergo discontinuities when crossing the crystallization temperature. As a result, an effective interface between liquid and solid phases HDPE is formed. Figure 2-19 demonstrates that by monitoring the advancement of the echoes reflected on the two solid/liquid interfaces (one from each cavity wall), information concerning solidification may be extracted.

Since ultrasonic wave velocity is less sensitive to temperature in the liquid phase than in the solid phase, by assuming a reasonable average temperature of the liquid layer, thickness of the liquid layer was determined using the P-V-T (pressure, ultrasonic wave velocity, and temperature) tripartite relationship. By partitioning the difference between the total distance between cavity walls and the liquid layer thickness in proportion to travel time in the two solid layers, the thicknesses of the solid layers on both sides of the liquid layer were also determined. By doing so, the physical locations of the solid/liquid interfaces were obtained, as shown in Figure 2-19.

In addition, since for HDPE the temperature zone for crystallization is very narrow, the temperature at solid/liquid interfaces (at 130°C crystallization temperature) can be determined with high accuracy (±5°C), and thus used as a temperature reference. This experimental observation can be used to verify the simulated solidification predicted by computer-aided engineering (CAE) software. Moreover, with the pressure held constant at holding pressure, and the average ultrasonic velocity derived from the time delay for a return trip of ultrasound inside the cavity, the average temperature of the molded part was determined as shown in Figure 2-13, using the P-V-T tripartite relationship.

The capability of ultrasound to determine part detachment was also demonstrated in Figures 2-11 and 2-21. When detachment occurs first from the internal mold, due to the change in interface, the reflection coefficient for the transmitted echo will increase. By identifying the increase, detachment from the internal mold can be known. On the other hand, if detachment occurs first from the external mold, energy transmitted into the molded part will diminish gradually to zero. No other echoes but the one reflected from the external mold cavity wall are observed. By identifying the point where the transmitted echoes start to diminish, detachment from the external mold can be known as well.

Based on the above results, a technique is established. It is claimed that by monitoring the reflection coefficient alone, the local polymer melt arrival, the end of filling, the pressure overshoot, the part detachment, and the release of holding pressure (plunger retraction) in the injection molding process can all be monitored on-line with

ultrasound, as summarized in Figure 2-23. Furthermore, ultrasonic techniques have other advantages over pressure transducers, such as their non-intrusive nature, which enables easy array implementation for multi-point monitoring, and their capability to monitor solidification of the part, and provide temperature and pressure information inside the molded part under certain conditions.

Monitoring of injection molding should also be carried out with materials other than HDPE. This is because for semi-crystalline materials like HDPE, material properties such as density and ultrasonic wave velocity are very different in solid than in liquid phase. Therefore very clear solid/liquid interfaces are present and observable. For amorphous material like polystyrene (PS), there exists no clear discontinuity in the aforementioned material properties when it solidifies or melts. In cases like this, flow front arrival, end of filling, and part detachment can still be monitored, though the solidification fronts might not be present.

On-line monitoring of gas-assisted injection molding was discussed in chapter 3. The monitoring was carried out on a 400-ton Husky injection molding machine with a Cinpres 2-cylinder gas generation system. The material used was HDPE.

As in injection molding, the arrival of polymer melt was identified. Moreover, as gas continued to advance inside the molded part, local gas arrival was also identified. When gas arrived locally, a gas/melt interface was formed. Not only was an echo reflected from this interface, but also the passage for ultrasound to the other cavity wall was blocked. As a result, the echo reflected from the internal mold cavity wall disappeared. The detectability of such a gas/melt interface was presented in Figure 3-7. Using array implementation, the development of gas channels might also be monitored.

Utilizing the reflection coefficients of the gas/melt interface echo and the echo reflected from the internal mold cavity wall, and their time delay with respect to the reflected echo from the external mold cavity wall, the polymer melt arrival, the start of

gas injection, the end of filling, the gas front arrival, the release of gas holding, and the gas blow-through were all identified on-line as shown in Figures 3-8, 3-10, and 3-11.

Since the gas generation system was of discontinuous type, gas pressure was not maintained constant throughout the process. Meanwhile, the gas was injected through the same nozzle as the polymer. As polymer injection stopped, since there was no gate to shut the barrel from the nozzle, compressed gas also penetrated into the barrel. Therefore the pressure inside the cavity dropped during monitoring. With both temperature and pressure of the molded part changing, it was difficult to measure the polymer wall thickness using the tripartite relationship.

Co-injected plates were also examined using ultrasound by the immersion method. Pure acrylonitrile-butadiene-styrene copolymer (ABS) was injected first, then ABS mixed with 2% carbon was injected as the core material. It was demonstrated that by placing two UTs, one on each side of the co-injected plate, interfaces between the two materials having slightly different elastic properties were discernible.

In chapter 4, ultrasonic temperature probes were fabricated and calibrated. One temperature probe was used in environments with elevated temperature to measure temperature during the polymer extrusion process. With cooling lines installed on the transducer end of the probe to bring down the temperature to below 50°C, the probing end was raised to a maximum of 275°C during calibration. The cladding provides advantages such as improvement in the signal-to-noise ratio (SNR) and machinability, so that this probe can be machined into the same shape as conventional temperature probes such as the Dynisco TPT463E-1M, in order to replace them conveniently.

Two discontinuities were made close to the probing end, so that part of the ultrasonic energy would be reflected. By measuring the change in ultrasonic wave velocity in the two sections (between the probe end and the 1<sup>st</sup> discontinuity and between discontinuities), the average temperatures of the two sections were determined, provided

the pressure was known. In principle, heat flux can then be determined and the temperature profile inside the polymer between cavity walls may also be calculated using an inverse algorithm. Two types of discontinuities were tested. The step type of discontinuity provided more symmetric geometry, and therefore the performance was more stable than the slot type design.

Such ultrasonic probes were calibrated at the Institute for National Measurement Standard, National Research Council (INMS-NRC). A 100Ω platinum resistance temperature detector (PRTD) was used as the reference thermometer. Together with a specifically designed high-performance oil bath, the accuracy of the overall system was better than 0.01°C. Steady state calibration curves between temperature and ultrasonic wave velocity using UTs of different central frequencies were established at atmospheric pressure as shown in Figure 4-11.

A calibrated ultrasonic probe and a Dynisco TPT463E-1M temperature probe were installed at symmetric positions onto the die ring of a PLACO co-extrusion blow molding machine to monitor the temperature during the polymer extrusion process. A digital compensator was used to correct the Dynisco temperature readings. Using a real-time Kalman filter to filter out noise in ultrasonic time delay measurement, and after correcting the shift bias of the ultrasonic temperature readings, the two readings were in good agreement as shown in Figure 4-15. Moreover, the ultrasonic probe has advantages such as faster response to temperature change, and higher sensitivity to heat flow, over the Dynisco TPT463E-1M. The ultrasonic probe can also measure the average temperature of the polymer, and is potentially capable of determining the temperature profile in the polymer between cavity walls at the probing location.

## 5.2 Original contributions

Several original contributions demonstrated in this study are summarized here:

- 1. We utilized reflection coefficients from interface echoes, obtained by a simple ultrasonic pulse/echo method, to monitor on-line several injection molding process features, such as local polymer melt arrival, the end of filling, pressure overshoot, part detachment, plunger retraction, and part ejection. Precise temperature information inside the polymer implied by the solidification interfaces was also extracted. Details can be found in references [78] [79] [80].
- 2. We utilized ultrasonic techniques to monitor the gas-assisted injection molding process. On-line monitoring of local polymer melt and gas arrival, the end of polymer injection, the start and end of gas injection, the end of filling, the gas penetration, and the gas blow-through were demonstrated. Details can be found in references [80] [81].
- 3. We calibrated and utilized an improved buffer rod as an ultrasonic temperature probe to measure temperatures at the probing end during the polymer extrusion process. Details can be found in references [77] [80] [81].

## 5.3 Future work

At the end of injection molding, several events may occur: part detachment, gate freezing, and release of holding pressure (plunger retraction). In this study, the effects of the part detachment and the plunger retraction on reflection coefficients were studied. Gate freezing was not studied. In the future, by shortening or prolonging the pressure holding time, the impact of plunger retraction and part detachment can be separated. Therefore more information can be obtained from reflection coefficient plots.

As demonstrated by Nishiwaki, et al. [39], after calibration, cavity pressure can be quantitatively measured using ultrasonic techniques; therefore an ultrasonic pressure probe may be developed. Meanwhile, the ultrasonic temperature probe should also be calibrated at different pressures, in order for it to be used in monitoring temperatures in the injection molding process, because ultrasonic wave velocity depends on both

temperature and pressure. Current calibration curves established under atmospheric pressure are sufficient for the polymer extrusion process, but inaccurate under high pressure circumstances, such as inside the cavity during injection molding.

Currently only time domain information of the reflection coefficient is used in interpreting and monitoring the injection molding process. In order to improve accuracy, not only time domain information about reflection coefficients should be considered, as indicated by Drinkwater [82], but frequency domain information should also be included in interpreting reflection coefficients under conditions such as non-uniformly or partially contacted interfaces.

## References:

- [1] R. Gendron and L.A. Utracki, "Material characteristics oriented computer control of extrusion part 1", *Proc. SPE ANTEC*, pp. 958-963, 1991.
- [2] A.R. Agrawal, I.O. Pandelidis, and M. Pecht, "Injection-molding process control a review", *Polym. Eng. Sci.*, 27, no.18, pp. 1345-1357, 1987.
- [3] R.E. Farrell and L. Dzeskiewicz, "Expert system for injection molding", *Proc. SPE ANTEC*, pp. 692-695, 1994.
- [4] J. Vann and Y. Shen, "Computer integrated information and control systems for improved quality and profit", Trans. the NADCA 15<sup>th</sup> Int. Die Casting Congress and Exposition, G-T89-021, 1989.
- [5] C.L. Thomas, "Sensor concepts for polymer injection molding", Ph.D. dissertation, Department of Mechanical Engineering, Drexel University, Philadelphia, PA, 1993.
- [6] J.F. Stevenson, *Innovation in Polymer Processing: Molding*, Hanser Publishers, New York, 1996.
- [7] P. Kennedy, Flow Analysis of Injection Molds, Hanser Publishers, New York, 1995.
- [8] M. Haupt, "Computer-assisted optimization of working points in plastics processing", *Proc. SPE ANTEC*, pp. 59-61, 1989.
- [9] V. Miranda and F.S. Lai, "A study of the effect of gate design on holding time by theoretical calculations, computer flow simulation and experimentation", *Proc. SPE ANTEC*, pp. 411-416, 1995.
- [10] C.P. Chiu and K.A. Liu, "A method for measuring PVT relationships of thermoplastics using an injection molding machine", *Polym. Eng. Sci.*, 35, no.19, pp. 1505-1510, 1995.

- [11] W.C. Bushko and V.K. Stokes, "Solidification of thermoviscoelastic melts. part 3: effects of mold surface temperature differences on warpage and residual stresses", *Polym. Eng. Sci.*, **36**, no. 3, pp. 322-335, 1996.
- [12] W.C. Bushko and V.K. Stokes, "Solidification of thermoviscoelastic melts. part 4: effects of boundary conditions on shrinkage and residual stresses", *Polym. Eng. Sci.*, **36**, no. 5, pp. 658-675, 1996.
- [13] Y. Yamamoto, Y. Iwata, M. Nakamira, and Y. Oukouchi, "Molten metal velocities and gas pressure in die cavity and defects in commercial aluminum pressure die castings", *Trans. the NADCA 15<sup>th</sup> Int. Die Casting Congress and Exposition*, G-T89-081, 1989.
- [14] J.R. Brevick, M. Duran, and Y. Karni, "Experimental determination of slow shot velocity-position profile to minimize air entrapment", *Trans. the NADCA 16<sup>th</sup> Int. Die Casting Congress and Exposition*, pp. 399-404, 1991.
- [15] M. Rafizadeh, W.I. Patterson, and M.R. Kamal, "Physically-based model of thermoplastics injection molding for control applications", *Int. Polym. Process.*, 11, no. 4, pp. 352-362, 1996.
- [16] D.M. Gao, K.T. Nguyen, P. Girard, and G. Salloum, "Numerical simulation of the sequential filling in injection molding process", *Proc. SPE ANTEC*, pp. 554-558, 1994.
- [17] P. Ehret, A. Davidoff, F. Jacque, and H. Bung, "Simulation of the complete injection cycle", *Proc. SPE ANTEC*, pp. 542-546, 1994.
- [18] D. Frayce, J.F. Hétu, and C.A. Loong, "Numerical modeling of filling and solidification in die casting", *Trans. the NADCA 17<sup>th</sup> Int. Die Casting Congress and Exposition*, pp. 13-17, 1993.

- [19] Y. Iwata, Y. Yamamoto, K. Yonekura, and Y. Kagami, "Computer simulation of molten metal flow in thin plate die castings", Trans. the NADCA 16<sup>th</sup> Int. Die Casting Congress and Exposition, pp. 311-320, 1991.
- [20] K.M.B. Jansen, D.J. van Dijk, and E.V. Burgers, "Experimental validation of shrinkage predictions for injection molded products", *Int. Polymer Processing*, 13, no. 1, pp. 99-104, 1998.
- [21] C.M. Hsiung and M. Cakmak, "Phenomenological modeling of structural gradient development in injection molding of slowly crystallizing polymers "poly-p-phenylene sulfide", *Proc. SPE ANTEC*, pp. 2378-2384, 1991.
- [22] L.J. Chien, C.L. Thomas, and D.R. Lawson, "Sensor/model fusion for improved process understanding and control in injection molding", CAE and Intelligent Processing of Polymer Materials, MD-79, pp. 189-197, 1997.
- [23] M.R. Kamal, W.I. Patterson, D.A. Fara, and A. Haber, "A study in injection molding dynamics", *Polym. Eng. Sci.*, 24, no. 9, pp. 686-691, 1984.
- [24] J.L. Wu, S.J. Chen, and R. Malloy, "Development of an on-line cavity pressure-based expert system for injection molding process" *Proc. SPE ANTEC*, pp. 444-449, 1991.
- [25] B. Souder, S. Woll, and D. Cooper, "Advanced methods for monitoring injection molding processes" *Proc. SPE ANTEC*, pp. 644-650, 1994.
- [26] Y. Mochiku, Y. Hatamura, and K. Shirahige, "Intelligent die casting and seven sensors", Trans. the NADCA 15<sup>th</sup> Int. Die Casting Congress and Exposition, G-T89-024, 1989.
- [27] F. Johannaber, *Injection Molding Machines a User's Guide, 3<sup>rd</sup> Edition*, Hanser Publishers, New York, 1994.

- [28] H.N.G. Wadley, S.J. Norton, F. Mauer, and B. Droney, "Ultrasonic measurement of internal temperature distribution", *Phil. Trans. R. Soc. London. A320*, pp. 341-361, 1986.
- [29] S.H. Patel, D.B. Todd, and M. Xanthos, "Recent developments in on-line analytical techniques applicable to the polymer industry", *Proc. SPE ANTEC*, pp. 2214-2219, 1994.
- [30] L.C. Lynnworth, *Ultrasonic Measurements for Process Control, Theory, Techniques, Applications*, Academic Press Inc., San Diego, 1989.
- [31] J. Krautkrämer and H. Krautkrämer, *Ultrasonic Testing of Materials*, 4<sup>th</sup> Fully Revised Edition, Springer-Verlag, Berlin Heidelberg, 1990.
- [32] B. Cao, H. Wang, C.-K. Jen, K.T. Nguyen, J.-G. Legoux, C.A. Loong, and M. Viens, "Ultrasonic monitoring of injection molding and die casting", *Proc. SPIE*, **2948**, pp. 173-186, 1996.
- [33] B. Cao, "On-line ultrasonic monitoring of injection molding and die casting processes", Master thesis, Department of Electrical Engineering, McGill University, Montréal, OC, 1996.
- [34] M.R. Kamal, W.I. Patterson, and V.G. Gomes, "An injection molding study. part 1: melt and barrel temperature dynamics", *Polym. Eng. Sci.*, 26, no. 12, pp. 854-866, 1986.
- [35] S. Mochizuki, M. Konno, A. Murata, N. Nishiwaki, A. Cui, and S. Hori, "Measurement of melted polymer temperature in injection molding machine by using ultrasonic techniques", *Proc. the* 7<sup>th</sup> *Int. Symposium on Transport Phenomena in Manufacturing Processes*, pp. 117-121, 1994.
- [36] J. Shen, R. Edwards, C.L. Thomas, and A.J. Bur, "Ultrasonic melt temperature measurement during extrusion", *Proc. SPE ANTEC*, pp. 2076-2079, 1998.

- [37] E.C. Brown, T.L.D. Collins, A.J. Dawson, P. Olley, and P.D. Coates, "Ultrasound: a virtual instrument approach for monitoring of polymer melt variables", *Proc. SPE ANTEC*, pp. 335-339, 1998.
- [38] L. Piché, A. Hamel, R. Gendron, M. Dumoulin, and J. Tatibouët, "Ultrasonic characterization of polymer melts under processing conditions", US Patent 5433112, July 18, 1995.
- [39] N. Nishiwaki, M. Konno, A. Cui, and S. Hori, "Pressure measurement in molding process by ultrasonic wave", *Proc. Seikei-Kakou*, 5, no. 11. pp. 779-785, 1993.
- [40] E.C. Brown, P. Olley, and P.D. Coates, "Ultrasonic velocity dependence on polymer melt variables", *Proc. SPE ANTEC*, pp. 1042-1046, 1997.
- [41] C.L. Thomas, M. Jiang, C.-C. Chen, and A.J. Bur, "An ultrasonic instrument for PVT characterization of polymer", *Proc. SPE ANTEC*, pp. 2707-2714, 1995.
- [42] B.A. Salamon and R.J. Donald, "Characterizing and controlling secondary flows in injection molds", *Proc. SPE ANTEC*, pp. 680-684, 1996.
- [43] N. Nishiwaki, S. Hori, K. Shimazaki, and T. Arai, "Visualization of plastics material characteristic by ultrasonic wave", *Proc. the 1<sup>st</sup> Pacific Symp. On Flow Visualization and Image Processing*, 1, pp. 225-230, 1997.
- [44] F. Gao, W.I. Patterson, and M.R. Kamal, "Dynamics and control of surface and mold temperatures in injection molding", *Int. Polym. Process.*, **8**, no. 2, pp. 147-157, 1993.
- [45] F. Manero, W.I. Patterson, and M.R. Kamal, "Cavity temperature profile measurement during injection moulding", *Proc. SPE ANTEC*, pp. 577-581, 1997.
- [46] G.C. Peischl and I. Bruker, "Melt homogeneity in injection molding: application of a ring-bar device", *Polym. Eng. Sci.*, **29**, no. 3, pp. 202-208, 1989.

- [47] O. Amano and S. Utsugi, "Temperature measurements of polymer melts in the heating barrel during injection molding. part 3: effects of screw geometry", *Polym. Eng. Sci.*, **30**, no. 7, pp. 385-393, 1990.
- [48] K.B. Migler and A.J. Bur, "Measurement of temperature profiles during polymer processing", *Proc. SPE ANTEC*, pp. 2278-2282, 1997.
- [49] S. Quilliet, Ph. Le Bot, D. Delaunay, and Y. Jarny, "Heat transfer at the polymer-metal interface. A method of analysis and its application to injection molding", ASME proc. 32<sup>nd</sup> National Heat Transfer Conf., 2, pp. 9-16, 1997.
- [50] R.G. Speight, E.P. Yazbak, and P.D. Coates, "In-line pressure and infrared temperature measurements for injection moulding process control", *Proc. SPE ANTEC*, pp. 647-651, 1995.
- [51] R.G. Speight, P. D'Agostino, and J.S. Herrmann, "Melt and mould temperature measurements for polymer injection moulding", *Proc. SPE ANTEC*, pp. 568-572, 1997.
- [52] C. Maier, "Infrared temperature measurement of polymers", *Polym. Eng. Sci.*, 36, no. 11, pp. 1502-1512, 1996.
- [53] A.J. Bur, F.W. Wang, C.L. Thomas, and J.L. Rose, "In-line optical monitoring of polymer injection molding", *Polym. Eng. Sci.*, **34**, no. 8, pp. 671-679, 1994.
- [54] A.J. Bur and C.L. Thomas, "A multi-functional optical sensor for monitoring polymer injection molding", *Proc. SPE ANTEC*, pp. 2798-2804, 1995.
- [55] N. Nishiwaki, A. Cui, M. Konno, and S. Hori, "Observation of solidified resin behavior in a cavity by ultrasonic waves", *Proc. Seikei-Kakou*, 5, no. 12, pp. 870-874, 1993.
- [56] C.J. Yu, J.E. Sunderland, and C. Poli, "Thermal contact resistance in injection molding", *Polym. Eng. Sci.*, 30, no. 24, pp. 1599-1606, 1990.

- [57] K.A. Narh and L. Sridhar, "Measurement and modeling of thermal contact resistance at a plastic metal interface", *Proc. SPE ANTEC*, pp. 2273-2277, 1997.
- [58] H. Wang, M. Prystay, J.-F. Hétu, B. Cao, and C.-K. Jen, "Gap between mold and part and its effect on cooling of injection-molded plastics", *Proc. SPE ANTEC*, pp. 1049-1053, 1996.
- [59] H. Wang, B. Cao, C.-K. Jen, K.T. Nguyen, and M. Viens, "On-line ultrasonic monitoring of the injection molding process", *Polym. Eng. Sci.*, 37, no. 2, pp. 363-376, 1997.
- [60] G. Crawford, "Technological advances in gas assist", Molding '98, the 8th Int'l Conf. and Exhibit, 1998.
- [61] R.G. Speight, E.P. Yazbak, and P.D. Coates, "In-line process measurements for integrated injection molding", *Proc. SPE ANTEC*, pp. 508-512, 1996.
- [62] R.G. Speight and J.B. Hull, "Pressure measurements for injection moulding control", *Proc. SPE ANTEC*, pp. 561-565, 1997.
- [63] G.S. Kino, Acoustic Waves: Devices, Imaging, and Analog Signal Processing, Prentice-Hall Inc., Englewood Cliffs, New Jersey, 1987.
- [64] J.J. Magda, M.L. Parrott, C.L. Thomas, and D.R. Lawson, "An ultrasonic technique for monitoring the interface in multi-layer polymer flows", *Proc. SPE ANTEC*, pp. 1182-1186, 1996.
- [65] L. Zou, M. Sayer, and C.-K. Jen, "Sol-gel fabricated thick piezoelectric ultrasonic transducers for potential applications in industrial material processes", *Proc. IEEE Ultrasonics Symp.*, pp. 1007-1011, 1997.
- [66] B.R. Marple, C.-K. Jen, and J. Voyer, "Ceramic-clad ceramic system for ultrasonic wave guidance"; *Proc. the 15<sup>th</sup> Int. Thermal Spray Conf., Thermal Spray: Meeting the Challenges of the 21<sup>st</sup> Century, pp. 1109-1114, 1998.*

- [67] J.-G. Legoux and C.-K. Jen, "Ultrasonic applications of thick metallic coatings", Proc. the 9<sup>th</sup> National Thermal Spray Conf., Thermal Spray: Practical Solutions for Engineering Problems, pp. 65-72, 1996.
- [68] C.-K. Jen and J.-G. Legoux, "High performance clad metallic buffer rods", *Proc. IEEE Ultrasonics Symp.*, pp. 771-776, 1996.
- [69] C.-K. Jen, B. Cao, K.T. Nguyen, C.A. Loong, and J.-G. Legoux, "On-line ultrasonic monitoring of a die-casting process using buffer rods", *Ultrasonics*, 35, pp. 335-344, 1997.
- [70] C.-K. Jen, J.-Y. Chen, S.V. Hoa, K.T. Nguyen, J.-G. Legoux, and H. Hébert, "Clad buffer rods for in-situ process monitoring", *Proc. IEEE Ultrasonics Symp.*, pp. 801-806, 1997.
- [71] L.C. Lynnworth, "Temperature profiling using multizone ultrasonic waveguides". Proc. the 6<sup>th</sup> Symp. on Temperature - It's Measurement and Control in Science and Industry, pp. 1181-1190, 1982.
- [72] H.A. Tasman, M. Campana, D. Pel, and J. Richter, "Ultrasonic thin-wire thermometry for nuclear applications", *Proc. the 6<sup>th</sup> Symp. on Temperature It's Measurement and Control in Science and Industry*, pp. 1191-1196, 1982.
- [73] S.C. Wilkins, "A single-crystal tungsten ultrasonic thermometer". Proc. the 7<sup>th</sup> Symp. on Temperature It's Measurement and Control in Science and Industry, pp. 1023-1026, 1986.
- [74] M. Hoersch, Manual on the Use of Thermocouples in Temperature Measurement, 4th Edition, American Society for Testing and Materials, Philadelphia, 1993.
- [75] T.-F. Chen, S. Lin, and J. C.-Y. Wang, "An application of Kalman filter and finite difference scheme to inverse heat conduction problems", *Inverse Problems in Engineering*, 3, pp. 163-175, 1996.

- [76] T.-F. Chen, "Analytical and experimental studies for space boundary and geometry inverse heat conduction problem", Ph.D. dissertation, Department of Mechanical Engineering, Concordia University, Montréal, QC, 1997.
- [77] T.-F. Chen, K.T. Nguyen, S.-S.L. Wen, and C.-K. Jen, "Temperature measurement of polymer extrusion by ultrasonic techniques", to be submitted to *Measurement Science and Technology*.
- [78] D. Ramos França, S.-S.L. Wen, C.-K. Jen, K.T. Nguyen, and H. Hébert, "Advances in on-line monitoring of polymer injection molding process", *Proc. IEEE Ultrasonics Symp.*, pp. 807-810, 1997.
- [79] S.-S.L. Wen, C.-K. Jen, and K.T. Nguyen, "Advances in ultrasonic monitoring of injection molding", to be submitted to *Int. Polym. Process*.
- [80] C.-K. Jen, K.T. Nguyen, S.-S.L. Wen, D. Ramos França, I. Ihara, T.-F. Chen, and H. Hébert, "Industrial material process monitoring using ultrasound". Invited talk, to be presented at *IEEE Ultrasonic Symp.*, Sendai, Japan, October 5-8, 1998.
- [81] S.-S.L. Wen, T.-F. Chen, D. Ramos França, K.T. Nguyen, C.-K. Jen, I. Ihara, A. Derdouri, and A. Garcia-Rejon, "Recent progress in on-line ultrasonic process monitoring", *Proc. SPIE*, **3399**, pp. 122-130, 1998.
- [82] B. Drinkwater and P. Cawley, "Measurement of the frequency dependence of the ultrasonic reflection coefficient from thin interface layers and partially contacting interfaces", *Ultrasonics*, **35**, pp. 479-488, 1997.